No. 19. (2015)
ISSN 1331-1611

KoG

SCIENTIFIC - PROFESSIONAL JOURNAL
OF CROATIAN SOCIETY FOR GEOMETRY AND GRAPHICS

Official publication of the Croatian Society for Geometry and Graphics publishes scientific and professional papers from the fields of geometry, applied geometry and computer graphics.

Founder and Publisher

Croatian Society for Geometry and Graphics

Design

Miroslav Ambruš-Kiš

Layout

Sonja Gorjanc, Ema Jurkin

Cover Illustration

F. V. Holi, photography

Print

SAND d.o.o., Zagreb

URL address

http://www.hdgg.hr/kog
http://hrcak.srce.hr

Edition

250

Published annually

Guide for authors
Please, see the next page

KoG is cited in: Mathematical Reviews, MathSciNet, Zentralblatt für Mathematik

INSTRUCTIONS FOR AUTHORS

SCOPE. "KoG" publishes scientific and professional papers from the fields of geometry, applied geometry and computer graphics.

SUBMISSION. Scientific papers submitted to this journal should be written in English or German, professional papers should be written in Croatian, English or German. The papers have not been published or submitted for publication elsewere.
The manuscript with wide margines and double spaced should be sent in PDF format via e-mail to one of the editors:

Sonja Gorjanc	Ema Jurkin
sgorjanc@grad.hr	ema.jurkin@rgn.hr

The first page should contain the article title, author and coauthor names, affiliation, a short abstract in English, a list of keywords and the Mathematical subject classification.

UPON ACCEPTANCE. After the manuscript has been accepted for publication authors are requested to send its LaTex file via e-mail to one of the addresses:

sgorjanc@grad.hr, ema.jurkin@rgn.hr

Figures should be titled by the figure number that match to the figure number in the text of the paper.

The corresponding author and coauthors will recieve hard copies of the issue free of charge.

UPUTE ZA AUTORE

PODRUČJE. "KoG" objavljuje znanstvene i stručne radove iz područja geometrije, primijenjene geometrije i računalne grafike.

UPUTSTVA ZA PREDAJU RADA. Znanstveni radovi trebaju biti napisani na engleskom ili njemačkom jeziku, a stručni na hrvatskom, engleskom ili njemačkom. Rad ne smije biti objavljen niti predan na recenziju u drugim časopisima.
Rukopis sa širokim marginama i dvostrukim proredom šalje se u PDF formatu elektronskom poštom na adresu jedne od urednica:

Sonja Gorjanc	Ema Jurkin
sgorjanc@grad.hr	ema.jurkin@rgn.hr

Prva stranica treba sadržavati naslov rada, imena autora i koautora, podatke o autoru i koautorima, sažetak na hrvatskom i engleskom, ključne riječi i MSC broj.

PO PRIHVAĆANJU RADA. Tekst prihvaćenog rada autor dostavlja elektronskom poštom kao LaTeX datoteku. Slike trebaju imati nazive koji odgovaraju rednom broju slike u tekstu članka. Adresa:

sgorjanc@grad.hr, ema.jurkin@rgn.hr

Svaki autor i koautor dobiva po jedan primjerak časopisa.

ISSN 1331–1611

No. 19
Zagreb, 2015

SCIENTIFIC AND PROFESSIONAL JOURNAL OF
CROATIAN SOCIETY FOR GEOMETRY AND GRAPHICS

CONTENTS

ORIGINAL SCIENTIFIC PAPERS

PROFESSIONAL PAPERS

ISSN 1331–1611

KoG

BROJ 19
Zagreb, 2015

ZNANSTVENO-STRUČNI ČASOPIS
HRVATSKOG DRUŠTVA ZA GEOMETRIJU I GRAFIKU

SADRŽAJ

ORIGINALNI ZNANSTVENI RADOVI

STRUČNI RADOVI

Original scientific paper
Accepted 23. 02. 2015.

BARBORA POKORNÁ
PAVEL CHALMOVIANSKÝ

Collision-free Piecewise Quadratic Spline with Regular Quadratic Obstacles

Collision-free Piecewise Quadratic Spline with Regular Quadratic Obstacles

ABSTRACT

We classify mutual position of a quadratic Bézier curve and a regular quadric in three dimensional Euclidean space. For given first and last control point, we find the set of all quadratic Bézier curves having no common point with a regular quadric. This system of such quadratic Bézier curves is represented by the set of their admissible middle control points. The spatial problem is reduced to a planar problem where the regular quadric is represented by a conic section. Then, the set of all middle control points is found for each type of conic section separately. The key issue is to find the boundary of this set. It is formed from the middle control points of the Bézier curves touching the given conic section. Our results are applicable in collision-free paths computation for virtual agents where the obstacles are represented or bounded by regular quadrics. Another application can be found in searching for pointwise spacelike curves in Minkowski space.

Key words: Bézier quadratic curve, regular quadric, intersection, collision-free paths

MSC2010: 65D17, 14P25, 51M04

Kvadratni splajnovi, po dijelovima bez kolizija, s regularnim kvadratnim barijerama

SAŽETAK

U trodimenzionalnom euklidskom prostoru klasificiramo međusobni odnos kvadratne Bézierove krivulje i regularne kvadrike. Za danu prvu i zadnju kontrolnu točku, nalazimo skup svih kvadratnih Bézierovih krivulja koje nemaju zajedničku točku s regularnom kvadrikom. Sustav ovakvih kvadratnih Bézierovih krivulja prikazuje se skupom njihovih dopustivih srednjih kontrolnih točaka. Prostorni problem svodi se na ravninski problem gdje konika predstavlja regularnu kvadriku. Tada se za svaku vrstu konike zasebno nalazi skup svih srednjih kontrolnih točaka. Glavna zadaća je naći granicu ovakvog skupa. Spomenutu granicu čine središnje kontrolne točke Bézierovih krivulja koje diraju koniku. Naši rezultati primjenjuju se u računanju putanja bez kolizija za virtualna sredstva gdje su barijere prikazane ili ograničene regularnim kvadrikama. Drugu primjenu nalazimo u istraživanju točkovnih prostornih krivulja u prostoru Minkowski.

Ključne riječi: Bézierove kvadratna krivulja, regularna kvadrika, presjek, dijelovi bez kolizija

1 Introduction

We consider a problem of finding conditions for collision-free piecewise quadratic path in $\mathbb{E}^d$ with respect to a regular quadric. If the quadric is a bounding domain of a complex object, we reduce the complexity of exact collision detection considerably.

For illustration, we work in three-dimensional space in which a regular quadric is situated. Taking two arbitrary fixed points out of the quadric in the same connected component, we find a set of all parabolic arcs connecting these two points such that this path and the regular quadric have no intersection. The spatial problem is reduced to a planar problem where the the regular quadric is represented by a conic section.

In most algorithms, the finding of collision-free path consists of two main steps. The first one is acquisition of linear spline path generated by sample-based planning algorithms. The second step is smoothing of the path because in mobile robotics a non smooth motions can cause slippage of wheels.

The finding of smooth collision-free path using Bézier curves was considered e.g. in [9], [11], [10]. But these algorithms are used as post processing, because they assume some linear collision-free path and they only smooth the path. Moreover, the algorithms provide only a numeri-

cal solution. Our method offers a direct analytical computation of all possible collision-free smooth paths without using sample-based planning algorithms. We assume an obstacle represented by a regular quadric and given start and end position of robot. We find all quadratic Bézier curves constituting the set of collision-free paths. One can use such a set for optimization of the sought path.

Sometimes the scene with obstacles is too much complicated and the smooth collision-free path cannot be found directly. Then, the use of sample-based planning algorithms is necessary. But the obtained linear path is jerky, because it contains many redundant nodes which was generated randomly. In order to remove these nodes the path pruning techniques as in [5] are used. Our results can also form a path pruning algorithm, where the node v_i can be removed if there is a quadratic Bézier collision-free path between nodes v_{i-1} and v_{i+1}. Such an algorithm is more flexible comparing with a piecewise linear approach.

There is another use for the affine three dimensional Minkowski space typically determined by a light cone. The points lying outside the cone are called space-like. If we take two space-like points as a first and a last control point, we can find all quadratic pointwise space-like Bézier curves. We analyze this problem in [3] for parabola. Some statements for other conic sections, we summarize in [13]

2 Theoretical background

In this section, we mention basic definitions of Bézier curves, regular quadrics and all concepts required later in the text.

Let $\mathbb{E}^3$ be three dimensional vector Euclidean space formed by vectors $x = (x_1, x_2, x_3)$ with scalar product $\langle \cdot, \cdot \rangle \colon \mathbb{E}^3 \times \mathbb{E}^3 \to \mathbb{R}$. By standard construction, we get an affine space with a Cartesian coordinate system $\langle O, e_1, e_2, e_3 \rangle$. Let $\mathbb{E}^2$ be a Euclidean plane. We assign to each family of parallel lines a unique point at infinity, at which "all of such lines meet". All the points at infinity define the line at infinity l^∞. The *extended Euclidean plane*, denoted by $\overline{\mathbb{E}^2}$, is obtained as $\overline{\mathbb{E}^2} = \mathbb{E}^2 \cup l^\infty$. More can be found in [1], [2].

Let $M_{3,3}(\mathbb{R})$ be the set of 3×3 matrices with real coefficients. A quadratic form is the map $q \colon \mathbb{R}^3 \to \mathbb{R}$, where $q(x) = xQx^\top$ for the symmetric $Q \in M_{3,3}(\mathbb{R})$. We talk about *regular quadratic form* if the matrix Q is diagonal with entries $\lambda_{1,2,3} \in \{-1, 1\}$ in a certain basis of $\mathbb{R}^3$. The unique symmetric bilinear form giving rise to q is denoted by P and called the *polar form* of q. We have $q(x) = P(x,x)$, $P(x,w) = xQw^\top$. In the associated affine space, we have $P(X,W) = XQW^\top$. Let Q be regular and the point $W \in \mathbb{R}^3$ be fixed. We call the set $W^\perp = \{X \in \mathbb{R}^3 \colon P(X,W) = 0\}$ the *polar (hyperplane)* of W. We say that X and W are conjugate with respect to the polar form P, and we denote this fact by $X \perp W$. For the *self-polar* point W holds $P(W,W) = 0$. In the affine space $\mathbb{R}^2$, the $W^\perp$ is the polar line determined by equation $WQX^\top = 0$, where the variable $X = (x, y, 1)$. An image of a *regular quadric* κ is the set of all points $X \in \mathbb{E}^3$ such that for its position vector $x = X - O$ the equality $q(x) = 0$ holds. The properties of quadrics are in [8].

Let $Q_K \in M_{3,3}(\mathbb{R})$ be a symmetric matrix. The algebraic curve of degree 2 called *conic section* is the set $K = \{[x,y] \in \mathbb{R}^2 \colon f(x,y) = 0 \text{ for } f(x,y) = (x\ y\ 1) Q_K (x\ y\ 1)^\top\}$. In appropriate cases, we consider the equation of the conic section instead of K due to the fact that the field $\mathbb{R}$ is not algebraically closed. In the extended Euclidean plane, it is necessary to homogenize the equation of conic section by replacing $(x, y, 1)$ with (x, y, z). We obtain the conic section $\overline{K} = \{[x,y,z] \in \overline{\mathbb{R}^2} \colon (x\ y\ z) Q_K (x\ y\ z)^\top = 0\}$ in homogeneous coordinates. More on plane algebraic curves we refer to the book [7]. The polar line $N^\perp$ of such a point N that $P(N,N) > 0$ splits the conic section K into some arcs. If $N^\perp \cap K = \{T_1, T_2\}$ then we denote the arc $\overset{\frown}{T_1 T_2} = \{X \in K \colon P(N,X) > 0\}$.

From each point $X \in \mathbb{R}^2$ lying outside the regular conic section K, one can construct two tangent lines to $\overline{K} \subset \overline{\mathbb{R}^2}$. The corresponding points of contact may be either *affine* or *at infinity*. In the case of point of the contact at infinity, the conic section $K \subset \mathbb{R}^2$ is a hyperbola and the projective tangent line is called asymptote a in affine space. We denote its point of contact with K at infinity by a^∞, see fig. 7 for an example. We denote the set of all tangent lines to K by T_K. Hence, $T_K = \{\ell \subset \mathbb{R}^2 : \text{ each point } X \in \ell \text{ satisfies } 0 = \langle \nabla f(X_0), X - X_0 \rangle \mid X_0 \in K \cap \ell\}$. We denote by $\nabla f(x_0, y_0)$ the gradient $\left(\frac{\partial f}{\partial x}(x_0, y_0), \frac{\partial f}{\partial y}(x_0, y_0)\right)$ of K at the point $[x_0, y_0] \in K$. Clearly, in a regular point, it is the normal vector of its tangent line.

For counting the number of real roots of real polynomial function in an interval, the theorem below is useful.

Theorem 1 (Budan-Fourier) *Let $f(x) = \sum_{i=0}^n a_i x^i \in P_n$, $n > 0, a_n \neq 0$. Let $\alpha < \beta$ and $f(\alpha) f(\beta) \neq 0$ and let $V(x)$ be the number of changes in sign in the sequence $\{f(x), f'(x), \ldots, f^{(n)}(x)\}$. Then, the number (including multiplicity) of real roots of the equation $f(x) = 0$ lying in the interval $\langle \alpha, \beta \rangle$ is equal to or is smaller, by an even number, than $V(\alpha) - V(\beta)$.*

We consider the collision-free path represented in Bézier form.

Definition 1 (Bézier curve) Bézier curve *of degree n in the space $\mathbb{E}^3$ is a polynomial map $b \colon [0,1] \to \mathbb{E}^3$ given by $b(t) = \sum_{i=0}^n B_i^n(t)\, b_i$. The points $b_i \in \mathbb{E}^3$ are called* control points*, the functions $B_i^n(t) = \binom{n}{i} (1-t)^{n-i} t^i$ for $i \in \{0, \ldots, n\}$ are Bernstein polynomials of degree n.*

More about the properties of Bézier curves can be found in [6], [4].

Lemma 1 (Determination of quadratic Bézier curve by its tangent) *Let the points $A,B,T \in \mathbb{R}^2$ be non-collinear and ℓ_T be a line such that segment $AB \cap \ell_T = \emptyset$, $T \in \ell_T$. Then, the quadratic Bézier curve $b(t)$ with the end points A,B, containing the point T and with the tangent line ℓ_T at the point T exists and is uniquely determined.*

Proof. Let the vector $\ell = (\ell_x, \ell_y) \neq (0,0)$ be the direction vector of the tangent line ℓ_T and $A = [a_x, a_y], B = [b_x, b_y], T = [t_x, t_y]$. Let the vector $n_\ell = (-\ell_y, \ell_x)$. We define the map τ such that $\tau(A,B,T,\ell) = C$ returns the middle control point of the Bézier curve $b(t)$.

$$\tau(A,B,T,\ell) = C = \frac{T - B_0^2(t_0)A - B_2^2(t_0)B}{B_1^2(t_0)} ,$$

where $t_0 \in (0,1)$ is a solution of the equation

$$0 = \alpha t^2 + 2\beta t + \gamma ,$$

and

$$\begin{aligned} \alpha &= \ell_x(b_y - a_y) - \ell_y(b_x - a_x) , \\ \beta &= \ell_x(a_y - t_y) - \ell_y(a_x - t_x) , \\ \gamma &= -\beta . \end{aligned}$$

The Bézier curve $b_{ACB}(t)$ with its control points A,C,B in this order satisfies the requirements of the theorem. For proving the existence of b_{ACB}, we use the affine transformation mapping the three independent points A,B,T to the points $A = [-1,0],\ B = [1,0],\ T = [0,1]$. We obtain the coefficients $\alpha = -2\ell_y,\ \beta = -\ell_x + \ell_y,\ \gamma = \ell_x - \ell_y$. After computing the discriminant, we do discussion with respect to direction of the vector ℓ. □

This statement is possible to extend in a natural way for degenerate situation in which collinearity of the points A,B,T or even $A = B$ hold.

3 Collision-free situation

Let us consider the Euclidean space $\mathbb{E}^3$, let $\langle O, e_1, e_2, e_3 \rangle$ be an affine coordinate system, with a regular quadric κ represented by the matrix Q. Let the points $A = [a_1, a_2, a_3]$ and $B = [b_1, b_2, b_3]$ be fixed and $a = A - O, b = B - O$ are their position vectors. Assuming the quadric is an enclosing volume of some obstacle and the points A,B are start and end position of a robot we require $q(a) > 0$ and $q(b) > 0$, i.e. A,B lie outside the quadric κ. We look for all collision-free (relative to quadric) paths supply by quadratic Bézier curves from the point A to the point B. In other words, we look for the set of all such points C that the Bézier curve $b_{ACB}(t)$ lie out of quadric. Thus, for all points $X \in b_{ACB}(t)$ and their position vectors $x = X - O$ the inequality $q(x) > 0$ holds. In applications, $A \neq B$ yields, however we solved also the case $A = B$ for the sake of completeness.

A generic quadratic Bézier curve is a part of a parabola, so it lies in the affine plane $\rho \subset \mathbb{E}^3$. Since the given points $A,B \in \rho$, the construction of the plane ρ may have several degrees of freedom depending on their positions. Using the equation $\rho = \{X \in \mathbb{E}^3; X = A + tv + sw, \text{ for } t,s \in \mathbb{R}\}$, the degree of freedom is represented by the $\dim[v,w]$. If $A \neq B$, the degree of freedom is 1. As the position of the point C changes, the plane ρ accordingly contains the axis $\overleftrightarrow{AB}$, so we can choose as $v = B - A$ and the choice of the vector w is free. If $A = B$, the degree of freedom is 2 and the choice of both vectors v,w is free (up to linear dependency).

In any case, the intersection of the quadric κ and the plane ρ is a conic section K (see fig. 1(a)). The figure 1(b) shows all cases how the set S of all points X that $q(x) > 0$ in the possible types of plane ρ looks like. The collision-free Bézier curve $b_{ACB}(t) \subset S$. We present a solution in the plane ρ for each type of conic section and the planar results can be put together to form the spatial result.

As we shall see later, it is useful to consider ρ as an extended Euclidean plane. However, the control points $A,B,C \notin l^\infty$. Let $\langle O,x,y \rangle_\rho$ be any Cartesian coordinate system in the plane ρ. Let $A = [a_x, a_y]$, $B = [b_x, b_y]$ a $C = [c_x, c_y]$ be the local affine coordinates of the control points in $\langle O,x,y \rangle_\rho$.

Definition 2 (Set of admissible solutions) *Let $V_\rho(A,B)$ be a set of points $C \in \rho$ such that the curve b_{ACB} is collision-free. Then, we say that $V_\rho(A,B)$ is a* set of admissible solutions *in the plane ρ with respect to A,B. If no confusion arises, we say the set of admissible solutions.*

By $V_\rho^v(A,B)$, we denote the set of points $C \in \rho$ such that $b_{ACB} \cap K = M$, where M is the set of contact points of order 2 between $b_{ACB}(t)$ and K. We denote the set of points $C \in \rho$ such that b_{ACB} and K have transversal intersection (i.e. directions of the intersecting curves at the intersection point are linearly independent) by $V_\rho^t(A,B)$. The set M contains at most two such points, since two componentwise different quadratic curves may have at most two common points of contact of order 2 (see e.g. Bézout theorem, [7]).

For the given points A,B, the union of disjoint sets $V_\rho(A,B) \cup V_\rho^v(A,B) \cup V_\rho^t(A,B)$ gives the whole plane ρ.

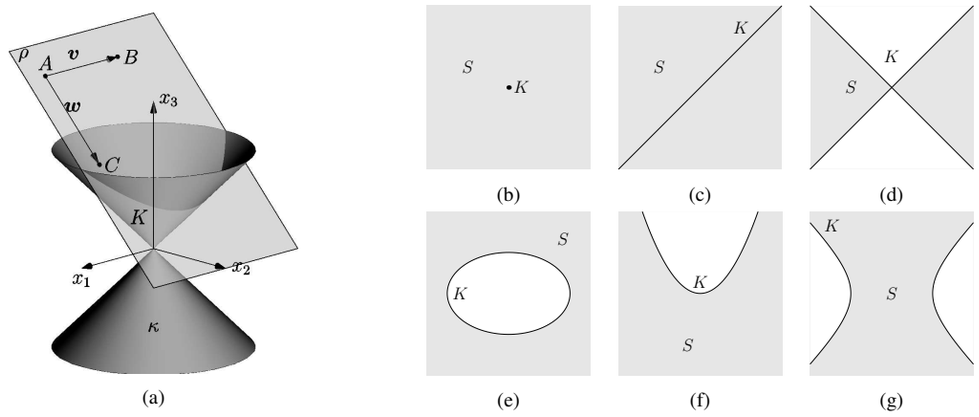

Figure 1: (a) *Plane* ρ *spans points* A,B,C. *In case of their non-collinearity, they generate* ρ *as affine hull. The conic section* K *is the intersection of the quadric* κ *and the plane* ρ.
(b–g) *Let* $K \subset \rho$ *be the conic section (point, double line, pair of lines, ellipse, parabola, hyperbola). The set* S *consists of all points lying out of quadric in the plane* ρ.

4 Exterior and interior points of contact

At first, we study the touching situation, that is the set $V_\rho^v(A,B)$.

Definition 3 (Set of points of contact) *We say that the set* $D \subset K$ *is the* set of points of contact *between* K *and the set of all* b_{ACB} *if for any point* $X_0 = [x_0, y_0] \in D$ *there is a point* C_0 *such that* $C_0 \in V_\rho^v(A,B)$ *and* $X_0 \in b_{AC_0B} \cap K$.

We say that b_{ACB} has *double contact*, if it has exactly two points of contact of order 2 with K (i.e. the set M contains exactly two points). We denote the middle control point of such Bézier curve by C_u. If K is a regular conic section, we denote the touching points by the letters $U_i, i = 1,2$ (see fig. 4). If K is a singular conic section, we denote the touching points by the symbol S_i, for $i = p,r$ (see fig. 5(b)).

When we obtain K as a connected component of a regular conic section, it may be an ellipse, a parabola or one component of a hyperbola. Since the connected component of regular conic section is convex, the tangent line is a supporting line of the component. In the case of singular conic section, the connected component may be a point (the top of the light-cone) or one isotropic line.

Let ℓ_T be a tangent line to a connected component K of conic section (regular or singular) at the point $T \in K$. It divides the plane ρ into two half-planes $\overline{H}_\ell^+, \overline{H}_\ell^-$ such that $K \subset \overline{H}_\ell^+$. We say, that ℓ_T *separates* the connected component K of the conic section and the arbitrary set of points O , if they lie in the different half-planes with respect to the tangent ℓ_T, i.e. $K \subset \overline{H}_\ell^+$ and $O \subset \overline{H}_\ell^-$. Additionally, in the case of hyperbola the asymptotes separate similarly K and O, but the corresponding touching point is infinite. We denote the set of all separating tangent lines and asymptotes by $T_{sep}(O,K)$. We denote by $S(O,K) \subset K$ the maximal open set of all *affine* points of contact of K and separating tangent lines.

Definition 4 (Exterior (interior) point of contact) *We say that the curve* b_{ACB} touches *a connected component of the regular conic section* K *from* outside (inside)*, if their common tangent is (is not) separating. Then, the point of contact is called* exterior (interior) point of contact*. The set of all exterior (interior) points of contact is denoted* D_{ext} (D_{in}).

The set of points of contact $D = D_{ext} \cup D_{in}$. Now, we describe the set of points of contact D for every type of conic section. First, we consider the regular conic sections, then we analyze the singular conic sections.

The polar line of the point A determined by the equation $AQ_KX^\top = 0$ splits the conic section K to some arcs. Let K be a regular conic section different from hyperbola. The condition that the point A is separated from K with respect to ℓ_T is that the point $T \in \{X \in K\colon AQ_KX^\top \geq 0\}$. So, the open set $S(A,K) = \{X \in K\colon AQ_KX^\top > 0\}$ (see fig. 2(a)). Now, let K_1, K_2 be the connected components of a hyperbola K. We consider each of them separately and we get $S(A,K_1) = \{X \in K_1\colon AQ_KX^\top > 0\}$ and $S(A,K_2)$ (see also fig. 2(b)).

Let K be a connected component of a regular conic section. Let $\ell_T \in T_K$ and the point $T \in K$ be its point of contact. The tangent line $\ell_T \in T_{sep}(AB,K)$ if and only if $T \in \overline{S}(A,K) \cap \overline{S}(B,K) = \{X \in K\colon AQ_KX^\top \geq 0 \wedge BQ_KX^\top \geq 0\}$ (see fig. 2(a)).

We denote the set of all $X \in K$ such that the corresponding tangent line ℓ_X to K at X contains both control points A,B by D_{AB}. The set $D_{AB} = \{X \in K\colon AQ_KX^\top = 0 \wedge BQ_KX^\top = 0\}$.

(a) (b)

Figure 2: (a) *The set of all tangent lines of K, which separate the point A and K, is determined by arc* $\overset{\frown}{T_1T_2^+} = S(A,K)$.
Similarly, the arc $\overset{\frown}{T_1^+T_2} = S(B,K)$. *The arc* $\overset{\frown}{T_1T_2}$ *determines all tangent lines* $T_{sep}(AB,K)$. *We obtain it as intersecion of the sets* $\overline{S}(A,K) \cap \overline{S}(B,K)$.
(b) *We have the set* $S(A,K_1) = \{X \in K_1 : AQ_KX^\top > 0\} = \overset{\frown}{Ta_2^\infty}$. *All tangent lines of connected component* K_2 *separate this component and the point A. Hence, we have the set* $S(A,K_2) = K_2$.

Theorem 2 (Set of exterior points of contact) *Let K be a regular connected component of conic section. The set of exterior points of contact* $D_{ext} \neq \emptyset$ *if and only if the segment* $AB \cap K = \emptyset$ *or* $AB \cap K = \{T\}$.
The set $D_{ext} = \{X \in K : AQ_KX^\top > 0 \wedge BQ_KX^\top > 0\} \cup D_{AB}$.

Proof. Sufficient condition. Let $AB \cap K = \{X_1, X_2\}$. Let ℓ be any tangent line to K. In order that the line ℓ separates AB and K (up to the point of contact if it exists), they must lie in the different half-planes with respect to ℓ (up to the point of contact). But the points $X_1, X_2 \in K$ lie in the same half-plane as AB. Hence, $\overline{S}(A,K) \cap \overline{S}(B,K) = \emptyset$ and there is no separating tangent line $\ell_T \in T_{sep}(AB,K)$. So, there exists no separating tangent line for any Bézier curve b_{ACB}. Consequently, the set $D_{ext} = \emptyset$.
Necessary condition. We discuss each case separately. Mainly, we use the fact that the quadratic Bézier curve is a convex curve, each of its tangent line defines a supporting half-plane to the curve. If $\ell_T \in T_{sep}(A,K)$ and $\ell_T \in T_{sep}(B,K)$, then $\ell_T \in T_{sep}(b_{ACB},K)$. So, for every $T \in \overline{S}(A,K) \cap \overline{S}(B,K)$ holds that $\ell_T \in T_{sep}(b_{ACB},K)$. At the end, we decide if endpoints T_1, T_2 of the intersection $\overline{S}(A,K) \cap \overline{S}(B,K)$ belong to the set D_{ext}. It is shown they do not in general. But if one of the triplets of points A,B,T_1 and A,B,T_2 is collinear, without loss of generality A,B,T_1, then the point $T_1 \in D_{AB}$. But $T_1 \in D_{ext}$ too, because the corresponding Bézier curve is a segment tangent to K. Hence, the set $D_{ext} = \{S(A,K) \cap S(B,K)\} \cup \{T_1\} \neq \emptyset$. □

Note, there might be two continuous arcs D_{ext}^1, D_{ext}^2, one on each connected component K_1, K_2 of the hyperbola K. Then, $D_{ext} = D_{ext}^1 \cup D_{ext}^2$.
The line $\overleftrightarrow{AB}$ divides the plane ρ into two half-planes, the open half-plane ρ_-, and the closed half-plane $\overline{\rho_+}$. Let us sort the tangent lines from A and B to K, that are not in $T_{sep}(AB,K)$, into pairs. If there are only two tangent lines not in $T_{sep}(AB,K)$, we denote them ℓ_1^+, ℓ_2^+ (see fig. 3(a)). If there are four tangent lines not in $T_{sep}(AB,K)$, we determine two pairs ℓ_1^+, ℓ_2^+ and ℓ_1^-, ℓ_2^- such that the corresponding points of contact $T_i^\pm = \ell_i^\pm \cap K, i = 1,2$ lie in the same half-plane $T_i^+ \in \overline{\rho_+}$ and $T_i^- \in \rho_-, i = 1,2$. If $\ell_1^+ \cap \ell_2^+ = P^+ \in \overline{\rho_+}$. We say the tangents ℓ_1^+, ℓ_2^+ *converge*. If $P^+ \in \rho_-$ or P^+ is a point at infinity, we say they *diverge* (see fig. 3(b)).

(a) (b)

Figure 3: (a) *There are only two tangent lines not in* $T_{sep}(AB,K)$. *The corresponding points of contact* $T_1^+, T_2^+ \in \overline{\rho_+}$, *so we denote the tangent lines* ℓ_1^+, ℓ_2^+. *They diverge, because their intersection lies in the half-plane* ρ_-.
(b) *If there are four tangent lines not in* $T_{sep}(AB,K)$, *we determine two pairs* ℓ_1^+, ℓ_2^+ *and* ℓ_1^-, ℓ_2^- *according to corresponding points of contact. The pair* ℓ_1^+, ℓ_2^+ *converge, because their intersection* $P^+ \in \overline{\rho_+}$. *However, the pair* ℓ_1^-, ℓ_2^- *diverge.*

Theorem 3 (Set of interior points of contact) *Let K be a regular connected conic section. The set of interior points of contact $D_{in}^{+} \neq \emptyset$ ($D_{in}^{-} \neq \emptyset$) iff the pair of tangents ℓ_1^{+}, ℓ_2^{+} (ℓ_1^{-}, ℓ_2^{-}) converges.*
Moreover, let $\ell_1, \ell_2 \notin T_{sep}(AB, K)$ be a pair of converging tangent lines and $P^{+} = \ell_1 \cap \ell_2 \in \rho_{+}$. If there exists a point $C_u \in \rho_{+}$ such that curve b_{AC_uB} has double contact (at the points U_1, U_2), then the set $D_{in}^{+} = \{X \in K \cap \rho_{+} : AQ_KX^{\top} < 0 \wedge BQ_KX^{\top} < 0\} \setminus \{\overset{\frown}{U_1U_2}\}$ (see fig. 4). Else, the set $D_{in}^{+} = \{X \in K \cap \rho_{+} : AQ_KX^{\top} < 0 \wedge BQ_KX^{\top} < 0\}$. A similar statement holds for a pair of tangent lines converging in the half-plane ρ_{-} and D_{in}^{-}.

Proof. Necessary condition of the existence $D_{in}^{+} \neq \emptyset$. Let the pair of tangent lines ℓ_1^{+}, ℓ_2^{+} converges in the half-plane ρ_{+}. We consider the parallel line v_a, resp. v_b containing the point A, resp. B, and have no common points with K in the half-plane ρ_{+}. Let the lines v_a, v_b determine the point at infinity v^{∞}. Let $C_m = \frac{1}{2}A + \frac{1}{2}B$ be. Let the line v_m be parallel to the lines v_a, v_b and $C_m \in v_m$. Let us construct the sequence $\{C_i\}_{i \in \mathbb{N}} \subset \rho_{+}$ such that $C_i \in v_m$ and $\lim_{i \to \infty} C_i = v^{\infty}$. There exists $n \in \mathbb{N}$ such that for each C_i, where $i > n$, the Bézier curve $b_{AC_iB} \cap K = \emptyset$. On the other hand, there exists $k \in \mathbb{N}$ such that for C_k the Bézier curve b_{AC_kB} intersects the conic section K. So there must exists some real $l \in (k, n)$ that for the Bézier curve $b_{AC_lB} \cap K \in D_{in}^{+}$. The proof for the set D_{in}^{-} can be done in a similar way.
Now, we indicate how to get the expression of the set D_{in}^{+}. Let us construct the curve $\Gamma(X) = \tau(A, B, X, \ell_X)$, where $X \in \{X \in K \cap \rho_{+} : AQ_KX^{\top} < 0 \wedge BQ_KX^{\top} < 0\} = \overset{\frown}{T_1T_2}$ and ℓ_X is the direction vector of the tangent line ℓ_X to the conic section K at the point X. The curve Γ is connected, because the continuous map τ maps the connected set $\overset{\frown}{T_1T_2}$ onto one connected curve. Let $s : (0,1) \to \overset{\frown}{T_1T_2}$ be any regular parameterization of the arc $\overset{\frown}{T_1T_2}$ such that for $s \to 0$ be $X \to T_1$ and for $s \to 1$ be $X \to T_2$. Then, we study a self-intersections of the curve $\Gamma(X)$. It can be proved the curve Γ has at most one self-intersection.
If Γ has one self-intersection $C_u = \Gamma(U_1)$, it means, there exists another point $U_2 \in \overset{\frown}{T_1T_2}$ that $C_u = \Gamma(U_2)$ and the Bézier curve b_{AC_uB} has double contact with K. There exist two special Bézier curves lying in $\overline{\rho_{+}}$, the curve $b_{AC_{2T}B}$ having two transversal intersections with K and the curve $b_{AC_{4T}B}$ having four transversal intersections with K. We construct the set of Bézier curves $L(w) = (1-w)b_{AC_{2T}B} + wb_{AC_{4T}B}$, where $w \in [0,1]$. According to the Hurwitz theorem (Th.(1,5) in [12]), there exists the point $C_3 \in \overline{\rho_{+}}$ that Bézier curve b_{AC_3B} has two transversal intersections and one common point of contact T_3 with the conic section K. The point $T_3 \in \overset{\frown}{T_1T_2}$ and then $C_3 \in \Gamma$ for some parameter $s_3, s_1 < s_3 < s_2$. Hence, the points of the arc $\overset{\frown}{U_1U_2}$ generate the Bézier curves with transversal intersections with K, because there is not other self-intersection of Γ except C_u. The set has the form $D_{in}^{+} = \{X \in K \cap \rho_{+} : AQ_KX^{\top} < 0 \wedge BQ_KX^{\top} < 0\} \setminus \{\overset{\frown}{U_1U_2}\}$. Note, that $U_1, U_2 \in D_{in}^{+}$.
If Γ does not have a self-intersection, for all the points $X \in \overset{\frown}{T_1T_2}$, the corresponding Bézier curves $b_{A\Gamma(X)B}$ have only one common point with K, the point of contact X. Hence, the set $D_{in}^{+} = \{X \in K \cap \rho_{+} : AQ_KX^{\top} < 0 \wedge BQ_KX^{\top} < 0\}$. □

5 Set of admissible points of contact

As we said, the set of all points of order 2 contact $D = D_{ext} \cup D_{in}$. The following theorem describes the set D for various regular types of the conic section K.

Theorem 4 (Set of points of contact)

(a) Let K be an ellipse. Then, the set of the points of contact D is either one arc of the exterior points of contact or one arc of exterior and one arc of interior points of contact or one or two arcs of interior points of contact.

(b) Let K be a parabola. Then, the set of the points of contact D is either one arc of the exterior points of contact or one arc of interior points of contact.

(c) Let K be a hyperbola. Then, the set of the points of contact D is either two arcs of the exterior points of contact or one arc of exterior and one arc of interior points of contact.

The arcs of the interior points of contact may have two affiliated components. The set of exterior points of contact may contains only one point T, when segment $AB \cap K = \{T\}$.

Proof. a) (Ellipse) Let $AB \cap K = \emptyset$. Then among all tangents passing through A or B to K, there are two in the set $T_{sep}(AB, K)$. They determine one arc D_{ext}. The other two tangents are not in the set $T_{sep}(AB, K)$. If they converge, then there is also one arc D_{in}. If they diverge, $D_{in} = \emptyset$. If $AB \cap K = \{T\}$, the only difference is that the separating pair of tangent lines becomes one line $\overleftrightarrow{AB}$ and $D_{ext} = \{T\}$. Let $AB \cap K = \{X_1, X_2\}$. Then, we consider two pairs of tangent lines ℓ_1^{+}, ℓ_2^{+} and ℓ_1^{-}, ℓ_2^{-}. One pair, without loss of generality the pair ℓ_1^{+}, ℓ_2^{+}, always converge so $D_{in}^{+} \neq \emptyset$. The pair ℓ_1^{-}, ℓ_2^{-} may converge or diverge, so we can obtain D as one or two arcs of D_{in}.
b) c) The proof for parabola and hyperbola is omitted, because it can be derived in a similar way. □

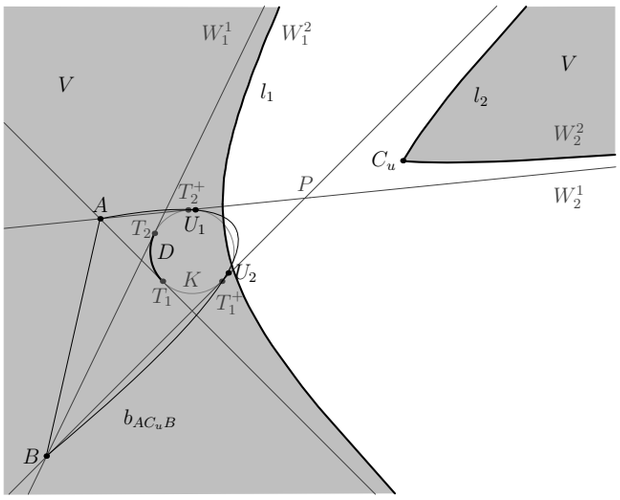

Figure 4: *The set* $D_{ext} = \{X \in K\colon AQ_KX^\top > 0 \wedge BQ_KX^\top > 0\} = \overset{\frown}{T_1T_2}$. *The set* $D_{in} \neq \emptyset$, *because the point* P *lies in the same half-plane generated by* $\overleftrightarrow{AB}$ *as the points* T_1^+, T_2^+. *The set* $D_{in} = \{X \in K\colon AQ_KX^\top < 0 \wedge BQ_KX^\top < 0\} \setminus \{\overset{\frown}{U_1U_2}\}$ *consists of two affiliated components* $T_2^+\overset{\frown}{U_1}U_2 \cup U_2\overset{\frown}{T_1^+} \cup \{U_1, U_2\}$. *The split of the arc is caused by the existence of the curve* b_{AC_uB}, *which has double contact with the conic section* K. *As one can see,* $b_{AC_uB} \cap K = \{U_1, U_2\}$. *Therefore, the set of points of contact* $D = D_{ext} \cup D_{in}$ *generates the curves* l_1, l_2 *such that* $l_1 \cup l_2 = \partial V_\rho(A,B)$. *Because the curve* l_1 *is generated by the exterior points of contact, the region* W_1^1 *containing the points* A, B *is subset* $W_1^1 \subset V_\rho(A,B)$. *The curve* l_2 *is generated by the interior points of contact. It bounds region* W_2^2 *not containing the points* A, B *and* $W_2^2 \subset V_\rho(A,B)$ *according to theorem 7 . The set of admissible solutions* $V_\rho(A,B) = W_1^1 \cup W_2^2$ *consists of two regions.*

Now, let K be a singular conic section. In the case of $K = \{V_Q\}$ (see fig. 1(b)), where V_Q is the top of the isotropic cone Q, we have $D = \{V_Q\}$ (see fig. 5(a)).
If $K = p$, where p is an isotropic double line (see fig. 1(c)), we must distinguish two cases. If A, B lie in the opposite half-planes generated by the line p, we have $D = \emptyset$. If A, B lie in the same half-plane, the set of points of contact $D = p$.
The last singular case is $K = p \cup r$, where p, r are a pair of distinct isotropic lines (see fig. 1(d)). Then, there are two regions of points lying out of K in the plane ρ. If A, B lie in the different regions, there is no collision-free Bézier curve b_{ACB}. Let A, B lie in the same region, which is determined by two half-lines $\overrightarrow{V_QP} \subset p$ and $\overrightarrow{V_QR} \subset r$ (see fig. 5(b)). Let $S_p \in p$ and $S_r \in r$ are the points of contact of the Bézier curve b_{AC_uB}, i.e. $b_{AC_uB} \cap K = \{S_p, S_r\}$ is double contact. Then $D = \overrightarrow{S_pP} \cup \overrightarrow{S_rR}$. The special case is $S_p = S_r = V_Q$.
In the tables 1 and 2, we see the structure of the set D for various types of conic sections. The numbers in the table 2 represent the number of connected arcs in the set D.

Table 1: *The set D for singular types of conic section K.*

	$\{V_Q\}$		p		$p \cup r$	
	D_{ext}	D_{in}	D_{ext}	D_{in}	D_{ext}	D_{in}
$AB \cap K = \emptyset \wedge \overleftrightarrow{AB} \cap K \neq \{T\}$	$\{V_Q\}$	$\emptyset$	p	$\emptyset$	$\overrightarrow{S_pP} \cup \overrightarrow{S_rR}$	$\emptyset$
$AB \cap K = \emptyset \wedge \overleftrightarrow{AB} \cap K = \{T\}$	$\{V_Q\}$	$\emptyset$	–	–	–	–
$AB \cap K = \{X_1, X_2\}$	–	–	–	–	–	–
$AB \cap K = \{T_0\}$	$\{V_Q\}$	$\emptyset$	–	–	–	–
$A = B$	$\{V_Q\}$	$\emptyset$	p	$\emptyset$	$\overrightarrow{V_QP} \cup \overrightarrow{V_QR}$	$\emptyset$

Table 2: *The set D for regular conic sections. The numbers indicate the number of connected arc components in the set D.*

	ellipse		parabola		hyperbola	
	D_{ext}	D_{in}	D_{ext}	D_{in}	D_{ext}	D_{in}
$AB \cap K = \emptyset \wedge \overleftrightarrow{AB} \cap K \neq \{T\}$	1	$\emptyset$,1	1	$\emptyset$	2	$\emptyset$
$AB \cap K = \emptyset \wedge \overleftrightarrow{AB} \cap K = \{T\}$	1	$\emptyset$	1	$\emptyset$	2	$\emptyset$
$AB \cap K = \{X_1, X_2\}$	$\emptyset$	1,2	$\emptyset$	1	1	1
$AB \cap K = \{T_0\}$	$\{T_0\}$	$\emptyset$,1	$\{T_0\}$	$\emptyset$	2	$\emptyset$
$A = B$	1	$\emptyset$	1	$\emptyset$	2	$\emptyset$

6 Boundary map

For the given points $A, B, X \in D \setminus D_{AB} \subseteq K$ and the tangent line ℓ_X at X to K, the Bézier curve b_{ACB} touching the conic section K is clearly identified. In order to find the middle control vertex C, we use the following map σ.

Definition 5 (Boundary map) *Let D be the set of points of contact for the given points A, B and K. The map $\sigma\colon D \setminus D_{AB} \to \rho$ is called* boundary map *if $\sigma(X) = C$ holds for some C from the definition 3 and $X \in D \setminus D_{AB}$ (see fig. 5(a)).*

It is not possible to define the map σ on the points in D_{AB}. If $T \in D_{AB} \subset K$ then the points A, B, T are collinear on the tangent line ℓ_T to K. Hence, there is an infinite number of points C such that the Bézier curve b_{ACB} touches K in T. All suitable C form a half-line, therefore we are interested in the end point of the half-line, the point C_S.

Theorem 5 *Let the conic section $K \neq \{V_Q\}$ and $X = [x_0, y_0] \in D \setminus D_{AB}$. Then, the corresponding boundary map $\sigma\colon D \setminus D_{AB} \to \rho$ has the form*

$$\sigma(X) = \frac{b(t_0) - B_0^2(t_0)A - B_2^2(t_0)B}{B_1^2(t_0)}, \tag{1}$$

where $t_0 \in [0,1]$ is a solution of the equation

$$0 = \alpha t^2 + 2\beta t + \gamma \tag{2}$$

and for $A = [a_x, a_y, 1]$, $B = [b_x, b_y, 1]$, $X = [x_0, y_0, 1]$ are

$$\alpha = (A-B)Q_K X^\top,$$
$$\beta = -AQ_K X^\top,$$
$$\gamma = -\beta.$$

Proof. Since we consider only affine points $C \in \rho$, let K be a conic section with the matrix Q_K. Since the point of contact $X \in b_{ACB}(t)$, there exists $t_0 \in [0,1]$ such that $X = b_{ACB}(t_0) = B_0^2(t_0)A + B_1^2(t_0)C + B_2^2(t_0)B$. For the point $X \in K$ the equality $XQ_K X^\top = 0$ holds. So, $X \notin \{A,B\}$ and $t_0 \notin \{0,1\}$. Because the point of contact $X = [x_0, y_0] \in D \setminus D_{AB}$, the equality $\left\langle \nabla f(x_0,y_0), \frac{d}{dt} b_{ACB}(t_0) \right\rangle = 0$ holds. The equation (2) has a real solution if the discriminant $\Delta = (AQ_K X^\top)(BQ_K X^\top) \geq 0$. It holds, because if $X \in D_{ext}$ then both brackets are positive. On the other hand, if $X \in D_{in}$ then both brackets are negative and their product is positive. From this quadratic equation, we obtain two roots t_1, t_2. The question is, if they are both within $\langle 0,1 \rangle$. We use the theorem 1. The table 3 shows the values of the sequences $\{f(t), f'(t), f''(t)\}$ in the end points of the interval $\langle 0,1 \rangle$ for $f(t) = \alpha t^2 + 2\beta t + \gamma$. From the previous, the expressions $AQ_K X^\top$ and $BQ_K X^\top$ have the same sign. Hence, the table 4 shows the number of sign changes of the sequences $\{f(t), f'(t), f''(t)\}$ with respect to the signs of $AQ_K X^\top$ and $BQ_K X^\top$. According to theorem 1 applied to the function $f(t)$, only one root is in $\langle 0,1 \rangle$. If both $t_1, t_2 \in (0,1)$ and $t_1 \neq t_2$ then $X \in D_{AB}$. Let $t_1 \in (0,1)$. Then, we substitute $t_0 = t_1$ into the Bézier curve equation and obtain the relevant point C from the definition 3 for the point of contact X. Hence, $C = \sigma(X)$. □

Table 3: *The values of derivatives of the function $f(t) = \alpha t^2 + 2\beta t + \gamma$ at the end points of the interval $\langle 0,1 \rangle$.*

	$t=0$	$t=1$
$f(t)$	$AQ_K X^\top$	$-BQ_K X^\top$
$f'(t)$	$-2AQ_K X^\top$	$-BQ_K X^\top$
$f''(t)$	$2(A-B)Q_K X^\top$	

Table 4: *If we look on the numbers of sign changes, the differences $2-1$ and $1-0$ are both equal to 1. So, the function $f(t)$ have one real solution within the interval $\langle 0,1 \rangle$.*

	$AQ_K X^\top > 0 \wedge BQ_K X^\top > 0$		$AQ_K X^\top < 0 \wedge BQ_K X^\top < 0$	
	$t=0$	$t=1$	$t=0$	$t=1$
$f(t)$	$+$	$-$	$-$	$+$
$f'(t)$	$-$	$-$	$+$	$+$
$f''(t)$	$\pm$	$\pm$	$\pm$	$\pm$
# of sign changes	2 1	1 0	1 2	0 1

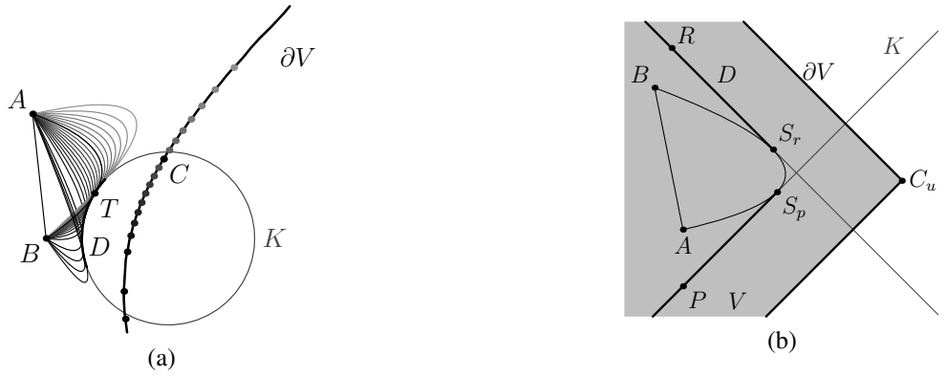

(a) (b)

Figure 5: (a) *The boundary map σ maps the points of the arc D to the points on ∂V, see that $\sigma(T) = C$.*
(b) *Let the conic section $K = p \cup r$. The points A, B have to lie in the same quadrant with respect to K. Let the quadrant be determined by two half-lines $\overrightarrow{V_Q P} \subset p$ and $\overrightarrow{V_Q R} \subset r$. If there exists a Bézier curve b_{AC_uB} with double contact $M = \{S_p, S_r\}$ with K, the set of exterior points of contact $D_{ext} = \overrightarrow{S_p P} \cup \overrightarrow{S_r R}$. Otherwise, we get $S_p = S_r = V_Q$ and $D_{ext} = \overrightarrow{V_Q P} \cup \overrightarrow{V_Q R}$. The set of interior points of contact is always $D_{in} = \emptyset$. The boundaries generated by the half-lines $\overrightarrow{S_p P}, \overrightarrow{S_r R}$ are connected due to the fact that $\sigma(S_p) = \sigma(S_r) = C_u$. Hence, the set of admissible solution $V_\rho(A,B)$ consist of one region. Because the boundary is generated by the exterior points of contact, $A, B \in V_\rho(A,B)$.*

For each $X \in D \setminus D_{AB}$, there exists exactly one point C such that the Bézier curve $b_{ACB}(t) \cap K = \{X\}$. How can we find the point C corresponding to a given point of contact $T \in D_{AB} \subset D$?

Lemma 2 *Let the points A,B and $T \in D_{AB} \subset K$ be collinear.*
(a) Let $AB \cap K = \{T\}$. The Bézier curve $b_{ACB} \cap K = \{T\}$ iff $C \in \overleftrightarrow{AB}$.
(b) Let $AB \cap K = \emptyset$. The Bézier curve $b_{ACB} \cap K = \{T\}$ if and only if $C \in \overrightarrow{C_S X} \subset \overleftrightarrow{AB}$, where $A,B \notin \overrightarrow{C_S X}$ and C_S is such that the derivative $\frac{d}{dt} b_{AC_SB}(t_0) = 0$ for $T = b_{AC_SB}(t_0)$. For the special case $A = B$, the point $C_S = A + 2(T - A)$.

In the equation (1) of the boundary map σ, the inequality $B_1^2(t_0) > 0$ holds for $t_0 \in (0,1)$, so the map σ is continuous. The σ maps the connected set $D_{ext} \setminus D_{AB}$ onto one connected curve l. If the point $T \in D_{AB} \neq \emptyset$, then $\lim_{X \to T} \sigma(X) = C_S$ and the union $l \cup \overrightarrow{C_S X}$ is a connected curve.

7 Set of admissible solutions

Theorem 6 (Boundary of the set $V_\rho(A,B)$) *The set of all such points C that for the Bézier curve $b_{ACB} \cap K \subset D$ yields, is the boundary of the set of admissible solutions $V_\rho(A,B)$. We denote it $\partial V_\rho(A,B)$.*

Proof. The point C belongs to the boundary of the set $V_\rho(A,B)$, if each neighborhood N of the point C contains both the point $C_1 \in V_\rho(A,B)$ and the point $C_2 \in \rho \setminus V_\rho(A,B)$. So, we prove the existence of points $C_1, C_2 \in N$ such that $b_{AC_1B} \cap K = \emptyset$ and $b_{AC_2B} \cap K = \{X_1, X_2\}$ with transversal intersection (see fig. 6).

Let A,B,u be given as in the lemma 1. Let C be such that $b_{ACB} \cap K \subset D$ and $T \in b_{ACB} \cap K$. Let the line ℓ_T with the direction vector u is the tangent line to K in T. Since $B_1^2(t_0) > 0$ for $t_0 \in (0,1)$, the map τ assigning to each point T its corresponding point C is continuous. It means, there exists a neighborhood M of the point T for each neighborhood N of the point C such that $\tau(M) \subset N$. For an arbitrary neighborhood N of the point C, the neighborhood M of the point T exists such that $\tau(M) \subset N$. Let $T_1 = T + k\nabla f(T)$ and $T_2 = T - k\nabla f(T)$, where $k > 0$ is such that $T_1, T_2 \in M$ and they satisfy the conditions of the lemma 1. Let the lines ℓ_1, ℓ_2 be parallel to the line ℓ_T (i.e. the vector u is their direction vector) and $T_1 \in \ell_1, T_2 \in \ell_2$. Then, the points $C_1 = \tau(A,B,T_1,u)$ and $C_2 = \tau(A,B,T_2,u)$ are $C_1, C_2 \in N$. We obtain the Bézier curves b_{AC_1B}, b_{AC_2B}. Since each tangent line ℓ_1, ℓ_2 defines the supporting half-plane to the convex quadratic Bézier curve and the points A,B lie out of K, it holds $b_{AC_1B} \cap K = \emptyset$ and $b_{AC_2B} \cap K = \{X_1, X_2\}$ with transversal intersection. □

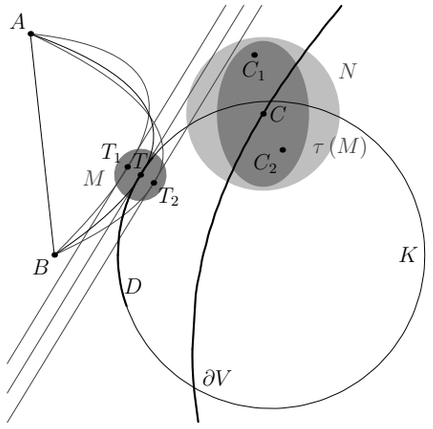

Figure 6: *Let C be such that $b_{ACB} \cap K \subset D$ and $T \in b_{ACB} \cap K$. For arbitrary neighborhood N of the point C, there exists a neighborhood M of the point T such that for $T_1, T_2 \in M$ the corresponding $C_1 = \tau(T_1), C_2 = \tau(T_2) \in N$. Moreover, $b_{AC_1B} \cap K = \emptyset$ and $b_{AC_2B} \cap K = \{X_1, X_2\}$ with transversal intersection. Hence, $C \in \partial V_\rho(A,B)$.*

We say that the boundary of the set of admissible solutions $\partial V_\rho(A,B)$ *is generated* by the set D mapped by the boundary map σ. The boundary of admissible solutions $\partial V_\rho(A,B)$ consists of one or two continuous unbounded curves. The degree of the curves is at most four in parameter t used in the map σ. It is clear from the expression for roots and the map σ in theorem 5.

If the conic section $K = p$, then the boundary of the set of admissible solutions ∂V is the parallel line with the line p. Let $K = p \cup r$. According to the table 1, the set of points of contact $D = \overrightarrow{S_p P} \cup \overrightarrow{S_r R}$ (in special case $S_p = S_r = V_Q$). The set ∂V consists from two half-lines parallel with p, resp. r, connected in the point C_u (see fig. 5(b)).

The region $V_\rho(A,B)$ is determined by its boundary. The boundary is parametrized piecewise using the map $\sigma\colon D \setminus D_{AB} \to \rho$. The next theorem determines, which parts of ρ with respect to the boundary belong to the region $V_\rho(A,B)$.

Theorem 7 (Set of admissible solutions)

(a) Let $K \neq \{V_Q\}$ be a connected component of the regular conic section. Let $l \subset \partial V_\rho(A,B)$ be a connected curve, which divides the plane into two regions W_1, W_2. If l is generated by D_{ext}, then $W_i \subseteq V_\rho(A,B)$ when $A,B \in W_i$. If l is generated by D_{ext} and $AB \subset l$, then $W_i \subseteq V_\rho(A,B)$ when $K \notin W_i$. If l is generated by D_{in}, then $W_i \subseteq V_\rho(A,B)$ when $A,B \notin W_i$.

(b) In the case of $K = \{V_Q\}$, both $W_1, W_2 \subset V_\rho(A,B)$. If $K = p$ or $K = p \cup r$, then $W_i \subseteq V_\rho(A,B)$ when $A,B \in W_i$.

Proof. (a) The intersection $AB \cap l \neq \emptyset$ iff $AB \cap K = \{T\}$. Then, the curve l is generated by exterior points of contact. The connected component K is a convex curve and the line $\overleftrightarrow{AB}$ determine the supporting half-plane to K. Hence, $W_i \subseteq V_\rho(A,B)$ if $K \notin W_i$.
If there exists only one curve $l = \partial V_\rho(A,B)$, we decide about W_i according to the point $C = \frac{1}{2}A + \frac{1}{2}B$.
Suppose that l_1 and l_2 exist such that $l_1 \cup l_2 = \partial V_\rho(A,B)$. According to the table 2, the conic section K is an ellipse. If both l_1, l_2 are generated by the sets of interior points of contact, in both cases we can decide about W_i according to the point $C = \frac{1}{2}A + \frac{1}{2}B$. The segment AB lies between the curves l_1, l_2 and the set $V_\rho(A,B)$ consists of two regions. Now, let the curve l_1 be generated by the set of exterior points of contact and the curve l_2 be generated by the set of interior points of contact (see fig. 4). The intersection $l_1 \cap l_2 = \emptyset$, because the Bézier curve with one exterior and one interior point of contact with K simultaneously does not exist. Let the curve l_1 divide the plane ρ into two components W_1, W_2 and $A, B \in W_1$. The curve $l_2 \subset W_2$, because for $C = \frac{1}{2}A + \frac{1}{2}B$ is $b_{ACB} \cap K = \emptyset$ and the set $W_1 \subset \partial V_\rho(A,B)$. Let the curve l_2 divide the region W_2 into two components W_3, W_4 and l_1 be the boundary between W_1, W_3. According to the theorem 6, the region W_3 consists of such points C that b_{ACB} and K have transversal intersections and the region $W_4 \subset \partial V_\rho(A,B)$. □

In the case of hyperbola, each component generates one set of admissible solutions. Hence, we obtain the regions $V_1(A,B), V_2(A,B)$ for the K_1, K_2. For every point $C \in V_1(A,B)$, the Bézier curve $b_{ACB} \cap K_1 = \emptyset$. We are looking for the set of points C, such that $b_{ACB} \cap (K_1 \cup K_2) = \emptyset$. It holds for every point $C \in V_1(A,B) \cap V_2(A,B)$, see fig. 7.

Finally, for the two given points A, B and the conic K, the set of acceptable solutions $V_\rho(A,B)$ consists of one or two regions, see the table 5. It depends on the number of arcs in the set D and on the type of the conic section K.

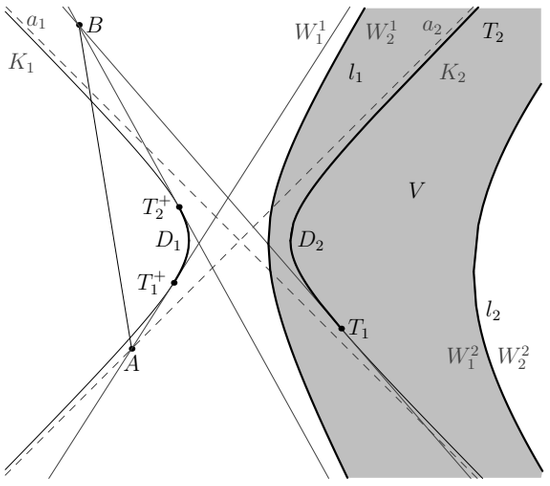

Figure 7: *For the component K_1, the set of exterior points of contact $D^1_{ext} = \emptyset$ and the set of interior points of contact $D^1_{in} = \overset{\frown}{T_1^+ T_2^+}$. The set of points of contact $D^1 = D^1_{in}$ generates the curve $l_1 \subset \partial V_\rho(A,B)$. The curve l_1 divides the plane ρ into two regions W_1^1, W_2^1. Let the points $A, B \in W_1^1$. According to the theorem 7, the set of admissible solutions for the component K_1 is $V^1(A,B) = W_2^1$.*
For the component K_2, since $T_2 = a_2^\infty$, the set of exterior points of contact $D^2_{ext} = \overset{\frown}{T_1 a_2^\infty}$ and the set of interior points of contact $D^2_{in} = \emptyset$. The set of points of contact $D^2 = D^2_{ext}$ generates the curve $l_2 \subset \partial V_\rho(A,B)$ and if the points $A, B \in W_1^2$, then $V^2(A,B) = W_1^2$.
Finally, the set of admissible solutions for the conic section K is $V_\rho(A,B) = V^1(A,B) \cap V^2(A,B)$.

Table 5: *The number of regions in the set of acceptable solutions $V_\rho(A,B)$.*

	$\{V_Q\}$	p	$p \cup r$	ellipse	parabola	hyperbola
$AB \cap K = \emptyset \wedge \overleftrightarrow{AB} \cap K \neq \{T\}$	2	1	1	1,2	1	1
$AB \cap K = \emptyset \wedge \overleftrightarrow{AB} \cap K = \{T\}$	1	–	–	1	1	1
$AB \cap K = \{X_1, X_2\}$	–	–	–	1,2	1	1
$AB \cap K = \{T_0\}$	2	–	–	1,2	1	1
$A = B$	1	1	1	1	1	1

8 Results and application

For the given regular quadric κ and the points A, B in three dimensional space, we described the set $V(A,B)$ of all such points C that the quadratic Bézier curve with control points A, C, B is collision-free path from the point A to the point B.

We solved the problem completely for each type of conic section K, which the plane ρ containing the points A, B cuts out in the regular quadric κ. The set $V_\rho(A,B)$ containing the admissible points $C \in \rho$ is described via the method of contact point. We proved, that the boundary of this set $\partial V_\rho(A,B)$ is determined by such points C that b_{ACB} touches the conic section K. Hence, we found the set of admissible points of contact D for the given points A, B as union of exterior and interior points of contact. Then, we showed how the set D determines the boundary $\partial V_\rho(A,B)$ using the boundary map σ.

We apply this study in the following example. Let the virtual agent starts at the point S_1 and needs to get to the point S_3 while passing through the point S_2. Moreover, he must avoid the house and two corn fields. First, we need to replace the obstacles with appropriate bounding objects. Conic sections as bounding objects well represent a wide range of obstacles. For example, ellipses are suitable for buildings, trees and things and hyperbolas and parabolas for coast or areas with special features. For our purpose, we choose an ellipse for house and a hyperbola for corn fields. The collision-free path is sought gradually. At first, we find the set V_e consisting of such points C that the Bézier curve $b_{S_1CS_2}$ is collision-free path between S_1, S_2 due to ellipse. Then, we find the set V_h consisting of such points C that the Bézier curve $b_{S_1CS_2}$ is collision-free path between S_1, S_2 due to hyperbola. Since we need to avoid both obstacles simultaneously, it is necessary to choose the final point $C_1 \in V_e \cap V_h$. The collision-free path between the points S_2, S_3 is found similarly as shown in fig. 8.

As can be seen in fig. 8, the points C_1, C_2 are chosen so that the spline is G^1-continuous. This choice may not be possible always. It depends on the existence of the segment C_1C_2 such that $S_2 \in C_1C_2$. All possible slopes of the segment C_1S_2 are determined by the tangent lines from the point S_2 to the set $V_e \cap V_h$. Possible slopes of the segment S_2C_2 are determined similarly. The necessary and sufficient condition for G^1-continuity of the spline is the existence of the same allowed slope for both segments.

9 Future work and conclusion

In the future, we look for the collision-free condition for Bézier curves of higher degree. They provide more natural-looking path and they are more flexible while avoiding obstacles including non-planar curves. We start to study conditions for cubic curves, using the knowledge and methods from the quadratic case. A possible application which is a matter of further work is the construction of collision-free splines with requirements for G^n continuity, for some $n \geq 2$.

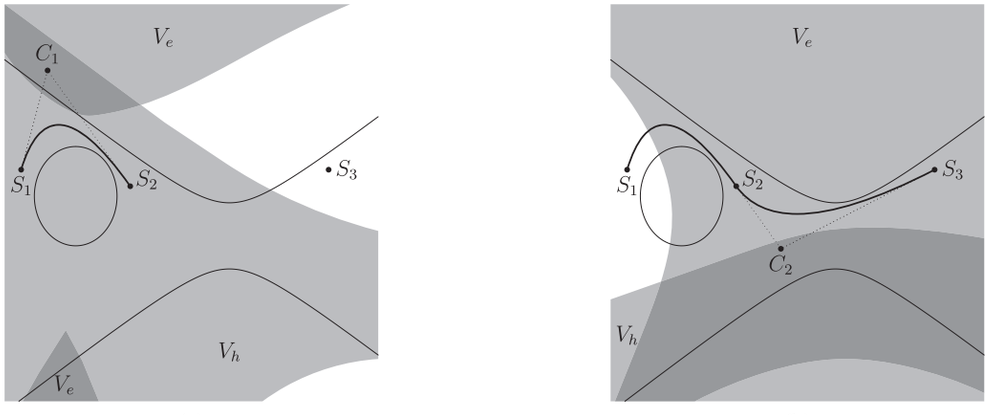

(a) (b)

Figure 8: (a) *At first, we search the collision-free path between the points S_1, S_2. After finding the sets of admissible solutions V_e, V_h for each obstacle separately, we choose the point $C_1 \in V_e \cap V_h$.*
(b) *Then, we find the sets V_e, V_h for the points S_2, S_3 and choose the point $C_2 \in V_e \cap V_h$. We choose it so that the final spline is G^1-continuous. This approach might help in some cases of narrow passages when the obstacles are wrapped with appropriate quadrics.*

Acknowledgement

The authors were supported by grant VEGA 1/0330/13. The authors would like to thank to the anonymous reviewers for helpful comments.

References

[1] M. BERGER, *Geometry I*, Universitext, Springer-Verlag, Berlin, 1987.

[2] M. BERGER, *Geometry II*, Universitext, Springer-Verlag, Berlin, 1987.

[3] P. CHALMOVIANSKÝ, B. POKORNÁ, Quadratic space-like Bézier curves in the three dimensional Minkowski space, *Proceedings of Symposium on Computer Geometry* **20** (2011), 104–110, `http://sccg.sk/~pokorna/publications.html`

[4] G. FARIN, J. HOSCHEK, M-S. KIM (eds.), *Handbook of computer aided geometric design*, North-Holland, Amsterdam, 2002.

[5] R. GERAERTS, M. OVERMARS, Creating high-quality paths for motion planning, *The International Journal of Robotics Research* **26**(8) (2007), 845–863.

[6] J. HOSCHEK, D. LASSER, *Fundamentals of computer aided geometric design*, A K Peters Ltd., Wellesley, MA, 1993.

[7] E. KUNZ, *Introduction to plane algebraic curves*, Birkhäuser Boston Inc., Boston, MA, 2005.

[8] W. KÜHNEL, *Differential Geometry: Curves - Surfaces - Manifolds*, American Mathematical Society, 2nd edition, 2006.

[9] Y. KWANGJIN, D. JUNG, S. SUKKARIEH, Continuous curvature pathsmoothing algorithm using cubic Bezier spiral curves for non-holonomic robots, *Advanced Robotics* **27**(4) (2013), 247–258.

[10] Y. KWANGJIN, S. SUKKARIEH, An analytical continuous-curvature path-smoothing algorithm, *IEEE Transactions on Robotics* **26**(3) (2010), 561–568.

[11] Y. KWANGJIN, S. SUKKARIEH, 3D smooth path planning for a UAV in cluttered natural environments, *Proceedings of IEEE/RSJ International Conference on Intelligent Robots and Systems*, 2008, 794–800.

[12] M. MARDEN, *Geometry of polynomials*, Second edition. Mathematical Surveys, No. 3, American Mathematical Society, Providence, R. I., 1966.

[13] B. POKORNÁ, Quadratic space-like Bézier curves in three dimensional Minkowski space, Project of Dissertation Thesis, 2012, `http://sccg.sk/~pokorna/publications.html`

Barbora Pokorná
e-mail: barbora.pokorna@fmph.uniba.sk

Pavel Chalmovianský
e-mail: pavel.chalmoviansky@fmph.uniba.sk

Faculty of Mathematics, Physics and Informatics
Mlynska dolina
84248 Bratislava
Slovak Republic

Original scientific paper
Accepted 11. 5. 2015.

ZEYNEP CAN
ÖZCAN GELIŞGEN
RÜSTEM KAYA

On the Metrics Induced by Icosidodecahedron and Rhombic Triacontahedron

On the Metrics Induced by Icosidodecahedron and Rhombic Triacontahedron

ABSTRACT

The theory of convex sets is a vibrant and classical field of modern mathematics with rich applications. If every points of a line segment that connects any two points of the set are in the set, then it is convex. The more geometric aspects of convex sets are developed introducing some notions, but primarily polyhedra. A polyhedra, when it is convex, is an extremely important special solid in $\mathbb{R}^n$. Some examples of convex subsets of Euclidean 3-dimensional space are Platonic Solids, Archimedean Solids and Archimedean Duals or Catalan Solids. In this study, we give two new metrics to be their spheres an archimedean solid icosidodecahedron and its archimedean dual rhombic triacontahedron.

Key words: Archimedean solids, Catalan solids, metric, Chinese Checkers metric, Icosidodecahedron, Rhombic triacontahedron

MSC2010: 51K05, 51K99, 51M20

O metrici induciranoj ikosadodekaedrom i trijakontaedrom

SAŽETAK

Teorija konveksnih skupova je vitalno i klasično područje moderne matematike s bogatom primjenom. Ako se sve točke dužine, koja spaja bilo koje dvije točke skupa, nalaze u tom skupu, tada je taj skup konveksan. Sve se više geometrijskih aspekata o konveksnim skupovima razvija uvodeći neke pojmove, ponajprije poliedre. Konveksni poliedar je iznimno važno posebno tijelo u $\mathbb{R}^n$. Neki primjeri konveksnih podskupova euklidskog trodimenzionalnog prostora su Platonova tijela, Arhimedova tijela, tijela dualna Arhimedovim tijelima i Catalanova tijela. U ovom članku prikazujemo dvije metrike koje su sfere Arhimedovom tijelu ikosadodekaedru i njemu dualnom tijelu, trijakontaedru.

Ključne riječi: Arhimedova tijela, Catalanova tijela, metrika kineskog šaha, ikosadodekaedar, trijakontaedar

1 Introduction

Some mathematicians studied on metrics and improved metric geometry (some of these are [2], [3], [6], [7], [8], [9]). Let $P_1 = (x_1, y_1, z_1)$ and $P_2 = (x_2, y_2, z_2)$ be two points in $\mathbb{R}^3$. The maximum metric $d_M : \mathbb{R}^3 \times \mathbb{R}^3 \to [0, \infty)$ is defined by

$$d_M(P_1, P_2) = \max\{|x_1 - x_2|, |y_1 - y_2|, |z_1 - z_2|\}.$$

Taxicab metric $d_T : \mathbb{R}^3 \times \mathbb{R}^3 \to [0, \infty)$ is defined by

$$d_T(P_1, P_2) = |x_1 - x_2| + |y_1 - y_2| + |z_1 - z_2|.$$

Then E. Krause asked the question of how to develop a metric which would be similar to movement made by playing Chinese Checkers [11]. An answer was given by G. Chen for plane [1]. In [5], Ö. Gelişgen, R. Kaya and M. Özcan extended Chinese-Checkers metric to $3-$dimensional space. The $CC-$metric $d_{CC} : \mathbb{R}^3 \times \mathbb{R}^3 \to [0, \infty)$ is defined by

$$d_{CC}(P_1, P_2) = d_L(P_1, P_2) + (\sqrt{2} - 1) d_S(P_1, P_2)$$

where $d_L(P_1, P_2) = \max\{|x_1 - x_2|, |y_1 - y_2|, |z_1 - z_2|\}$ and $d_S(P_1, P_2) = \min\{|x_1 - x_2| + |y_1 - y_2|, |x_1 - x_2| + |z_1 - z_2|, |y_1 - y_2| + |z_1 - z_2|\}$.
Each of geometries induced by these metrics is a Minkowski geometry. Minkowski geometry is a non-euclidean geometry in a finite number of dimensions that is different from elliptic and hyperbolic geometry (and from the Minkowskian geometry of space-time). In a Minkowski geometry, the linear structure is just like the

Euclidean one but distance is not uniform in all directions. That is, the points, lines and planes are the same, and the angles are measured in the same way, but the distance function is different. Instead of the usual sphere in Euclidean space, the unit ball is a certain symmetric closed convex set [13].

A polyhedron is a solid in three dimensions with flat faces, straight edges and vertices. A regular polyhedron is a polyhedron with congruent faces and identical vertices. There are only five regular convex polyhedra which are called platonic solids. Archimedes discovered the semiregular convex solids. However, several centuries passed before their rediscovery by the renaissance mathematicians. Finally, Kepler completed the work in 1620 by introducing prisms and antiprisms as well as four regular nonconvex polyhedra, now known as the Kepler–Poinsot polyhedra. Construction of the dual solids of the Archimedean solids was completed in 1865 by Catalan nearly two centuries after Kepler (see [10]). A convex polyhedron is said to be semiregular if its faces have a similar configuration of nonintersecting regular plane convex polygons of two or more different types about each vertex. These solids are commonly called the Archimedean solids. The duals are known as the Catalan solids. The Catalan solids are all convex. They are face-transitive when all its faces are the same but not vertex-transitive. Unlike Platonic solids and Archimedean solids, the face of Catalan solids are not regular polygons.

According to studies of mentioned researches unit spheres of Minkowski geometries which are furnished by these metrics are associated with convex solids. For example, unit spheres of maximum space and taxicab space are cubes and octahedrons, respectively, which are Platonic Solids [4], [6]. And unit sphere of CC-space is a deltoidal icositetrahedron which is a Catalan solid [5]. Therefore, there are some metrics in which unit spheres of space furnished by them are convex polyhedra. That is, convex polyhedra are associated with some metrics. When a metric is given we can find its unit sphere. On the contrary a question can be asked; "Is it possible to find the metric when a convex polyhedron is given?". In this study we find the metrics of which unit spheres are an icosidodecahedron, one of the Archimedean Solids and a rhombic triacontahedron which is Archimedean dual (a catalan solid) of icosidodecahedron.

2 Icosidodecahedron Metric

One type of convex polyhedrons is the Archimedean solids. The fifth book of the "Synagoge" or "Collection" of the Greek mathematician Pappus of Alexandria, who lived in the beginning of the fourth century AD, gives the first known mention of the thirteen "Archimedean solids". Although, Archimedes makes no mention of these solids in any of his extant works, Pappus lists this solids and attributes to Archimedes in his book [16].

An Archimedean solid is a symmetric, semiregular convex polyhedron composed of two or more types of regular polygons meeting in identical vertices. A polyhedron is called semiregular if its faces are all regular polygons and its corners are alike. And, identical vertices are usually means that for two taken vertices there must be an isometry of the entire solid that transforms one vertex to the other.

One of the Archimedean solids is the icosidodecahedron. An icosidodecahedron is a polyhedron which has 32 faces, 60 edges and 30 vertices. Twelve of its faces are regular pentagons and twenty of them are equilateral triangles [14].

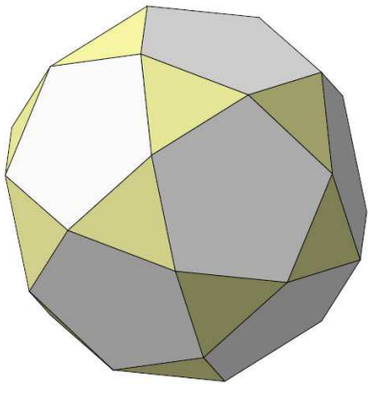

(a)

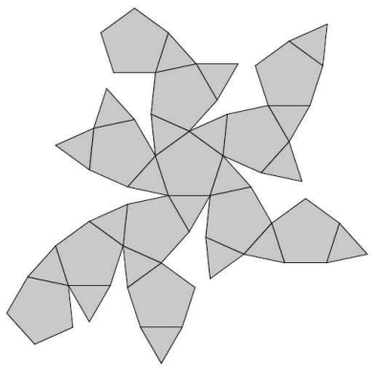

(b)

Figure 1: (a) *Icosidodecahedron*, (b) *Net of icosidodecahedron*

To find the metrics of which unit spheres are convex polyhedrons, firstly, the related polyhedra are placed in the 3-dimensional space in such a way that they are symmetric with respect to the origin. And then the coordinates of vertices are found. Later one can obtain metric which always supply plane equation related with solid's surface. Therefore we describe the metric which unit sphere is an icosidodecahedron as following:

Definition 1 *Let $P_1 = (x_1, y_1, z_1)$ and $P_2 = (x_2, y_2, z_2)$ be two points in $\mathbb{R}^3$.*
The distance function $d_{ID} : \mathbb{R}^3 \times \mathbb{R}^3 \to [0, \infty)$ icosidodecahedron distance between P_1 and P_2 is defined by

$$d_{ID}(P_1, P_2) = \max \left\{ \begin{array}{l} u + (\varphi - 1)\max\{v, (\varphi-1)w, (1-\varphi)u + v + w\}, \\ v + (\varphi - 1)\max\{w, (\varphi-1)u, u + (1-\varphi)v + w\}, \\ w + (\varphi - 1)\max\{u, (\varphi-1)v, u + v + (1-\varphi)w\} \end{array} \right\}$$

where $u = |x_1 - x_2|$, $v = |y_1 - y_2|$, $w = |z_1 - z_2|$ and $\varphi = \frac{1+\sqrt{5}}{2}$ the golden ratio.

According to icosidodecahedron distance, there are three different paths from P_1 to P_2. These paths are
i) union of two line segments which one is parallel to a coordinate axis and other line segment makes $\arctan(\frac{\sqrt{5}}{2})$ angle with another coordinate axis.
ii) union of two line segments which one is parallel to a coordinate axis and other line segment makes $\arctan(\frac{1}{2})$ angle with another coordinate axis.
iii) union of three line segments each of which is parallel to a coordinate axis.

Thus icosidodecahedron distance between P_1 and P_2 is the sum of Euclidean lengths of these two line segments or $\frac{\sqrt{5}-1}{2}$ times the sum of Euclidean lengths of these three line segments.
Figure 2 illustrates icosidodecahedron way from P_1 to P_2 if maximum value is $|x_1 - x_2| + (\frac{\sqrt{5}-1}{2})|y_1 - y_2|$, $|x_1 - x_2| + (\frac{\sqrt{5}-1}{2})^2|z_1 - z_2|$ or $(\frac{\sqrt{5}-1}{2})(|x_1 - x_2| + |y_1 - y_2| + |z_1 - z_2|)$.

Lemma 1 *Let $P_1 = (x_1, y_1, z_1)$ and $P_2 = (x_2, y_2, z_2)$ be distinct two points in $\mathbb{R}^3$. u, v, w denote $|x_1 - x_2|$, $|y_1 - y_2|$, $|z_1 - z_2|$, respectively. Then*

$$d_{ID}(P_1, P_2) \geq u + (\varphi-1)\max\{v, (\varphi-1)w, (1-\varphi)u + v + w\},$$
$$d_{ID}(P_1, P_2) \geq v + (\varphi-1)\max\{w, (\varphi-1)u, u + (1-\varphi)v + w\},$$
$$d_{ID}(P_1, P_2) \geq w + (\varphi-1)\max\{u, (\varphi-1)v, u + v + (1-\varphi)w\}.$$

Proof. Proof is trivial by the definition of maximum function. □

Theorem 1 *The distance function d_{ID} is a metric. Also according to d_{ID}, the unit sphere is an icosidodecahedron in $\mathbb{R}^3$.*

Proof. Let $d_{ID} : \mathbb{R}^3 \times \mathbb{R}^3 \to [0, \infty)$ be the icosidodecahedron distance function and $P_1 = (x_1, y_1, z_1)$, $P_2 = (x_2, y_2, z_2)$ and $P_3 = (x_3, y_3, z_3)$ are distinct three points in $\mathbb{R}^3$. u, v, w denote $|x_1 - x_2|$, $|y_1 - y_2|$, $|z_1 - z_2|$, respectively. To show that d_{ID} is a metric in $\mathbb{R}^3$, the following axioms hold true for all P_1, P_2 and $P_3 \in \mathbb{R}^3$.

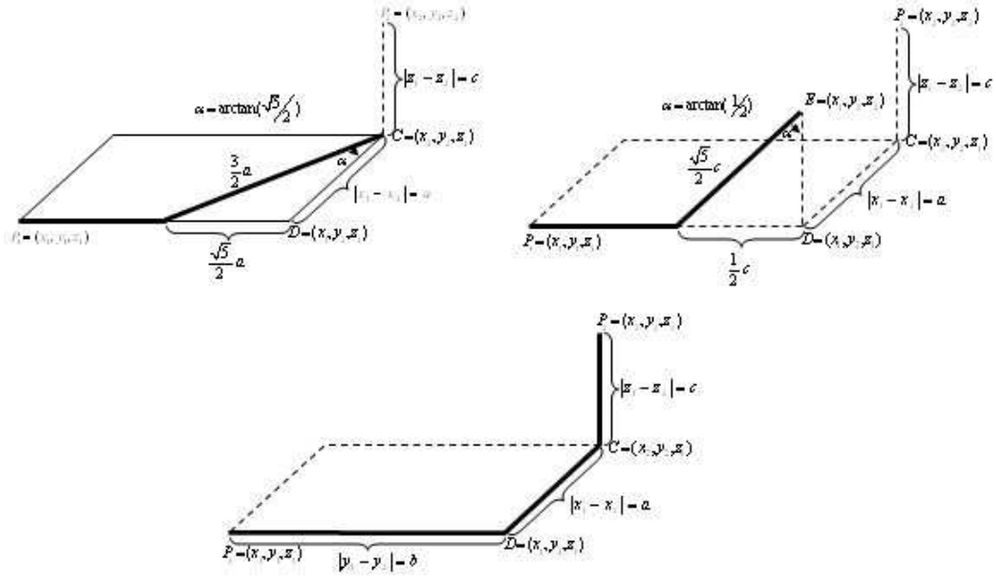

Figure 2: *ID way from P_1 to P_2*

M1) $d_{ID}(P_1,P_2) \geq 0$ and $d_{ID}(P_1,P_2) = 0$ iff $P_1 = P_2$
M2) $d_{ID}(P_1,P_2) = d_{ID}(P_2,P_1)$
M3) $d_{ID}(P_1,P_3) \leq d_{ID}(P_1,P_2) + d_{ID}(P_2,P_3)$.
Since absolute values is always nonnegative value $d_{ID}(P_1,P_2) \geq 0$. If $d_{ID}(P_1,P_2) = 0$ then there are possible three cases. These cases are
Case I:
$d_{ID}(P_1,P_2) = u+(\varphi-1)\max\{v,(\varphi-1)w,(1-\varphi)u+v+w\}$
Case II:
$d_{ID}(P_1,P_2) = v+(\varphi-1)\max\{w,(\varphi-1)u,u+(1-\varphi)v+w\}$
Case III:
$d_{ID}(P_1,P_2) = w+(\varphi-1)\max\{u,(\varphi-1)v,u+v+(1-\varphi)w\}$.

Case I: If $d_{ID}(P_1,P_2) = u+(\varphi-1)\max\{v,(\varphi-1)w,(1-\varphi)u+v+w\}$, then

$$\begin{aligned}
&u+(\varphi-1)\max\{v,(\varphi-1)w,(1-\varphi)u+v+w\}=0\\
&\Leftrightarrow u=0 \text{ and } (\varphi-1)\max\{v,(\varphi-1)w,(1-\varphi)u+v+w\}=0\\
&\Leftrightarrow x_1=x_2,\ y_1=y_2,\ z_1=z_2\\
&\Leftrightarrow (x_1,y_1,z_1)=(x_2,y_2,z_2)\\
&\Leftrightarrow P_1=P_2
\end{aligned}$$

The other cases can be shown by similar way in Case I. Thus we get $d_{ID}(P_1,P_2) = 0$ iff $P_1 = P_2$.
Since $|x_1-x_2| = |x_2-x_1|$, $|y_1-y_2| = |y_2-y_1|$ and $|z_1-z_2| = |z_2-z_1|$, obviously $d_{ID}(P_1,P_2) = d_{ID}(P_2,P_1)$. That is, d_{ID} is symmetric.
Let $P_1 = (x_1,y_1,z_1)$, $P_2 = (x_2,y_2,z_2)$ and $P_3 = (x_3,y_3,z_3)$ are distinct three points in $\mathbb{R}^3$. u_1, v_1, w_1, u_2, v_2, w_2 denote $|x_1-x_3|$, $|y_1-y_3|$, $|z_1-z_3|$, $|x_2-x_3|$, $|y_2-y_3|$, $|z_2-z_3|$, respectively.
Then by using the property $|a-b+b-c| \leq |a-b| + |b-c|$ we get

$$\begin{aligned}
&d_{ID}(P_1,P_3)\\
&=\max\left\{\begin{array}{l} u_1+(\varphi-1)\max\{v_1,\ (\varphi-1)w_1,(1-\varphi)u_1+v_1+w_1\},\\ v_1+(\varphi-1)\max\{w_1,\ (\varphi-1)u_1,u_1+(1-\varphi)v_1+w_1\},\\ w_1+(\varphi-1)\max\{u_1,\ (\varphi-1)v_1,u_1+v_1+(1-\varphi)w_1\}\end{array}\right\}\\
&\leq\max\left\{\begin{array}{l} u_1+u_2+(\varphi-1)\max\left\{\begin{array}{l} v_1+v_2,\ (\varphi-1)(w_1+w_2),\\ (1-\varphi)(u_1+u_2)\\ +v_1+v_2+w_1+w_2\end{array}\right\},\\ v_1+v_2+(\varphi-1)\max\left\{\begin{array}{l} w_1+w_2,\ (\varphi-1)(u_1+u_2),\\ u_1+u_2+(1-\varphi)(v_1+v_2)\\ +w_1+w_2\end{array}\right\},\\ w_1+w_2+(\varphi-1)\max\left\{\begin{array}{l} u_1+u_2,\ (\varphi-1)(v_1+v_2),\\ u_1+u_2+v_1+v_2\\ +(1-\varphi)(w_1+w_2)\end{array}\right\}\end{array}\right\}\\
&=I.
\end{aligned}$$

Therefore one can easily find that $I \leq d_{ID}(P_1,P_2) + d_{ID}(P_2,P_3)$ from Lemma 1. So, $d_{ID}(P_1,P_3) \leq d_{ID}(P_1,P_2) + d_{ID}(P_2,P_3)$. Consequently, icosidodecahedron distance is a metric in 3-dimensional analytical space.
Finally, the set of all points $X = (x,y,z) \in \mathbb{R}^3$ that icosidodecahedron distance is 1 from $O = (0,0,0)$ is

$$S_{ID} = \left\{(x,y,z): \max\left\{\begin{array}{l} |x|+(\varphi\text{-}1)\max\left\{\begin{array}{l}|y|,(\varphi\text{-}1)|z|,\\ (1\text{-}\varphi)|x|+|y|+|z|\end{array}\right\},\\ |y|+(\varphi\text{-}1)\max\left\{\begin{array}{l}|z|,(\varphi\text{-}1)|x|,\\ |x|+(1\text{-}\varphi)|y|+|z|\end{array}\right\},\\ |z|+(\varphi\text{-}1)\max\left\{\begin{array}{l}|x|,(\varphi\text{-}1)|y|,\\ |x|+|y|+(1\text{-}\varphi)|z|\end{array}\right\}\end{array}\right\}=1\right\}.$$

Thus the graph of S_{ID} is as in Figure 3. □

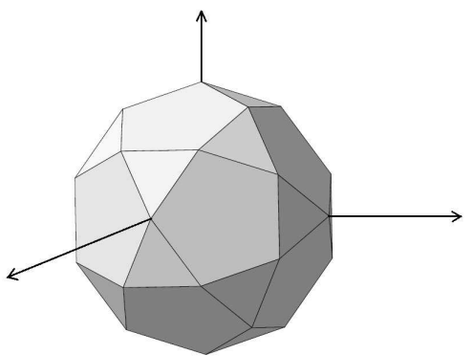

Figure 3: *Icosidodecahedron*

Corollary 1 *The equation of the icosidodecahedron with center* (x_0,y_0,z_0) *and radius r is*

$$\max\left\{\begin{array}{l} |x-x_0|+(\varphi-1)\max\left\{\begin{array}{l}|y-y_0|,(\varphi-1)|z-z_0|,\\ (1-\varphi)|x-x_0|\\ +|y-y_0|+|z-z_0|\end{array}\right\},\\ |y-y_0|+(\varphi-1)\max\left\{\begin{array}{l}|z-z_0|,(\varphi-1)|x-x_0|,\\ (1-\varphi)|y-y_0|\\ +|x-x_0|+|z-z_0|\end{array}\right\},\\ |z-z_0|+(\varphi-1)\max\left\{\begin{array}{l}|x-x_0|,(\varphi-1)|y-y_0|,\\ (1-\varphi)|z-z_0|\\ +|x-x_0|+|y-y_0|\end{array}\right\}\end{array}\right\} = r$$

which is a polyhedron which has 32 faces with vertices; such that all permutations of the three axis components and all posible +/- sign changes of each axis component of $(0,0,r)$, *and* $(\frac{\varphi-1}{2}r,\frac{1}{2}r,\frac{\varphi}{2}r)$, *where* $\varphi = \frac{1+\sqrt{5}}{2}$ *the golden ratio.*

Lemma 2 *Let l be the line through the points* $P_1 = (x_1,y_1,z_1)$ *and* $P_2 = (x_2,y_2,z_2)$ *in the analytical 3-dimensional space and* d_E *denote the Euclidean metric. If l has direction vector*(p,q,r), *then*

$$d_{ID}(P_1,P_2) = \mu(P_1P_2)d_E(P_1,P_2)$$

where $\mu(P_1P_2) =$

$$\frac{\max\left\{\begin{array}{l}|p|+(\varphi-1)\max\{|q|,(\varphi-1)|r|,(1-\varphi)|p|+|q|+|r|\},\\ |q|+(\varphi-1)\max\{|r|,(\varphi-1)|p|,|p|+(1-\varphi)|q|+|r|\},\\ |r|+(\varphi-1)\max\{|p|,(\varphi-1)|q|,|p|+|q|+(1-\varphi)|r|\}\end{array}\right\}}{\sqrt{p^2+q^2+r^2}}.$$

Proof. Equation of l gives us $x_1 - x_2 = \lambda p$, $y_1 - y_2 = \lambda q$, $z_1 - z_2 = \lambda r$, $r \in \mathbb{R}$. Thus, $d_{ID}(P_1, P_2)$ is equal to

$$|\lambda| \left(\max \left\{ \begin{array}{l} |p| + (\varphi - 1) \max \left\{ \begin{array}{l} |q|, (\varphi - 1)|r|, \\ (1-\varphi)|p| + |q| + |r| \end{array} \right\}, \\ |q| + (\varphi - 1) \max \left\{ \begin{array}{l} |r|, (\varphi - 1)|p|, \\ |p| + (1-\varphi)|q| + |r| \end{array} \right\}, \\ |r| + (\varphi - 1) \max \left\{ \begin{array}{l} |p|, (\varphi - 1)|q|, \\ |p| + |q| + (1-\varphi)|r| \end{array} \right\} \end{array} \right\} \right)$$

and $d_E(A,B) = |\lambda| \sqrt{p^2 + q^2 + r^2}$ which implies the required result. □

The lemma above says that $d_{ID}-$distance along any line is some positive constant multiple of Euclidean distance along same line. Thus, one can immediately state the following corollaries.

Corollary 2 *If P_1, P_2 and X are any three collinear points in $\mathbb{R}^3$, then $d_E(P_1,X) = d_E(P_2,X)$ if and only if $d_{ID}(P_1,X) = d_{ID}(P_2,X)$.*

Corollary 3 *If P_1, P_2 and X are any three distinct collinear points in the real 3-dimensional space, then*

$$d_{ID}(X,P_1) \,/\, d_{ID}(X,P_2) = d_E(X,P_1) \,/\, d_E(X,P_2) \,.$$

That is, the ratios of the Euclidean and $d_{ID}-$distances along a line are the same.

3 Rhombic Triacontahedron Metric

The duals of thirteen Archimedean solids are known as Catalan solids. Unlike Platonic and Archimedean solids, faces of Catalan solids are not regular polygons. Rhombic triacontahedron is one of the Catalan solids with 30 faces, 32 vertices and 60 edges. Its faces are rhombuses. The ratio of the long diagonal to the short diagonal of each face is exactly equal to $\varphi = \frac{1+\sqrt{5}}{2}$, which is the golden ratio [15].

Definition 2 *Let $P_1 = (x_1, y_1, z_1)$ and $P_2 = (x_2, y_2, z_2)$ be two points in $\mathbb{R}^3$. The distance function $d_{RT} : \mathbb{R}^3 \times \mathbb{R}^3 \to [0, \infty)$ Rhombic triacontahedron distance between P_1 and P_2 is defined by $d_{RT}(P_1, P_2) =$*

$$\frac{\varphi}{2} \max \left\{ \begin{array}{l} |x_1 - x_2| + (2\varphi - 3) \max \left\{ \begin{array}{l} (\varphi+1)|z_1 - z_2| + \varphi |y_1 - y_2|, \\ |x_1 - x_2| \end{array} \right\}, \\ |y_1 - y_2| + (2\varphi - 3) \max \left\{ \begin{array}{l} (\varphi+1)|x_1 - x_2| + \varphi |z_1 - z_2|, \\ |y_1 - y_2| \end{array} \right\}, \\ |z_1 - z_2| + (2\varphi - 3) \max \left\{ \begin{array}{l} (\varphi+1)|y_1 - y_2| + \varphi |x_1 - x_2|, \\ |z_1 - z_2| \end{array} \right\} \end{array} \right\}$$

where $\varphi = \frac{1+\sqrt{5}}{2}$, the golden ratio.

According to the rhombic triacontahedron distance, there are two types path from P_1 to P_2. These paths are:

i) union of three line segments which one is parallel to a coordinate axis and other line segments are made $\arctan(\frac{1}{2})$ and $\arctan(\frac{\sqrt{5}}{2})$ angle with other coordinate axes.

ii) a line segment which is parallel to a coordinate axis.

Thus rhombic triacontahedron distance between P_1 and P_2 is the Euclidean length of line segment which is parallel to a coordinate axis or $\frac{\sqrt{5}+1}{4}$ times the sum of Euclidean lengths of three line segments. Figure 5 shows that the path between P_1 and P_2 in case of the maximum is $|y_1 - y_2| + \frac{3-\sqrt{5}}{2}|z_1 - z_2| + \frac{\sqrt{5}-1}{2}|x_1 - x_2|$.

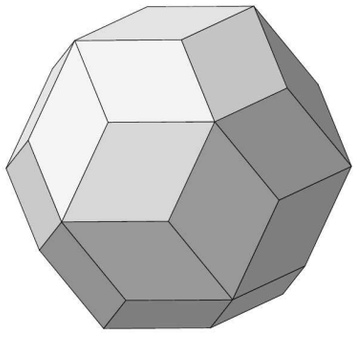

(a)

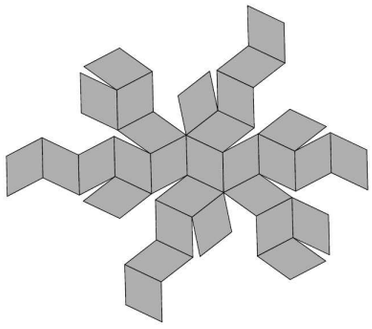

(b)

Figure 4: (a) *Rhombic triacontahedron*, (b) *Net of rhombic triacontahedron*

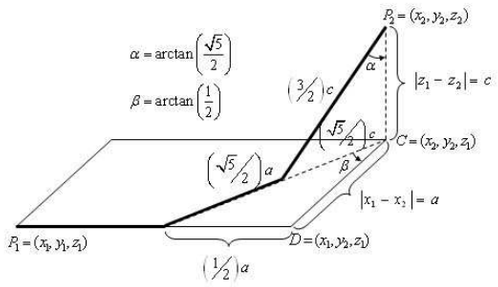

Figure 5: *RT way from P_1 to P_2 in the case $|y_1-y_2|\geq|x_1-x_2|\geq|z_1-z_2|$*

Lemma 3 *Let $P_1=(x_1,y_1,z_1)$ and $P_2=(x_2,y_2,z_2)$ be distinct two points in $\mathbb{R}^3$. Then*

$$d_{RT}(P_1,P_2)\geq \frac{\varphi}{2}\left(|x_1-x_2|+(2\varphi-3)\max\left\{(\varphi+1)|z_1-z_2|+\varphi|y_1-y_2|,|x_1-x_2|\right\}\right)$$
$$d_{RT}(P_1,P_2)\geq \frac{\varphi}{2}\left(|y_1-y_2|+(2\varphi-3)\max\left\{(\varphi+1)|x_1-x_2|+\varphi|z_1-z_2|,|y_1-y_2|\right\}\right)$$
$$d_{RT}(P_1,P_2)\geq \frac{\varphi}{2}\left(|z_1-z_2|+(2\varphi-3)\max\left\{(\varphi+1)|y_1-y_2|+\varphi|x_1-x_2|,|z_1-z_2|\right\}\right).$$

where $\varphi=\frac{1+\sqrt{5}}{2}$.

Proof. Proof is trivial by the definition of maximum function. □

Theorem 2 *The distance function d_{RT} is a metric. Also according to d_{RT}, unit sphere is a rhombic triacontahedron in $\mathbb{R}^3$.*

Proof. Let $d_{RT}:\mathbb{R}^3\times\mathbb{R}^3\to[0,\infty)$ be the rhombic triacontahedron distance function and $P_1=(x_1,y_1,z_1)$, $P_2=(x_2,y_2,z_2)$ and $P_3=(x_3,y_3,z_3)$ are distinct three points in $\mathbb{R}^3$. To show that d_{RT} is a metric in $\mathbb{R}^3$, the following axioms hold true for all P_1, P_2 and $P_3\in\mathbb{R}^3$.
M1) $d_{RT}(P_1,P_2)\geq 0$ and $d_{RT}(P_1,P_2)=0$ iff $P_1=P_2$
M2) $d_{RT}(P_1,P_2)=d_{RT}(P_2,P_1)$
M3) $d_{RT}(P_1,P_3)\leq d_{RT}(P_1,P_2)+d_{RT}(P_2,P_3)$.
One can easily show that the rhombic triacontahedron distance function satisfies above axioms by similar way in Theorem 1.
Consequently, the set of all points $X=(x,y,z)\in\mathbb{R}^3$ that rhombic triacontahedron distance is 1 from $O=(0,0,0)$ is $S_{RT}=$

$$\left\{(x,y,z):\frac{\varphi}{2}\max\left\{\begin{array}{l}|x|+(2\varphi-3)\max\{(\varphi+1)|z|+\varphi|y|,|x|\},\\ |y|+(2\varphi-3)\max\{(\varphi+1)|x|+\varphi|z|,|y|\},\\ |z|+(2\varphi-3)\max\{(\varphi+1)|y|+\varphi|x|,|z|\}\end{array}\right\}=1\right\}.$$

Thus the graph of S_{RT} is as in Figure 6. □

Corollary 4 *The equation of the rhombic triacontahedron with center (x_0,y_0,z_0) and radius r is*

$$\frac{\varphi}{2}\max\left\{\begin{array}{l}|x-x_0|+(2\varphi-3)\max\left\{\begin{array}{l}(\varphi+1)|z-z_0|+\varphi|y-y_0|,\\ |x-x_0|\end{array}\right\},\\ |y-y_0|+(2\varphi-3)\max\left\{\begin{array}{l}(\varphi+1)|x-x_0|+\varphi|z-z_0|,\\ |y-y_0|\end{array}\right\},\\ |z-z_0|+(2\varphi-3)\max\left\{\begin{array}{l}(\varphi+1)|y-y_0|+\varphi|x-x_0|,\\ |z-z_0|\end{array}\right\}\end{array}\right\}=r.$$

which is a polyhedron which has 30 faces with vertices; such that all permutations of the three axis components and all posible +/- sign changes of each axis component of $(\mu r,0,r)$, $(0,\delta r,r)$ and $(\mu r,\mu r,\mu r)$, where $\mu=\frac{\sqrt{5}-1}{2}$ and $\delta=\frac{3-\sqrt{5}}{2}$.

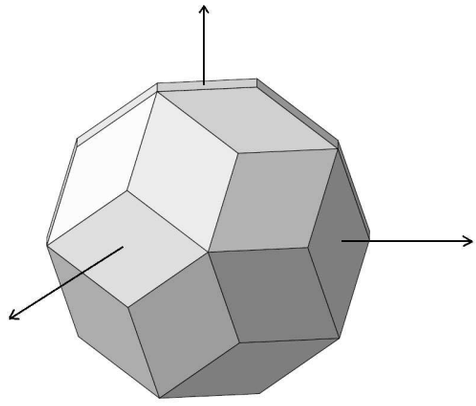

Figure 6: *Rhombic Triacontahedron*

Lemma 4 *Let l be the line through the points $P_1=(x_1,y_1,z_1)$ and $P_2=(x_2,y_2,z_2)$ in the analytical 3-dimensional space and d_E denote the Euclidean metric. If l has direction vector (p,q,r), then*

$$d_{RT}(P_1,P_2)=\mu(P_1P_2)d_E(P_1,P_2)$$

where

$$\mu(P_1P_2)=\frac{\frac{\varphi}{2}\max\left\{\begin{array}{l}|p|+(2\varphi-3)\max\{(\varphi+1)|r|+\varphi|q|,|p|\},\\ |q|+(2\varphi-3)\max\{(\varphi+1)|p|+\varphi|r|,|q|\},\\ |r|+(2\varphi-3)\max\{(\varphi+1)|q|+\varphi|p|,|r|\}\end{array}\right\}}{\sqrt{p^2+q^2+r^2}}.$$

Proof. Equation of l gives us $x_1-x_2=\lambda p$, $y_1-y_2=\lambda q$, $z_1-z_2=\lambda r$, $r\in\mathbb{R}$. Thus,
$d_{RT}(P_1,P_2)=$

$$|\lambda|\left(\frac{\varphi}{2}\max\left\{\begin{array}{l}|p|+(2\varphi-3)\max\{(\varphi+1)|r|+\varphi|q|,|p|\},\\ |q|+(2\varphi-3)\max\{(\varphi+1)|p|+\varphi|r|,|q|\},\\ |r|+(2\varphi-3)\max\{(\varphi+1)|q|+\varphi|p|,|r|\}\end{array}\right\}\right)$$

and $d_E(A,B)=|\lambda|\sqrt{p^2+q^2+r^2}$ which implies the required result. □

The previous lemma says that $d_{RT}-$distance along any line is some positive constant multiple of Euclidean distance along same line. Thus, one can immediately state the following corollaries:

Corollary 5 *If P_1, P_2 and X are any three collinear points in $\mathbb{R}^3$, then $d_E(P_1,X) = d_E(P_2,X)$ if and only if $d_{RT}(P_1,X) = d_{RT}(P_2,X)$.*

Corollary 6 *If P_1, P_2 and X are any three distinct collinear points in the real 3-dimensional space, then*

$$d_{RT}(X,P_1) \,/\, d_{RT}(X,P_2) = d_E(X,P_1) \,/\, d_E(X,P_2)\,.$$

That is, the ratios of the Euclidean and $d_{RT}-$distances along a line are the same.

References

[1] G. CHEN, *Lines and Circles in Taxicab Geometry*, Master Thesis, Department of Mathematics and Computer Science, University of Central Missouri, 1992.

[2] H. B. COLAKOGLU, O. GELIŞGEN, R. KAYA, Area formulas for a triangle in the alpha plane *Mathematical Communications* **18**(1) (2013), 123–132.

[3] T. ERMIS, O. GELISGEN, R. KAYA, On Taxicab Incircle and Circumcircle of a Triangle, *KoG* **16** (2012), 3–12.

[4] T. ERMIS, R. KAYA, Isometries the of 3-Dimensional Maximum Space, *Konuralp Journal of Mathematics* **3**(1) (2015), 103–114.

[5] O. GELIŞGEN, R. KAYA, M. OZCAN, Distance Formulae in The Chinese Checker Space, *Int. J. Pure Appl. Math.* **26**(1) (2006), 35–44.

[6] O. GELIŞGEN, R. KAYA, The Taxicab Space Group, *Acta Mathematica Hungarica* **122**(1-2) (2019), 187–200.

[7] O. GELIŞGEN, R. KAYA, Alpha(i) Distance in n-dimensional Space, *Applied Sciences* **10** (2008), 88–93.

[8] O. GELIŞGEN, R. KAYA, Generalization of Alpha -distance to n-Dimensional Space, *KoG* **10** (2006), 33–35.

[9] R. KAYA, O. GELISGEN, S. EKMEKCI, A. BAYAR, On The Group of Isometries of The Plane with Generalized Absolute Value Metric, *Rocky Mountain Journal of Mathematics* **39**(2) (2009), 591–603.

[10] M. KOCA, N. KOCA, R. KOÇ, Catalan solids derived from three-dimensional-root systems and quaternions, *Journal of Mathematical Physics* **51** (2010), 043501.

[11] E. F. KRAUSE, *Taxicab Geometry*, Addison-Wesley Publishing Company, Menlo Park, CA, 88p., 1975.

[12] R. S. MILLMANN, G. D. PARKER, *Geometry a Metric Approach with Models*, Springer, 370p., 1991.

[13] A. C. THOMPSON, *Minkowski Geometry*, Cambridge University Press, Cambridge, 1996.

[14] `http://en.wikipedia.org/wiki/Icosidodecahedron`

[15] `http://en.wikipedia.org/wiki/Rhombic\_triacontahedron`

[16] `http://www.math.nyu.edu/\symbol{126}crorres/Archimedes/Solids/Pappus.html`

Zeynep Can
e-mail: zeynepcan@aksaray.edu.tr
Aksaray University, Faculty of Arts and Sciences
400084 Aksaray,Turkey

Özcan Gelişgen
e-mail: gelisgen@ogu.edu.tr
Eskişehir Osmangazi University,
Faculty of Arts and Sciences
26480 Eskişehir, Turkey

Rüstem Kaya
e-mail: rkaya@ogu.edu.tr
Eskişehir Osmangazi University,
Faculty of Arts and Sciences
26480 Eskişehir, Turkey

Original scientific paper
Accepted 13. 11. 2015.

GUNTER WEISS

Elementary Constructions for Conics in Hyperbolic and Elliptic Planes

Dedicated to Prof. Dr. Klaus Meirer on the occasion of his 75th birthday.

Elementary Constructions for Conics in Hyperbolic and Elliptic Planes

ABSTRACT

In the Euclidean plane there are well-known constructions of points and tangents of e.g. an ellipse c based on the given axes of c, which make use of the Apollonius definition of c via its focal points or via two perspective affinities (de la Hire's construction). Even there is no parallel relation neither in a hyperbolic plane nor in an elliptic plane it is still possible to modify many of the elementary geometric constructions for conics, such that they also hold for those (regular) non-Euclidean planes. Some of these modifications just replace Euclidean straight lines by non-Euclidean circles. Furthermore we also study properties of Thales conics, which are generated by two pencils of (non-Euclidean) orthogonal lines.

Key words: hyperbolic plane, elliptic plane, conic sections, de la Hire, Apollonius, Thales

MSC2010: 51M04, 51M09

Elementarne konstrukcije konika u hiperboličnoj i eliptičnoj ravnini

SAŽETAK

U Euklidskoj ravnini poznate su konstrukcije točaka i tangenata za npr. elipsu c zadanu osima, pri čemu se koristi Apolonijeva definicija za c preko fokusa ili dva afiniteta (de la Hireova konstrukcija). Iako ne postoje paralelne relacije s hiperboličnom niti eliptičnom ravninom, ipak je moguće modificirati mnoge elementarne konstrukcije vezane za konike tako da one vrijede za (regularne) neeuklidske ravnine. U nekim modifikacijama samo je euklidski pravac zamijenjen s neeuklidskom kružnicom. Također će se proučiti svojstva Talesovih konika koje su generirane s dva pramena (neeuklidskih) okomitih pravaca.

Ključne riječi: hiperbolična ravnina, eliptična ravnina, konika, de la Hire, Apolonije, Tales

1 Introduction: Euclidean focal points

We aim at modifying Euclidean constructions for points and tangents of conics, such that they hold for conics in hyperbolic and elliptic planes. In the Euclidean plane, due to Apollonius, a hyperbola or an ellipse c is defined as geometric locus, where the focal points of c are the essential givens of c. To construct e.g. an ellipse via the classical "gardener's construction" in a hyperbolic plane necessitates the concept of focus in a hyperbolic resp. elliptic geometry. For visualizing the hyperbolic plane we use F. Klein's projective geometric model, elliptic geometry will be visualized on the sphere.

In a Euclidean plane a focus of a conic can be defined in several ways:

Definition 1 (Euclidean) *Given $c = \{P\}$ (ellipse resp. hyperbola), F_1, F_2 are (real) focal points, iff $\overline{PF_1} \pm \overline{PF_2} = const$. $\forall P \in c$, (and similar for a parabola c).*

Definition 2 (Euclidean) *Given $c = \{P\}$ (ellipse resp. hyperbola resp. parabola), F_i are focal points, iff each line through F_i is orthogonal to its conjugate line through F_i, (Figure 1).*

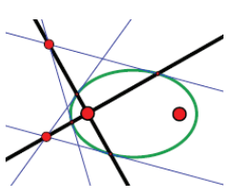

Figure 1: *Conjugate lines through a focus of a conic are orthogonal.*

Definition 3 (Euclidean) *Given $c = \{P\}$ (ellipse resp. hyperbola resp. parabola in the projectively and complex extended Euclidean plane π), F_i are focal points, iff they are intersections of tangents of c passing through the (conjugate imaginary) absolute points I, J of π.*

From Definition 3 follows that an ellipse and a hyperbola have four focal points, two of which are real and the other two are conjugate imaginary. For the extension of the concept "focus" to a projective extended hyperbolic or elliptic plane it seems to be an advantage to interpret the pair of Euclidean absolute points I, J at the ideal line u of π as degenerate absolute conic ω. Then the four tangents mentioned in Definition 3 become the common tangents of ω and c, which intersect also in I, J. Therewith one might count the pair of absolute points I, J also as an additional pair of focal points, such that, from an algebraic-geometric point of view, one has three pairs of focal points. A parabola and a circle have one real proper focal point. For the circle, considered as a limit figure of an ellipse, this focal point is the centre and counts for four focal points, while I, J forms the ideal pair of focal points. For a parabola, considered as a limit figure of a hyperbola, the ideal point is a real ideal focal point, while the pair I, J counts twice as imaginary pair of ideal focal points. In Figure 2 the situation is visualized symbolically showing conics "near" the limit cases.

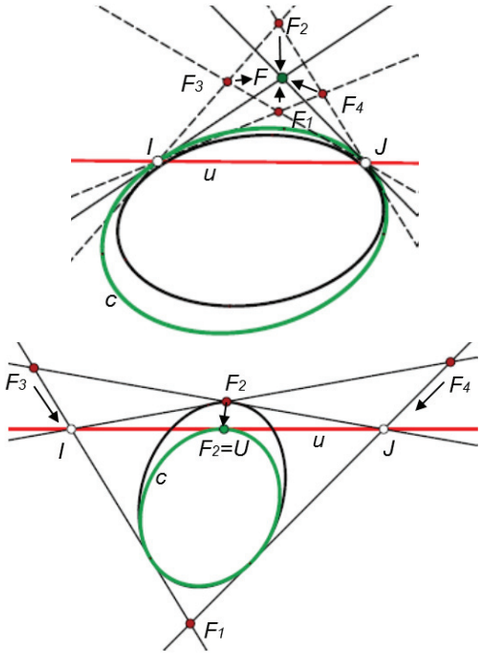

Figure 2: *Symbolic visualization of the 6 focal points of limit cases of a conic c.*

2 Introduction: de la Hire's construction of an ellipse and extensions

In the Euclidean plane π let an ellipse c be given by its axis segments. Then, due to Philippe de la Hire, one constructs points and tangents of an ellipse via two orthogonal perspective affine transformations of c to its two vertex circles, see Figure 3.

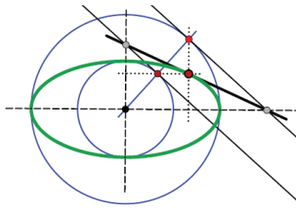

Figure 3: *De la Hire's construction of an ellipse via two orthogonal affinities.*

Remark 1 *It might not be so well-known that de la Hire's construction of an ellipse can easily be modified to construct a hyperbola c given by its axis rectangle (resp. its half axis segments a, b) using two perspective collineations $\kappa_i : c \mapsto c_i$. Thereby c_i is the (twice counted) vertex circle of c and the centres C_i of κ_i are the vertices of c, see Figure 4. Using e.g. the vanishing line v_1 of κ_1 one finds the first image O_1 of the point O of c. Let P_0 be an arbitrary point on c_i and let P_1 be the second intersection point of c_i with line $O_1 \vee P_0$, and P_2 the second intersection point of c_i with line $O \vee P_0$, then the mappings $P_0 \mapsto P_1$, $P_0 \mapsto P_2$ are involutions and $P_1 \mapsto P_2$ is a projectivity on the circle c_i. Therewith the pencils $\{C_1P_1\}$ and $\{C_2P_2\}$ are projective pencils and generate, according to J. Steiner, a conic. If the point O_1 is outside c_i, then this conic is a hyperbola with vertices C_i. If the point $O_1 (\neq C_i)$ is inside c_i, then the conic c becomes an ellipse with vertices C_i.*

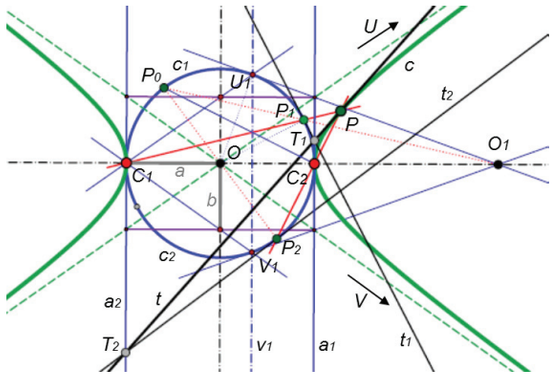

Figure 4: *Modified de la Hire's construction of a hyperbola via two perspective collineations.*

This construction principle is also applicable for constructing a parabola c given by its focal point F and its directrix line l, resp. its vertex C. The construction becomes very simple, if one uses the circle c_1 with centre F and radius $r = |FC|$ as collinear image of c. The diameters d of c_1 different form the axis of the parabola c intersect c in pairs of points with orthogonal tangents intersecting in a point $S \in l$, see Figure 5. The tangents of c_1 in the intersection points $d \cup c_1$ intersect the vertex tangent of c in points of this pair of parabola tangents and $d \perp FS$ according to focus Definition 2.

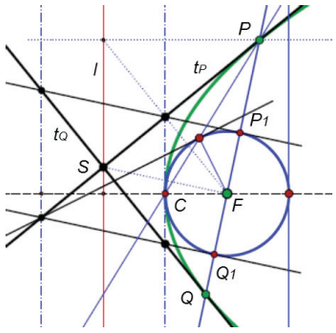

Figure 5: *Modified de la Hire's construction of a parabola via two perspective collineations.*

3 Conics in the hyperbolic and elliptic plane based on focus Definition 1

Starting with two real focus points F_i and the length of the main axis of a conic c it is possible to perform the usual Euclidean construction of points and tangents of c also in a (projectively extended) hyperbolic or an elliptic plane π, see Figure 6.

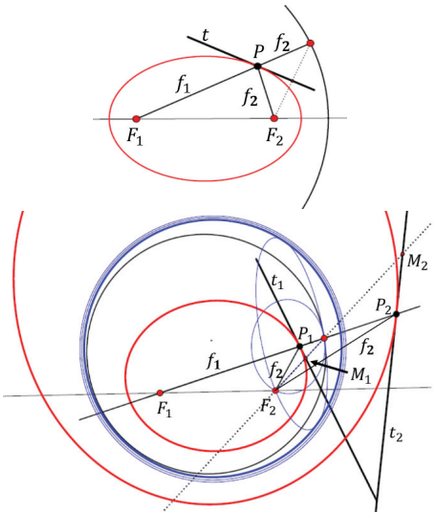

Figure 6: *"Gardener's construction" of an ellipse in the Euclidean and a hyperbolic plane.*

Note that a segment in a regular non-Euclidean plane has two midpoints M_i and therefore one gets two conics to a given proper pair of focal points and main axis length.
It turns out that also focus Definition 2 remains valid in non-Euclidean planes, see Figure 7.

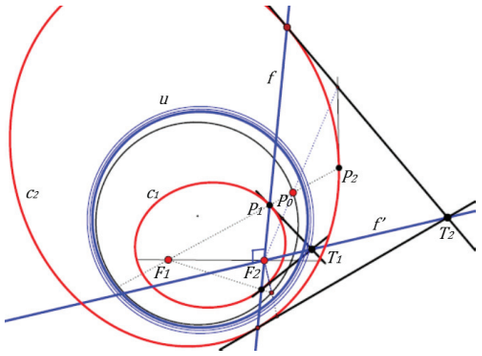

Figure 7: *In a non-Euclidean plane pairs of conjugate lines through a focus of a conic are orthogonal.*

4 Conics in the hyperbolic and elliptic plane based on de la Hire's construction

Obviously it is possible to perform de la Hire's construction (Figure 3) line by line also on the sphere just by avoiding the interpretation of orthogonal perspective affinities, see Figure 8. Central projection of the spherical figure from the midpoint of the sphere onto e.g. the plane of the main vertex circle of the spherical ellipse c gives the Euclidean version of de la Hire's construction.

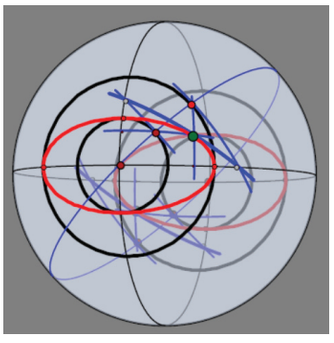

Figure 8: *Spherical version of de la Hire's construction of an ellipse.*

Similarly we can perform de la Hire's construction line by line also in the hyperbolic plane, see Figure 9. Note that in a (regular) non-Euclidean plane a conic c in general has three midpoints, which are the vertices of the polar triangle common to c and the absolute conic (resp. the absolute polarity). In Figure 9 we show a case with three real midpoints, labelled as M_1, M_2, M_3. We call M_1 the proper

midpoint and M_2, M_3 ideal midpoints. In Figure 9 conic c has real axes a, b and reality of the axes is a necessary (and sufficient) condition to perform de la Hire's construction. Furthermore, as long as the correspondence between vertex circle and axis is not explicitly given one has two possibilities for de la Hire's construction and gets two conics as results. (Also in the Euclidean case one could permute the two perspective affinities and would get the second solution.)

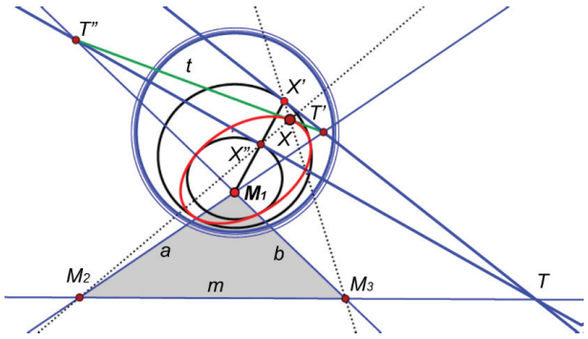

Figure 9: *De la Hire's construction of an ellipse in a hyperbolic plane.*

5 Conics in the hyperbolic and elliptic plane have, in general, six focal points

In the hyperbolic plane it is possible that a conic c has three real pairs of focal points F_i. This is the case, if c and the absolute conic u have four real tangents in common forming a quadrilateral, see Figure 10. All conics c (except u) touching this quadrilateral are hyperbolic confocal. The diagonal triangle of the common tangent quadrilateral is the common midpoint triangle (M_1, M_2, M_3) of all confocal conics. Let c_1 be one of the conics and let P be one of its points. Then it is of interest, whether the "gardener's construction" based on different pairs of focal points will deliver the same conic c_1:

From Projective Geometry (see e.g. [1]) follows that the pairs of lines (PF_1, PF_2), (PF_3, PF_4) and (PF_5, PF_6) are pairs of a hyperbolic involutoric projectivity, which has the tangent t and normal n of c in P as (orthogonal) fixed lines.

The common tangents of a general real conic c and the imaginary absolute conic u of an elliptic plane occur in two conjugate imaginary pairs, such that only one pair of focal points is real.

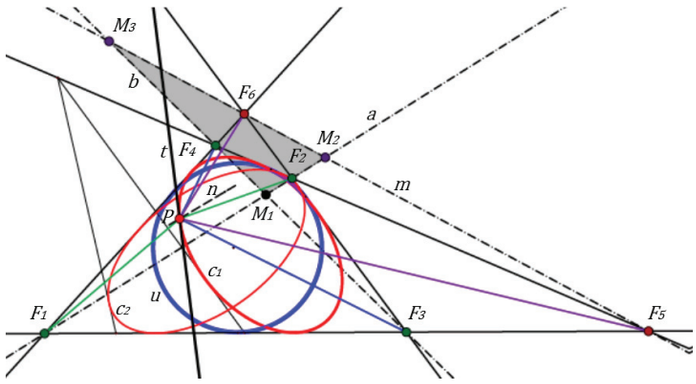

Figure 10: *Confocal pencil of conics with 6 real focal points in the hyperbolic plane.*

Concluding we state that all real pairs of focal points of a conic c in a hyperbolic plane are equivalent with respect to focus definitions 1, 2 and 3.

6 The orthoptic of a conic in hyperbolic and elliptic planes

The orthoptic of a given curve c is the set of points, from which one can draw orthogonal tangents to c, see [8]. In a Euclidean plane it is well-known that ellipses c have a real orthoptic circle, hyperbolas have a real or imaginary orthoptic circle, too. (For an equilateral hyperbola c in the projective extended Euclidean plane the pair of asymptotes is the only pair of real orthogonal tangents, such that the orthoptic degenerates into the centerpoint of c alone.) Parabolas have an orthoptic line, the directrix line. So we can say that *conics c have an orthoptic Möbius circle concentric to c*. Figure 11 shows the case of an ellipse in the Euclidean plane. In addition the "pedal curve" for the foci as poles is depicted, too. This pedal curve is the main vertex circle of c. Furthermore we note that this pedal circle is the same for each of the two foci of an ellipse or hyperbola. For a parabola this pedal curve is the vertex tangent, such that also the pedal curve of a conic c for a focus as pole is again a Möbius circle.

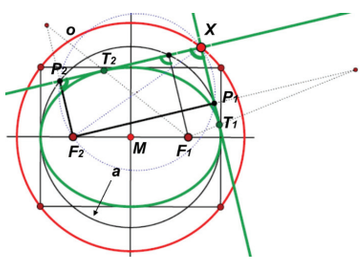

Figure 11: *Orthoptic circle o of an ellipse and its pedal circle for the foci as poles.*

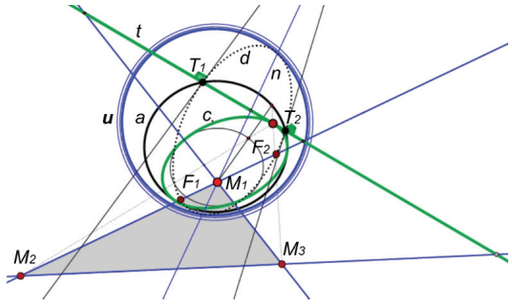

Figure 12: *In a hyperbolic plane π the intersections T_i of a tangent t to an ellipse c with the main vertex circle a and the focal points F_i are concyclic.*

In a hyperbolic plane π it turns out that the main vertex circle a is not the pedal curve of c with respect to a focus as pole, but the intersections T_i of a tangent t to an ellipse c with the main vertex circle a and the focal points F_i are points of a circle, see Figure 12.
Similar to the Euclidean case there is a "Poncelet-circle" p concentric with an ellipse c, containing the vertices of quadrangles subscribed to c. These quadrangles have metric properties with respect to hyperbolic geometry, but the circle p is not the hyperbolic orthoptic curve of the conic c, see Figure 13. This is obvious because of
***Poncelet's Theorem**: If a closed $n-$gon is subscribed to a conic p and inscribed to another c, then there exist infinitely many such $n-$gons.*
In the Euclidean case p coincides with the orthoptic o and all Poncelet 4-gons are rectangles.

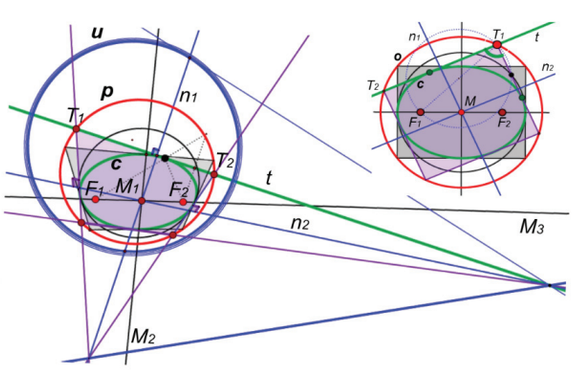

Figure 13: *An ellipse c in a Euclidean or non-Euclidean plane possesses a concentric circle p containing the vertices of Poncelet quadrangles subscribed to c.*

The presented results show that in a (regular) non-Euclidean geometry neither the orthoptic of a conic nor its pedal curve for a focus as pole can be a concentric circle.

Theorem 1 *The orthoptic curve of a conic c in a non-Euclidean plane π is a concentric conic o.*

Proof by applying the absolute polarity to conic c, which maps c to a conic c': The tangent $t' \perp t$ of c maps to an intersection point $T' \in T \cap c'$, see Figure 14.

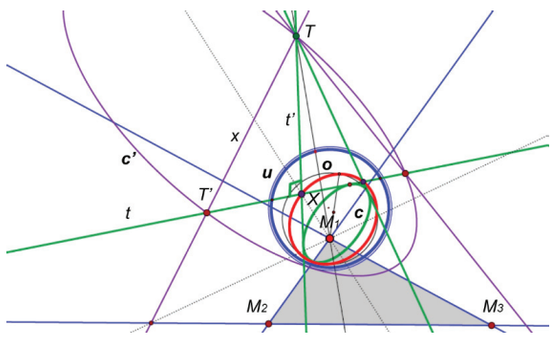

Figure 14: *In a hyperbolic plane π to an ellipse c there exists a concentric orthoptic conic o.*

7 Thales conics as orthoptics of a segment

A segment can be regarded as a singular conic c. Applying Theorem 1 follows:
The non-Euclidean orthoptic curve of a segment c is a concentric conic o, the "Thales-conic" of c.
The orthoptic o of segment c is generated by projective pencils of lines and therefore it is a conic.

Remark 2 *N. Wildberger calls the orthoptic of a segment its "thaloid". As the Euclidean case is called "Thales-circle" we prefer the concept "Thales-conic" comprising also the Euclidean case, c.f. [6]. For generalisations of the classical Thales-circle to Thales-surfaces see also [7].*

The orthoptic o of segment c is generated by projective pencils of lines and therefore it is a conic. It also allows a kinematic generation, see Figure 15: The orthogonal slider cross Σ_3 defines a forced motion keeping the two rods Σ_1, Σ_2 orthogonal, which rotate at the fixed poles P_{01}, P_{02}. Via the three-pole theorem of Aronhold (see [9]) it is possible to construct the instantaneous pole P_{03} and therewith also the tangents of o.

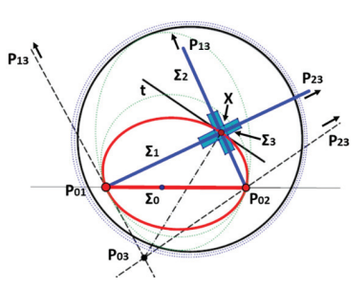

Figure 15: *Kinematic construction of points and tangents of a Thales-conic in a hyperbolic plane.*

8 Bodenmiller's theorem and its non-Euclidean counterparts

As an application of the concepts Thales-conic and orthoptic conic we start with the Euclidean theorem of Bodenmiller and study non-Euclidean versions of it. The theorem reads as follows, see e.g. [2] and Figure 16:

Theorem 2 (Bodenmiller) *Given a general quadrilateral in the Euclidean plane, then its three diagonal segments have Thales-circles belonging to a pencil of circles.*

Usually one calls the (real, coinciding or conjugate imaginary) common points of the Bodenmiller-circles the "Bodenmiller-points" of the quadrilateral. There are several extensions of this theorem, see also [2]:

(1) The midpoints of the Bodenmiller-Thales-circles are collinear with the Gauss-line g. (The Gauss-line of a quadrilateral contains the centres of all regular and singular conics c touching the quadrilateral; such a set of conics is called a 'dual pencil of conics'. The Gauss-line g is an affine geometric concept!)

(2) The common cord b of the three Bodenmiller-Thales-circles of a quadrilateral Q contains four orthocentres O_i of the four partial triangles of Q. (Obviously b is orthogonal to the Gauss-line g and it contains, in algebraic sense, 6 remarkable points of Q.)

(3) The pencil of Bodenmiller-Thales-circles of a quadrilateral Q consists of the orthoptics to the conics of the dual pencil of conics to Q.

Even though statement (3) is obvious and easy to prove, it seems not to be mentioned explicitly in relevant references:

For the proof we use a linear combination of two diagonal segments of Q, interpreted as singular conics of the dual pencil to Q and get a certain conic c of this pencil. The same linear combination of the corresponding Bodenmiller-Thales-circles then gives the orthoptic circle of that c.

Now the question arises, what about the Bodenmiller statements in non-Euclidean geometries?

Theorem 3 (Non-Euclidean Bodenmiller)

Given a quadrilateral Q, then the Thales-conics over the 3 diagonal segments belong to a pencil of conics.

With a special linear combination of two singular conics (i.e. two diagonal segments) of the dual pencil of conics to Q one might get the third singular conic. Applying the same linear combination to the corresponding "Bodenmiller-Thales-conics" will give the Bodenmiller-conic of the third diagonal segment, see Figure 17. We call the common points of the Bodenmiller-Thales-circles again "Bodenmiller-points".

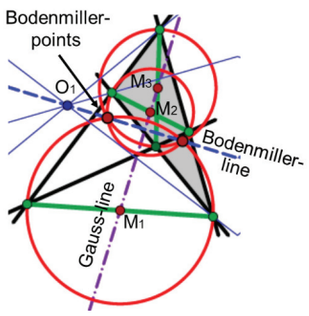

Figure 16: *Bodenmiller-circles, Bodenmiller-points and Gauss-line of a quadrilateral.*

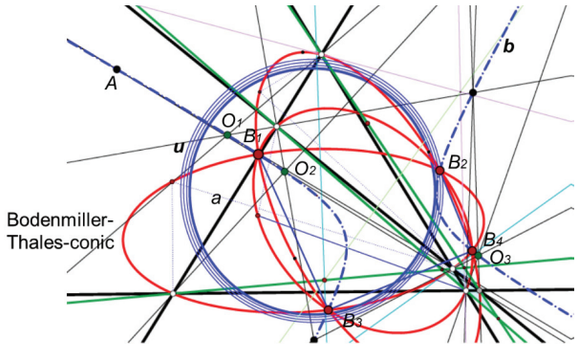

Figure 17: *Quadrilateral Q in a hyperbolic plane and its 3 Bodenmiller-Thales-conics. Its Bodenmiller-conic b contains 4 Bodenmiller-points B_i, the absolute poles of the sides of Q and 4 orthocentres O_i of the partial triangles of Q.*

Furthermore we conclude with the same arguments that the pencil of Bodenmiller-Thales-conics consists of the orthoptic conics to the dual pencil of conics touching quadrilateral Q, thus extending statement (3) also to non-Euclidean cases.

As a counterpart to the extension (2) of Bodenmiller's theorem we find the following:

Theorem 4 (non-Euclidean version of Bodenmiller property (2)) *Given a general quadrilateral Q in a hyperbolic or elliptic plane π, then (in algebraic sense) the four Bodenmiller-points B_i, the four absolute poles of the sides of Q, and the four orthocentres O_i of the partial triangles of Q are points of a single conic b, the "Bodenmiller-conic" of Q, (see Figure 17).*

Remark 3 *We mentioned that in the Euclidean case the Bodenmiller-line b contains 6 points, the two Bodenmiller-points and the four orthocentres of the partial triangles of quadrilateral Q. If we add the ideal line u to b, thus receiving a "singular Bodenmiller-conic", then we find the*

Euclidean absolute points as well as the ideal points of the directions orthogonal to the four sides of Q as additional points on the singular Bodenmiller-conic $(b \cup u)$. Therewith we find 12 remarkable points of a quadrilateral on its Bodenmiller-conic in all cases, the Euclidean and non-Euclidean planes.

It still remains to ask for the non-Euclidean counterpart of the Gauss-line g of a quadrilateral Q. Each diagonal segment has two non-Euclidean midpoints and it is not surprising that these all together 6 points belong to one conic, which we might call "Gauss-conic" g of Q. But note that this Gauss-conic does not contain the midpoint triplets of the regular conics c of the dual pencil of conics to Q! Therefore this conic cannot act as a suitable counterpart for the Euclidean Gauss-line. Let us add the absolute pole of each diagonal d_i to its midpoint pair M_1, M_2 as the third midpoint M_3 of a singular conic, see Figure 18. So we have set of 9 midpoints, which define a one parameter set of cubic curves.

This gives rise to following:

Conjecture (non-Euclidean version of Gauss-line property (1)) *Given a general quadrilateral Q in a hyperbolic or elliptic plane π, then the midpoint triplets of all conics touching Q belong to a cubic curve, the "Gauss-cubic" g_3.*

To prove this conjecture one might again use the idea of linear combining two singular conics: In the dual pencil of conics touching Q we use a pencil parameter t such that the singular conics correspond to parameter values 0, ∞, 1. To each of these special parameter values there will be a point triplet (M_1, M_2, M_3) $(t = 0, 1, \infty)$ of midpoints forming the basis points of a pencil of cubics. By a continuity argument with $t \in \mathbb{R}$ it will be possible to find an ordering within the triplets. Then $\{M_1(t)\} =: g_1$, $\{M_2(t)\} =: g_2$, $\{M_3(t)\} =: g_3$ are three parameterized arcs of curves which are conjectured to belong to one cubic of the pencil.

9 Concluding remarks

Even though there exist already many results on "elementary non-Euclidean geometry", see for example recent KoG-issues, there are still many open questions concerning circles and conics connected with triangles, quadrangles and quadrilaterals. In this article we focussed on the concept orthoptic of a conic and, as a special case, the Thales-conic to a segment and applied the results generalizing theorems for quadrilaterals, which are well-known in Euclidean geometry, namely the theorems of Bodenmiller and Gauss.

Still open questions are e.g. the focus loci of (dual) pencils of conics, Wallace-Simson's theorem, its extension to quadrilaterals as well as its connections with Miquel's theorem. One also could look for conics which have one or more properties of an equilateral hyperbola. Especially in higher dimensional non-Euclidean spaces (see [3]) there is little known about classical elementary geometry and one will find a large field of activity there.

Maybe this topics seem not to be "mathematical mainstream", but as C. Kimberling's incredibly growing list of now more than 7000 remarkable points of a triangle shows, see [5], there is a worldwide community dealing with what can be called "advanced elementary geometry". This might justify that paper, too.

After finishing this paper the author found an announcement of a book concerning conics, see [4], which will be available in Spring 2016 and also contains a chapter about conics in non-Euclidean geometries.

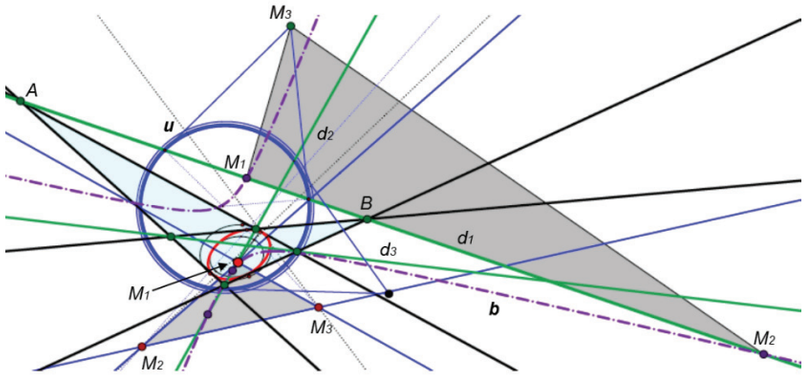

Figure 18: *Quadrilateral Q in a hyperbolic plane and its Gauss-conic g, which does not contain the midpoint triplets of the conics touching Q.*

References

[1] H. BRAUNER, *Geometrie projektiver Räume 1, 2*, B. I. Wissenschaftsverlag Mannheim-Wien-Zürich, 1976.

[2] R. FRITSCH, Gudermann, Bodenmiller und der Satz von Bodenmiller-Steimer, *Didaktik der Mathematik*, 20. Jahrg., 1992, 165–187.

[3] O. GIERING, *Vorlesungen über höhere Geometrie*, Vieweg, Braunschweig, 1982.

[4] G. GLAESER, H. STACHEL, B. ODENHAL, *The Universe of Conics: From the ancient Greeks to 21st century developments*, Springer Spektrum, 2016.

[5] C. KIMBERLING, *Encyclopedia of Triangle Centers-ETC. centers*, `ttp://faculty.evansville.edu/ck6/encyclopedia/ETC.tml`

[6] G. WEISS, *Die Vierseiteigenschaften von Bodenmiller und Steiner*, math.–stat. Section Forschungszentrum Graz, Austria, Bericht 167, 1981, 1–20.

[7] G. WEISS, F. GRUBER, Den Satz von Thales verallgemeinern – aber wie?, *KoG* **12** (2008), 7–18.

[8] W. WUNDERLICH, Kurven mit isoptischem Kreis, *Aequationes math.* **6** (1971), 71–81.

[9] W. WUNDERLICH, *Ebene Kinematik*, B. I. Hochschultaschenbücher 447/447a, Mannheim-Wien-Zürich, 1970.

Gunter Weiss
e-mail: weissgunter@hotmail.com
University of Technology Vienna
Karlsplatz 13, 1040 Vienna, Austria

Original scientific paper
Accepted 17. 12. 2015.

SÜLEYMAN YÜKSEL
MÜNEVVER ÖZCAN

On Some Regular Polygons in the Taxicab 3−Space

On Some Regular Polygons in the Taxicab 3−Space

ABSTRACT

In this study, it has been researched which Euclidean regular polygons are also taxicab regular and which are not. The existence of non-Euclidean taxicab regular polygons in the taxicab 3-space has also been investigated.

Key words: taxicab geometry, Euclidean geometry, regular polygons

MSC2010: 51K05, 51K99, 51N25

O nekim pravilnim mnogokutima u taxicab trodimenzionalnom prostoru

SAŽETAK

U ovom se radu proučava koji su euklidski pravilni mnogokuti ujedno i taxicab pravilni, a koji to nisu. Također se istražuje postojanje taxicab pravinih mnogokuta koji nisu pravilni u euklidskom smislu.

Ključne riječi: taxicab geometrija, euklidska geometrija, pravilni mnogokuti

1 Introduction

The taxicab 3-dimensional space $\mathbb{R}^3_T$ is almost the same as the Euclidean analytical 3-dimensional space $\mathbb{R}^3$. The points, lines and planes are the same in Euclidean and taxicab geometry and the angles are measured in the same way, but the distance function is different. The taxicab metric is defined using the distance function as in [4], [6]

$$d_T(A,B) = |b_1 - a_1| + |b_2 - a_2| + |b_3 - a_3|. \tag{1}$$

Also, for a vector $\overrightarrow{V} = (v_1, v_2, v_3) \in \mathbb{R}^3$, taxicab norm of $\overrightarrow{V}$ is noted as $\left\|\overrightarrow{V}\right\|_T$ as in [5] and

$$\left\|\overrightarrow{V}\right\|_T = |v_1| + |v_2| + |v_3|. \tag{2}$$

Since taxicab plane and 3-dimensional taxicab space have different distance function from that in the Euclidean plane and 3-dimensional space, it is interesting to study the taxicab analogues of topics that include the distance concept in the Euclidean plane and 3-dimensional space. During the recent years, many such topics have been studied in the taxicab plane and 3-dimensional space (see [1], [2], [3], [5], [6], [7], [8], [9], [10]).
In $\mathbb{R}^2$, the equation of taxicab circle is

$$|x - x_0| + |y - y_0| = r \tag{3}$$

which is centered at $M = (x_0, y_0)$ point with radius r.
In $\mathbb{R}^3$, the equation of taxicab sphere is

$$|x - x_0| + |y - y_0| + |z - z_0| = r \tag{4}$$

which is centered at $M = (x_0, y_0, z_0)$ point with radius r (see [7], [8], [9]). Then, a taxicab circle can be defined by a plane and a taxicab sphere.
In $\mathbb{R}^3$, the taxicab circle is the intersection set of taxicab sphere and $ax + by + cz + d = 0$, $(a,b,c,d \in \mathbb{R})$, plane which passes through the center of taxicab sphere.
Recently regular polygons have been studied in the taxicab plane (see [3]). Although there do not exist Euclidean and taxicab regular triangles in the taxicab plane (see [3]), there exist Euclidean and taxicab regular triangles in the taxicab 3-dimensional space $\mathbb{R}^3_T$ (see Example 1, 2). Therefore, it can be interesting to study regular polygons in the taxicab 3-dimensional space. On the $x = k_1, y = k_2, z = k_3$ $(k_1, k_2, k_3 \in \mathbb{R})$ planes in the $\mathbb{R}^3_T$, Euclidean and taxicab regular polygons can be investigated in the same way as in the taxicab plane $\mathbb{R}^2_T$. Therefore, in this study, regular polygons which are not on $x = k_1, y = k_2, z = k_3$ $(k_1, k_2, k_3 \in \mathbb{R})$ planes are researched and we answer the following question: Which Euclidean regular polygons are also the taxicab regular, and which are not? In addition, we investigate the existence and nonexistence of taxicab regular polygons in the taxicab 3-dimensional space $\mathbb{R}^3_T$.

2 Taxicab Regular Polygons

As in the Euclidean 3-space, a polygon in the taxicab 3-space consists of three or more coplanar line segments, the line segments (sides) intersect only at endpoints, each endpoint (vertex) belongs to exactly two line segments and no two line segments with a common endpoint are collinear. If the number of sides of a polygon is n for $n \geq 3$ and $n \in \mathbb{N}$, then the polygon is called an $n-$gon. The following definitions for polygons in the taxicab 3-space are given by means of the taxicab lengths instead of the Euclidean lengths:

Definition 1 *A polygon in the plane is said to be taxicab equilateral if the taxicab lengths of its sides are equal.*

Definition 2 *A polygon in the plane is said to be taxicab equiangular if the measures of its interior angles are equal.*

Definition 3 *A polygon in the plane is said to be taxicab regular if it is both taxicab equilateral and equiangular.*

Definition 2 does not give a new equiangular concept because the taxicab and the Euclidean measure of an angle are the same. That is, every Euclidean equiangular polygon is also the taxicab equiangular, and vice versa. However, since the taxicab 3-space has a different distance function, Definition 1 and Definition 3 are new concepts [3].
An n-gon can be formed by n vectors with a total of zero on a plane. If the lengths of n vectors are the same and all the angles between two consecutive vectors are equal, the n-gon is regular (see Figure 1). Therefore, we need to find n vectors that allow these requirements to form a regular n-gon.

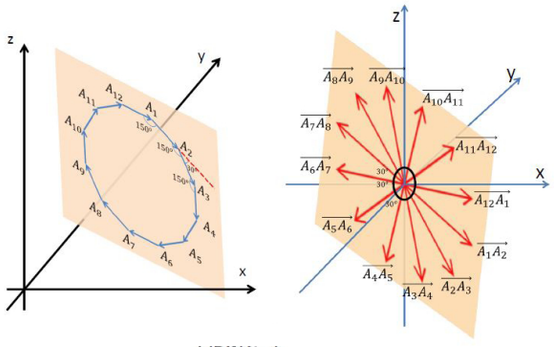

Figure 1.

Let W be a vector set and the members of W are sides of taxicab regular polygon as in Figure 1. It is clear that all the vectors are on the same plane and all the angles between two consecutive vectors are equal.
Let w be a vector in $\mathbb{R}^3$. We would like to find geometric locations of the w_i vectors where $\|w\|_E = \|w_i\|_E$ and $\|w\|_T = \|w_i\|_T$ (since there exist an infinite number of points on a circle as in Case 2, it can be said that $i \in \mathbb{N}$). Let $k \in \mathbb{R}$.
If the direction vector of w is $(\pm k, \pm k, \pm k)$, then $\|w\|_E = \frac{\|w\|_T}{\sqrt{3}}$.
If the direction vector of w is a member of $\{(\pm k,0,0),(0,\pm k,0),(0,0,\pm k)\}$, then $\|w\|_E = \|w\|_T$.
If the direction vector of w is not a member of $\{(\pm k,0,0),(0,\pm k,0),(0,0,\pm k),(\pm k,\pm k,\pm k)\}$, then $\frac{\|w\|_T}{\sqrt{3}} < \|w\|_E < \|w\|_T$.
To determine w_i vectors, there exist three different cases depending on the Euclidean and taxicab lengths of the w vector.
Case 1. For $\|w\|_E = \frac{\|w\|_T}{\sqrt{3}}$, as it is shown in Figure 2, the members of the intersection set of the Euclidean and taxicab sphere are

$$w_i = (\pm\frac{\|w\|_T}{3}, \pm\frac{\|w\|_T}{3}, \pm\frac{\|w\|_T}{3}). \tag{5}$$

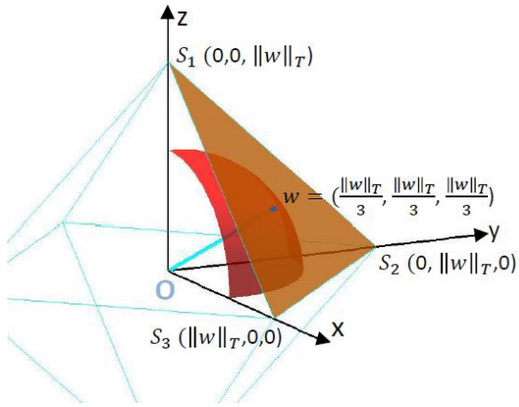

Figure 2.

Case 2. For $\frac{\|w\|_T}{\sqrt{3}} < \|w\|_E < \|w\|_T$, as it is shown in Figure 3, the intersection sets are 8 circles on the taxicab sphere. One of the circles, C, is on $x+y+z = \|w\|_T$ plane and points of C are intersection of

$$x+y+z = \|w\|_T \tag{6}$$

plane and

$$\left(x-\frac{\|w\|_T}{3}\right)^2+\left(y-\frac{\|w\|_T}{3}\right)^2+\left(z-\frac{\|w\|_T}{3}\right)^2=\frac{3\|w\|_E^2-\|w\|_T^2}{3} \tag{7}$$

Euclidean sphere. All the circles, for $1 \leq j \leq 8$ C_j, are intersection of

$$\left(x\pm\frac{\|w\|_T}{3}\right)^2+\left(y\pm\frac{\|w\|_T}{3}\right)^2+\left(z\pm\frac{\|w\|_T}{3}\right)^2=\frac{3\|w\|_E^2-\|w\|_T^2}{3} \tag{8}$$

Euclidean spheres and

$$\pm x \pm y \pm z = \|w\|_T \tag{9}$$

planes. Thus, w_i vectors where $\|w\|_E = \|w_i\|_E$ and $\|w\|_T = \|w_i\|_T$ are members of $\bigcup_{j=1}^{8} C_j$.

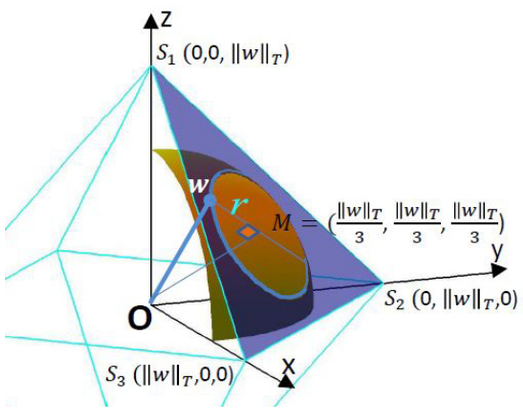

Figure 3.

Case 3. For $\|w\|_E = \|w\|_T$, as it is shown in Figure 20, the members of the intersection set of Euclidean and taxicab sphere are

$$w_i = (\pm\|w\|_T, 0, 0), (0, \pm\|w\|_T, 0), (0, 0, \pm\|w\|_T). \tag{10}$$

Let us introduce the following abbreviations for the following Proposition 1.
$\pm x \pm y \pm z = \|\overrightarrow{w}\|_T$ plane equation is shown as $P_{\pm,\pm,\pm}$ and $\left(x \pm \frac{\|w\|_T}{3}\right)^2 + \left(y \pm \frac{\|w\|_T}{3}\right)^2 + \left(z \pm \frac{\|w\|_T}{3}\right)^2 = \frac{3\|w\|_E^2 - \|w\|_T^2}{3}$ sphere equation is shown as $S_{\pm,\pm,\pm}$.

Proposition 1 *Let w be a vector. The geometric locations of the w_i ($i \in \mathbb{N}$) vectors which fulfill the following conditions $\|w\|_E = \|w_i\|_E$ and $\|w\|_T = \|w_i\|_T$ are $\bigcup_{j=1}^{9} C_j$ and C_j, for $0 \le j \le 9$, can be defined as:*

Assume $\|w\|_E \neq \|w\|_T$
If $0 \le x,y,z \le \|w\|_T$ then $C_1 = S_{-,-,-} \cap P_{+,+,+}$.
If $0 \le x,z \le \|w\|_T$ and $-\|w\|_T \le y \le 0$ then $C_2 = S_{-,+,-} \cap P_{+,-,+}$.
If $0 \le z \le \|w\|_T$ and $-\|w\|_T \le x,y \le 0$ then $C_3 = S_{+,+,-} \cap P_{-,-,+}$.
If $0 \le y,z \le \|w\|_T$ and $-\|w\|_T \le x \le 0$ then $C_4 = S_{+,-,-} \cap P_{-,+,+}$.
If $0 \le x,y \le \|w\|_T$ and $-\|w\|_T \le z \le 0$ then $C_5 = S_{-,-,+} \cap P_{+,+,-}$.
If $0 \le x \le \|w\|_T$ and $-\|w\|_T \le y,z \le 0$ then $C_6 = S_{-,+,+} \cap P_{+,-,-}$.
If $-\|w\|_T \le x,y,z \le 0$ then $C_7 = S_{+,+,+} \cap P_{-,-,-}$.
If $0 \le y \le \|w\|_T$ and $-\|w\|_T \le x,z \le 0$ then $C_8 = S_{+,-,+} \cap P_{-,+,-}$.
Assume $\|w\|_E = \|w\|_T$.
$C_9 = \{(\pm\|w\|_T, 0, 0), (0, \pm\|w\|_T, 0), (0, 0, \pm\|w\|_T)\}$.

Corollary 1 *Let W be a vector set of the edges of Euclidean regular polygon and $w \in W$. A Euclidean regular polygon is also taxicab regular if only if $W \subseteq \bigcup_{j=1}^{9} C_j$ where $\bigcup_{j=1}^{9} C_j$ is the same as in Proposition 1.*

Proof. For $n \ge 3$, if an $n-$gon is Euclidean and taxicab regular, then all the w side vectors of $n-$gon are members of the intersection set of an origin-centered taxicab sphere with a radius of $\|w\|_T$ and an origin-centered Euclidean sphere with a radius of $\|w\|_E$. It is clear that the intersection set is $\bigcup_{j=1}^{9} C_j$ as in Proposition 1. □

3 Euclidean Regular Polygons in Taxicab 3-Space

Euclidean regular polygons are Euclidean equiangular. Since the taxicab angles are measured in the same way as Euclidean (see [3], [6]), the polygons are also taxicab equiangular. Thus, we are just interested in which Euclidean regular polygons are taxicab equilateral and which are not (see Definitions 1, 2, 3).

Theorem 1 *None of Euclidean regular $n-$gon ($n > 12$) is taxicab regular.*

Proof. All the regular polygons are planar and the intersection set of Euclidean and taxicab spheres forms eight circles (see Figure 4). A plane can intersect only 6 out of 8 circles on the taxicab sphere. Thus, the number of intersection points of the plane and 6 circles are max 12 (see Figures 4, 5). Therefore, maximum 12 parts of lines which have equal taxicab length and equal Euclidean length can be obtained. As a result, no Euclidean regular $n-$gon ($n > 12$) is taxicab regular. □

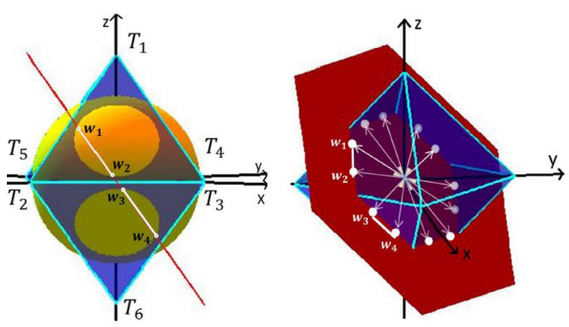

Figure 4.

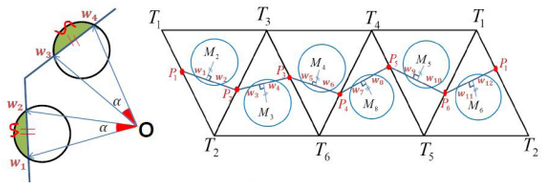

Figure 5.

Theorem 2 *There exist* 12*-gons that are Euclidean and taxicab regular and they are lying on a plane parallel to one of the* $\pm x \pm y \pm z = 0$ *planes.*

Proof. According to the proof presented in Theorem 1, it is possible that there exist 12 points on the intersection set of Euclidean and taxicab spheres and a plane. Thus, we need to prove that the angle between two consecutive vectors can be 30^o and that all the points can lay on a plane parallel to one of the $\pm x \pm y \pm z = 0$ planes.
As it was stated before, it is easy to see that the plane can intersect max 6 out of 8 circles (see Figure 4) with $r = \frac{1}{\sqrt{3}}\sqrt{3\|w\|_E^2 - \|w\|_T^2}$ radius and $M = \left(\pm\frac{\|w\|_T}{3}, \pm\frac{\|w\|_T}{3}, \pm\frac{\|w\|_T}{3}\right)$ center. When $a,b,c > 0$, $ax + by + cz = 0$ plane intersect octahedron (taxicab sphere) on its $T_1T_2T_3$, $T_6T_2T_3$, $T_6T_3T_4$, $T_6T_4T_5$, $T_1T_5T_4$, $T_1T_2T_5$ faces. For $k,m,n \in \mathbb{R}$, the intersection set of plane and edges of octahedron is

$$\left\{ \begin{array}{c} P_1 = (-k, 0, k - \|w\|_T), P_2 = (0, -m, \|w\|_T - m), \\ P_3 = (n, n - \|w\|_T, 0), P_4 = (k, 0, k - \|w\|_T), \\ P_5 = (0, m, m - \|w\|_T), P_6 = (-n, \|w\|_T - n, 0) \end{array} \right\}.$$

For $1 \le i \le 6$, the plane P_i are on

$$ax + by + cz = 0. \tag{11}$$

To obtain

$$\begin{aligned} \measuredangle w_1Ow_2 = \measuredangle w_3Ow_4 = \measuredangle w_5Ow_6 = \measuredangle w_7Ow_8 \\ = \measuredangle w_9Ow_{10} = \measuredangle w_{11}Ow_{12} = \alpha, \end{aligned}$$

it should be satisfied that

$$\|\overrightarrow{w_1w_2}\| = \|\overrightarrow{w_3w_4}\| = \|\overrightarrow{w_5w_6}\| = \|\overrightarrow{w_7w_8}\| = \|\overrightarrow{w_9w_{10}}\| = \|\overrightarrow{w_{11}w_{12}}\| \tag{12}$$

(see Figures 4, 5). Also, to obtain (12) it should be satisfied that

$$\begin{aligned} d_E(M_2,[P_1P_2]) = d_E(M_3,[P_2P_3]) = d_E(M_4,[P_3P_4]) \\ = d_E(M_8,[P_4P_5]) = d_E(M_5,[P_5P_6]) \\ = d_E(M_6,[P_6P_1]). \end{aligned} \tag{13}$$

For $\|w\|_T = 3$, each of equations (11) and (13) are solved on the Maple Computer Math Program. It is seen that $|a| = |b| = |c|$ and $m = k = n = \frac{\|w\|_T}{2}$. Therefore, $ax + by + cz = 0$ planes are $\pm x \pm y \pm z = 0$.
If $w_1 = P_1$ and $w_2 = P_2$, then $\alpha = 60^o$ (see Figure 6).
If $w_1 = w_2$, then $\alpha = 0^o$ (see Figure 7). So $0^o \le \alpha \le 60^o$. Then, it is possible that $\alpha = 30^o$. For $\alpha = 30^o$ and $1 \le i \le 12$, Euclidean and taxicab regular 12−gon can be created by w_i vectors. □

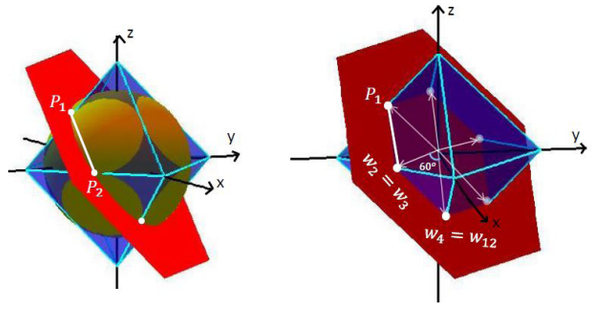

Figure 6.

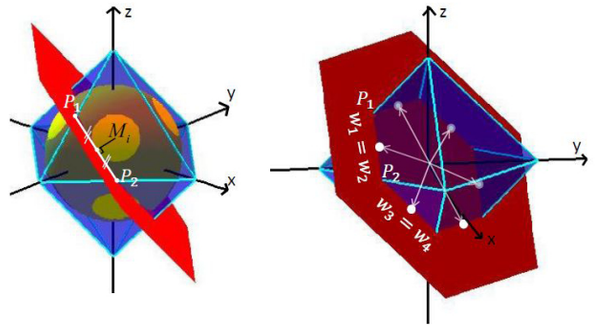

Figure 7.

Now we are going to explain the connection between taxicab and Euclidean lengths of the sides of a regular 12−gon: Because of $P_2 = (0, -\frac{\|w\|_T}{2}, \frac{\|w\|_T}{2})$ and $P_3 = (\frac{\|w\|_T}{2}, -\frac{\|w\|_T}{2}, 0)$, P_2 and P_3 points have an equal distance from the origin. Therefore, the midpoint of the line segment $[P_2P_3]$ is $S_{23} = (\frac{\|w\|_T}{4}, -\frac{\|w\|_T}{2}, \frac{\|w\|_T}{4})$ and this point, S_{23}, is on the taxicab sphere.
The angles of the right triangle $S_{23}V_4O$ are $15^o, 75^o, 90^o$ (see Figure 8). As a result,

$$d_E(S_{23}, O) = \cos 15^o d_E(w_4, O) \tag{14}$$

and

$$\begin{aligned} d_E(S_{23}, O) &= \sqrt{\left(\frac{\|w\|_T}{4}\right)^2 + \left(-\frac{\|w\|_T}{2}\right)^2 + \left(\frac{\|w\|_T}{4}\right)^2} \\ &= \frac{\sqrt{6}}{4}\|w\|_T \end{aligned} \tag{15}$$

$$d_E(w_4, O) = \|w\|_E \tag{16}$$

$$cos15^o = \frac{2+\sqrt{3}}{\sqrt{6}+\sqrt{2}}. \tag{17}$$

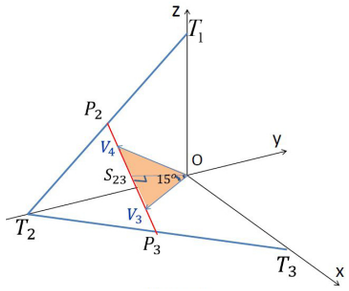

Figure 8.

When equations (15), (16) and (17) are written in 14, it is found that

$$\|w\|_T = \frac{3+\sqrt{3}}{3}\|w\|_T\,. \tag{18}$$

Thus we can get the following corollary.

Corollary 2 *Let $A_1A_2...A_{12}$ be a Euclidean regular polygon on one of the $\pm x \pm y \pm z = k$ planes, $k \in \mathbb{R}$. If the taxicab length of one of the sides is $\frac{3+\sqrt{3}}{3}$ times of the Euclidean length, $A_1A_2...A_{12}$ is also taxicab regular.*

Theorem 3 *There do not exist Euclidean regular* 10*-gons that are taxicab regular at the same time.*

Proof. Let $A_1A_2A_3A_4A_5A_6A_7A_8A_9A_{10}$ be a taxicab and Euclidean regular 10-gon. In this case, taxicab lengths of vectors $\overrightarrow{A_1A_2}$, $\overrightarrow{A_2A_3}$, $\overrightarrow{A_3A_4}$, $\overrightarrow{A_4A_5}$, $\overrightarrow{A_5A_6}$, $\overrightarrow{A_6A_7}$, $\overrightarrow{A_7A_8}$, $\overrightarrow{A_8A_9}$, $\overrightarrow{A_9A_{10}}$, $\overrightarrow{A_{10}A_1}$ are the same. Thus, these vectors are on the intersection set of an origin centered taxicab sphere with a radius of $d_T(A_1,A_2)$ and an origin-centered Euclidean sphere with a radius of $d_E(A_1,A_2)$ and the plane $ax+by+cz=0$. Also, the angle between each consecutive vectors is 36^o. For the number of intersection points between 6 circles and the plane to be 10, the plane must intersect four or five circles with two points. Since all the circles are symmetric with respect to the origin, the plane must intersect 4 circles with two points and 2 circles with 1 point as shown in Figures 9, 10.

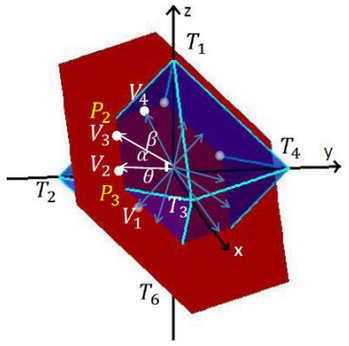

Figure 9.

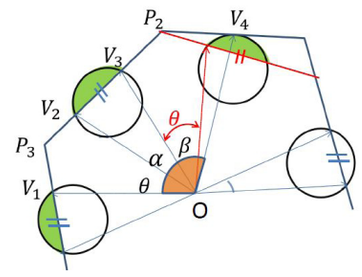

Figure 10.

Let $\measuredangle V_1OV_2 = \theta$, $\measuredangle V_2OV_3 = \alpha$ and $\measuredangle V_3OV_4 = \beta$ (see Figures 9, 10). Since $\beta > \theta$, β and θ cannot be 36^o at the same time. As a result, no Euclidean regular 10−gon is taxicab regular. □

Theorem 4 *None of the Euclidean regular* $5,7,9,11-$*gons is taxicab regular at the same time.*

Proof. Let $A_1A_2A_3A_4A_5$ Euclidean regular 5−gon be also taxicab regular. Then, the taxicab lengths of $\overrightarrow{A_1A_2}$, $\overrightarrow{A_2A_3}$, $\overrightarrow{A_3A_4}$, $\overrightarrow{A_4A_5}$, $\overrightarrow{A_5A_1}$ vectors of the 5−gon are the same. If $\overrightarrow{A_2A_1}$, $\overrightarrow{A_3A_2}$, $\overrightarrow{A_4A_3}$, $\overrightarrow{A_5A_4}$, $\overrightarrow{A_1A_5}$ vectors are added into $\overrightarrow{A_1A_2}$, $\overrightarrow{A_2A_3}$, $\overrightarrow{A_3A_4}$, $\overrightarrow{A_4A_5}$, $\overrightarrow{A_5A_1}$ vectors, ten vectors on the same plane are obtained. The taxicab lengths of 10 vectors are the same and the angle between each consecutive vectors is 36^o (see Figure 11). This is a contradiction, because it is shown in Theorem 3 that none of the Euclidean regular 10−gons is taxicab regular. Also, in Theorem 1, no Euclidean regular $n-$gon ($n > 12$) is taxicab regular, so there is not any Euclidean and taxicab regular $n-$gon for $n = 14,18,22$. Similarly, it can be understood that there is not Euclidean and taxicab regular $n-$gon for $n = 7,9,11$. □

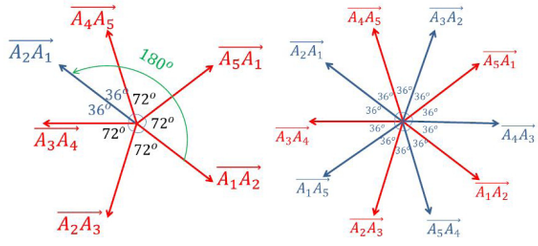

Figure 11.

Theorem 5 *If two symmetry planes of Euclidean regular* $8,6,4,3-$*gons satisfy the following conditions, these polygons are taxicab regular at the same time.*

i) Two symmetry planes are not orthogonal.

ii) At least one of them is on the corners of polygons.

iii) Two symmetry planes are members of

$\{x \mp y = k_1,\ x \mp z = k_2, y \mp z = k_3, x = k_4, y = k_5, z = k_6\}$ *set (for* $1 \le i \le 6,\ k_i \in \mathbb{R}$*)*

Proof. A reflection about the plane set is a taxicab isometry [6]. Let $A_1A_2A_3A_4A_5A_6A_7A_8$ be a Euclidean regular polygon, A_1A_5 and A_2A_6 are symmetry planes. According to the A_1A_5 symmetry plane;

$$d_T(A_1,A_2)=d_T(A_1,A_8),\ d_T(A_2,A_3)=d_T(A_8,A_7)$$
$$d_T(A_3,A_4)=d_T(A_7,A_6),\ d_T(A_4,A_5)=d_T(A_6,A_5) \quad (19)$$

According to the A_2A_6 symmetry plane;

$$d_T(A_2,A_3)=d_T(A_2,A_1),\ d_T(A_3,A_4)=d_T(A_1,A_8)$$
$$d_T(A_4,A_5)=d_T(A_8,A_7),\ d_T(A_5,A_6)=d_T(A_7,A_6) \quad (20)$$

From (19) and (20) equations, it is obtained that taxicab lengths of polygon sides are the same. It is clear that the other symmetry planes can give the same result.
As it is known that the angles between two non-orthogonal symmetry planes of a Euclidean regular 8−gon are 22.5^o, 45^o and 67.5^o (see Figure 12). The angle between $x+z=k_2$ and $x=k_4$ planes is 45^o. Thus, if the following three features are present in the Euclidean regular 8−gon, then it is said to be taxicab regular.
i) Polygon center of gravity is on the intersection line of $x+z=k_2$ and $x=k_4$,
ii) Polygon is orthogonal to $x+z=k_2$ and $x=k_4$,
iii) One of the corner of the polygon on $x+z=k_2$, the other corner on $x=k_4$.
Similarly, other pairs of planes can be found. □

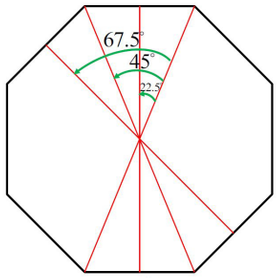

Figure 12.

In addition to Theorem 5, while a regular 8−gon is on one of the $x=k_4$, $y=k_5$, $z=k_6$ planes, the connection between taxicab length and Euclidean length of the sides of the regular 8−gon are researched. As it is shown in Figure 13 the result is researched for $z=0$.

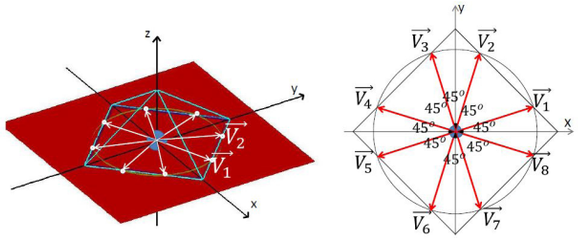

Figure 13.

Let $S_1=(d_T(A_1,A_2),0,0)$ and $S_2=(0,d_T(A_1,A_2),0)$. Midpoint of S_1 and S_2 is $S_{12}=(\frac{d_T(A_1,A_2)}{2},\frac{d_T(A_1,A_2)}{2},0)$ on the taxicab sphere. The angles of $S_{12}\vec{V_1}O$ right triangle are $22.5^o,67.5^o,90^o$ (see Figure 14). Hence,

$$d_E(S_{12},O)=\cos(22,5^o).d_E(V_1,O) \quad (21)$$

and

$$d_E(S_{12},O)=\sqrt{\left(\frac{d_T(A_1,A_2)}{2}\right)^2+\left(\frac{d_T(A_1,A_2)}{2}\right)^2+0^2}$$
$$=\frac{\sqrt{2}}{2}d_T(A_1,A_2) \quad (22)$$

$$d_E(V_1,O)=d_E(A_1,A_2) \quad (23)$$

$$\cos 22,5^o=\frac{1+\sqrt{2}}{\sqrt{4+2\sqrt{2}}}. \quad (24)$$

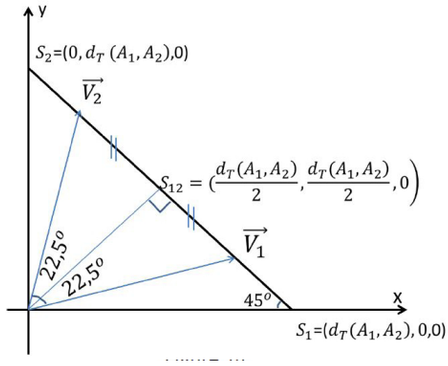

Figure 14.

When equations (22), (23) and (24) are written in (21), the following equation can be found

$$d_T(A_1,A_2)=\frac{\sqrt{2\sqrt{2}+2}}{2}\cdot d_E(A_1,A_2). \quad (25)$$

Since every Euclidean translation of $\mathbb{R}^3$ is an isometry of $\mathbb{R}^3_T$ [6], this result is also the same on $z=k$ $(k\in\mathbb{R})$ planes. Thus, we can give the following corollary.

Corollary 3 *Let $A_1A_2A_3A_4A_5A_6A_7A_8$ be a Euclidean regular polygon on one of the $x=k_1,y=k_2,z=k_3$ planes. If the taxicab length of one of the sides is $\frac{\sqrt{2\sqrt{2}+2}}{2}$ times of the Euclidean length, $A_1A_2A_3A_4A_5A_6A_7A_8$ is also taxicab regular.*

Example 1 *For $A(0,1,0)$, $B(1,0,0)$, $C(0,0,1)$ points, ABC is a triangle. Since*

$$d_E(A,B)=d_E(A,B)=d_E(A,B)=\sqrt{2},$$
$$d_T(A,B)=d_T(A,B)=d_T(A,B)=2$$

ABC is also Euclidean and taxicab regular. Symmetry axes of the triangle are $x-y=0$, $y-z=0$, $x-z=0$.

Symmetry planes are not enough to determine taxicab regular polygons. Because, all the symmetry planes of taxicab regular polygons are not members of

$$\{x\mp y=k_1, x\mp z=k_2, y\mp z=k_3, x=k_4, y=k_5, z=k_6\}$$

set (for $1\leq i\leq 6$, $k_i\in\mathbb{R}$).

Example 2 *For $A(0,0,1)$, $B(-\frac{1}{3},-\frac{1}{3},-\frac{1}{3})$, $C(1,0,0)$ points, ABC is a taxicab regular triangle. But only one of the symmetry planes is a member of*

$$\{x\mp y=k_1, x\mp z=k_2, y\mp z=k_3, x=k_4, y=k_5, z=k_6\}$$

set (for $1\leq i\leq 6$, $k_i\in\mathbb{R}$). Other two symmetry planes are not members.

Corollary 4 *Let $A_1A_2A_3A_4A_5A_6$ be a Euclidean regular polygon on one of the $\pm x\pm y\pm z=k$ planes ($k\in\mathbb{R}$). If the taxicab length of one of the sides is $\sqrt{2}$ times of the Euclidean length, $A_1A_2A_3A_4A_5A_6$ is also taxicab regular.*

Proof. Let $d_T(A_1,A_2)=\sqrt{2}d_E(A_1,A_2)$. The intersection points between $x+y+z=0$ plane and an origin-centered taxicab sphere with a radius of $d_T(A_1,A_2)$ are the midpoints of the 6 edges.

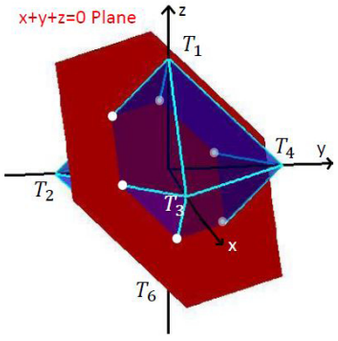

Figure 15.

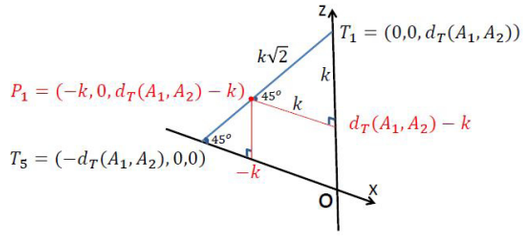

Figure 16.

Also $P_1=(-\frac{d_T(A_1,A_2)}{2},0,\frac{d_T(A_1,A_2)}{2})$. Since

$$d_E(P_1,O)=\sqrt{(-\frac{d_T(A_1,A_2)}{2})^2+0^2+\left(\frac{d_T(A_1,A_2)}{2}\right)^2}$$
$$=\frac{\sqrt{2}}{2}d_T(A_1,A_2),$$

then $d_E(P_1,O)=d_E(A_1,A_2)$. Thus, the intersection points between $x+y+z=0$ plane and an origin-centered Euclidean sphere with a radius of $d_E(A_1,A_2)$ and an origin-centered taxicab sphere with a radius of $d_T(A_1,A_2)$ are the midpoints of the 6 edges. The angle between each consecutive vectors is 60^o (see Figure 17). Thus, the polygon $A_1A_2A_3A_4A_5A_6$ is taxicab regular at the same time. □

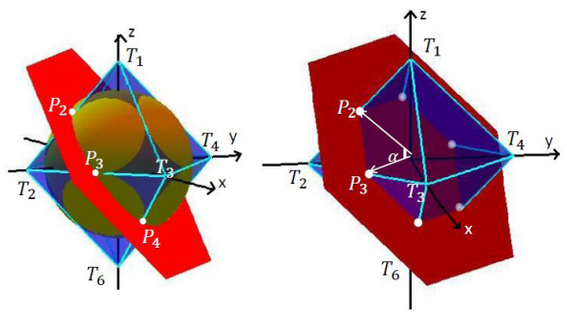

Figure 17.

Example 3 *Let us consider $A_1=(0,0,0)$, $A_2=(0,-1,1)$, $A_3=(1,-2,1)$, $A_4=(2,-2,0)$, $A_5=(2,-1,-1)$, $A_6=(1,0,-1)$. It is clear that $A_1A_2...A_6$ is a Euclidean and taxicab regular 6−gon. Besides, $d_T(A_1,A_2)=\sqrt{2}d_E(A_1,A_2)$ and A_1,A_2,A_3,A_4,A_5,A_6 points are on the $x+y+z=0$ plane.*

Corollary 5 *For $n=3,4$ and 6, $n-$gons on one of the $\pm x\pm y\pm z=k$ planes are Euclidean regular. If the taxicab length of one of the sides is $\frac{3+\sqrt{3}}{3}$ times of Euclidean length, $n-$gon is also taxicab regular.*

Proof. As it is seen in Theorem 2, there are 12 vectors on the same plane with the same taxicab length and the angles between two consecutive vectors are 30^o (see Figure 18).

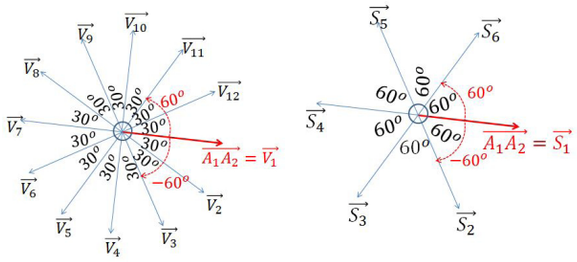

Figure 18.

If we choose 6 vectors whose angles between two consecutive vectors are 60^o, these vectors can create a taxicab regular 6−gon. □

Corollary 6 *Let us consider, $A_1A_2A_3A_4A_5A_6$ is a Euclidean regular polygon on one of the $\pm x \pm y \pm z = k$ planes. If the taxicab length of one of the sides is $\frac{2\sqrt{6}}{3}$ times of the Euclidean length, $A_1A_2A_3A_4A_5A_6$ is also taxicab regular.*

Proof. Let $A_1A_2A_3A_4A_5A_6$ be a Euclidean regular 6−gon on $x+y+z=k$ plane and the taxicab length of the $\overrightarrow{A_1A_2}$ vector is $\frac{2\sqrt{6}}{3}$ times of the Euclidean length. Then $d_T(A_1,A_2)=\frac{2\sqrt{6}}{3}d_E(A_1,A_2)$ and let the intersection points between $x+y+z=0$ plane and a origin-centered Euclidean sphere with a radius of $d_E(A_1,A_2)$ and a origin-centered taxicab sphere with a radius of $d_T(A_1,A_2)$ be $w_i=(x,y,z)$ for $i\in\mathbb{N}$. Then

$$\|\overrightarrow{w_i}\|_T = \frac{2\sqrt{6}}{3}\|\overrightarrow{w_i}\|_E \tag{26}$$

$$|x|+|y|+|z| = \frac{2\sqrt{6}}{3}\sqrt{x^2+y^2+z^2} \tag{27}$$

and

$$x+y+z=0 \tag{28}$$

and

$$\|\overrightarrow{w_i}\|_T = d_T(A_1,A_2) \tag{29}$$

$$|x|+|y|+|z| = d_T(A_1,A_2). \tag{30}$$

Equations (27), (28) and (30) are solved by the Maple math program. As a result, it is found that all points are

$$w_1=(-\frac{d_T(A_1,A_2)}{2},\frac{d_T(A_1,A_2)}{4},\frac{d_T(A_1,A_2)}{4}),$$
$$w_2=(-\frac{d_T(A_1,A_2)}{4},-\frac{d_T(A_1,A_2)}{4},\frac{d_T(A_1,A_2)}{2}),$$
$$w_3=(\frac{d_T(A_1,A_2)}{4},-\frac{d_T(A_1,A_2)}{2},\frac{d_T(A_1,A_2)}{4}),$$
$$w_4=(\frac{d_T(A_1,A_2)}{2},-\frac{d_T(A_1,A_2)}{4},-\frac{d_T(A_1,A_2)}{4}),$$
$$w_5=(\frac{d_T(A_1,A_2)}{4},\frac{d_T(A_1,A_2)}{4},-\frac{d_T(A_1,A_2)}{2}),$$
$$w_6=(-\frac{d_T(A_1,A_2)}{4},\frac{d_T(A_1,A_2)}{2},-\frac{d_T(A_1,A_2)}{4}).$$

It is clear that $\|\overrightarrow{w_i}\|=\|\overrightarrow{w_j}\|$ and $\|\overrightarrow{w_i}\|_T=\|\overrightarrow{w_i}\|_T$ for $1\le i,j\le 6$. Also the angle between $\overrightarrow{w_1}$ and $\overrightarrow{w_2}$ is α and $\alpha=60^o$. Similarly, it can be shown that the angles between $\overrightarrow{w_i}$ and $\overrightarrow{w_j}$ $(1\le i,j\le 6)$ are also 60^o. Therefore, it can be concluded that the Euclidean polygon is a taxicab regular at the same time. □

Example 4 *By using $A_1=(0,0,0)$, $A_2=(3,-6,3)$, $A_3=(9,-9,0)$, $A_4=(12,-6,-6)$, $A_5=(9,0,-9)$, $A_6=(3,3,-6)$ points, we can create $A_2A_3A_4A_5A_6$ Euclidean and taxicab regular 6−gon. Also $d_T(A_1,A_2)=\frac{2\sqrt{6}}{3}d_E(A_1,A_2)$ and all the A_1, A_2, A_3, A_4, A_5, A_6 points are on the $x+y+z=0$ plane.*

Corollary 7 *Let $\overrightarrow{V}\in\{(1,0,0),(0,1,0),(0,0,1)\}$. If there is a rotation whose axis is $\overrightarrow{V}$ between two consecutive sides of a quadrilateral, it is Euclidean and taxicab regular.*

Proof. Let $A_1A_2A_3A_4$ be a Euclidean regular quadrilateral and there is a rotation between $[A_1A_2]$ and $[A_1A_4]$. Since the angle between $[A_1A_2]$ and $[A_1A_4]$ is $\frac{\pi}{2}$, the rotation angle is $\frac{\pi}{2}$. Therefore, the rotation is a taxicab isometry [6]. Thus $d_T(A_1,A_2)=d_T(A_1,A_4)$ and $d_E(A_1,A_2)=d_E(A_1,A_4)$. As a result, the quadrilateral is Euclidean and taxicab regular. □

Corollary 8 *Let $A_1A_2A_3$ be a Euclidean regular triangle on one of the $\pm x\pm y\pm z=k$ planes. If the taxicab length of one of the sides is $\sqrt{2}$ or $\frac{2\sqrt{6}}{3}$ times of the Euclidean length, $A_1A_2A_3$ is also taxicab regular.*

Proof. As it is seen in Corollary 6, there are 6 vectors on the same plane with the same taxicab length and the angles between two consecutive vectors are 60^o. If we choose 3 vectors whose angles between two consecutive vectors are 120^o (see Figure 19), these vectors can create a taxicab regular 3−gon. □

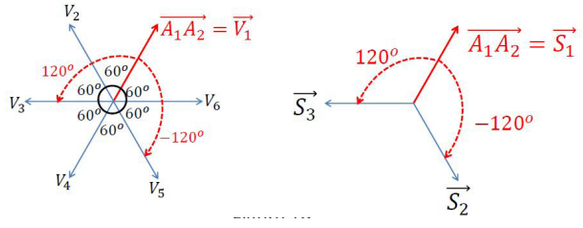

Figure 19.

Example 5 *For $A_1=(1,2,-1)$, $A_2=(4,-4,2)$, $A_3=(7,-1,-4)$ points, ABC is a Euclidean and taxicab regular triangle.*

In addition, $d_T(A_1,A_2)=\frac{2\sqrt{6}}{3}d_E(A_1,A_2)$ and A_1, A_2, A_3, A_4, A_5, A_6 points are on $x+y+z=2$ plane.

Example 6 *For $A_1=(0,0,0)$, $A_2=(0,-1,1)$, $A_3=(1,-1,0)$ points, ABC is a Euclidean and taxicab regular triangle.*

Furthermore, $d_T(A_1,A_2)=\sqrt{2}d_E(A_1,A_2)$ and A_1, A_2, A_3, A_4, A_5, A_6 points are on $x+y+z=0$ plane.

4 Taxicab Regular Polygons in Taxicab 3-Space

Theorem 6 *There do not exist any taxicab regular triangles which are not Euclidean.*

Proof. Let ABC be non-Euclidean taxicab regular triangle. Then $s(\hat{A}) = s(\hat{B}) = s(\hat{C}) = 60^o$. Thus, ABC is a Euclidean regular triangle and this is a contradiction. □

Theorem 7 *There exist taxicab regular* $4-$*gons which are not Euclidean.*

Proof. Draw an origin-centered Euclidean and taxicab sphere with a radius 1 (see Figure 20). Let $P \in]AE[$ line segment.

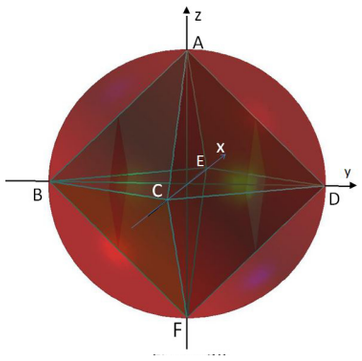

Figure 20.

Since part of line $[OD]$ is perpendicular to the $x = 0$ plane and the AEO triangle is on the $x = 0$ plane, $[OP] \perp [OD]$. Besides, $d_E(O,D) = d_T(O,D) = d_T(O,P) = 1$ but $d_E(O,P) < 1$. Because OPH is a right triangle and $d_E(O,P) < d_E(O,H) + d_E(H,P) = d_T(O,P) = 1$ as it is shown in Figure 21. According to [6] Proposition 3.1, every Euclidean translation is a taxicab isometry. Thus, we can create a non-Euclidean taxicab regular $4-$gon by translating $[OP], [OD]$ parts of the lines as in Figure 22. Since $P \in]AE[$ line segment, there are many P points. Therefore, there exist many non-Euclidean taxicab regular $4-$gons. □

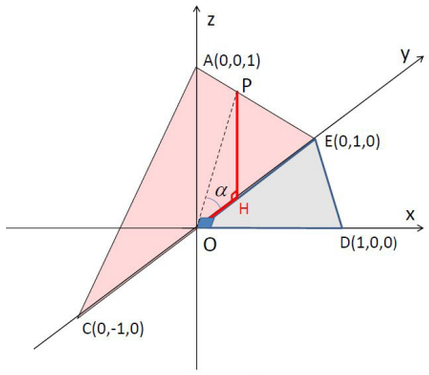

Figure 21.

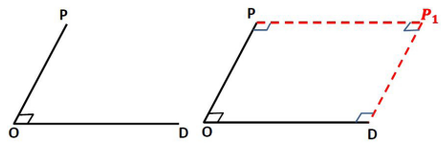

Figure 22.

Example 7 *Let us consider* $A(0,0,0)$, $B(2,0,0)$, $C(2,1,1)$, $D(0,1,1)$ *points. ABCD is a* $4-$*gon. It is clear that;*

$$[AB] \perp [BC], [BC] \perp [CD], [CD] \perp [AD], [AD] \perp [AB]$$

and

$$d_T(A,D) = d_T(B,C) = d_T(A,B) = d_T(C,D) = 2$$

but $d_E(A,D) \neq d_E(A,B)$. *Thus, ABCD is a non-Euclidean taxicab regular* $4-$*gon.*

Theorem 8 *When a line segment is given as a side, it is possible to create a taxicab regular* $2n-$*gons* $(n \geq 2)$ *including the given side.*

Proof. In $\mathbb{R}^3$, let us consider now any given line segment $[A_1A_2]$ in the taxicab plane. Since all the corners of polygons are planar, a plane E must be chosen which includes the given line segment to draw a $2n$-sided polygon (see Figure 23). After then, let us draw an A_1-centered taxicab sphere with a radius of $d_T(A_1,A_2)$ (see Figure 24).

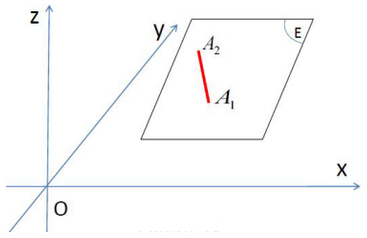

Figure 23.

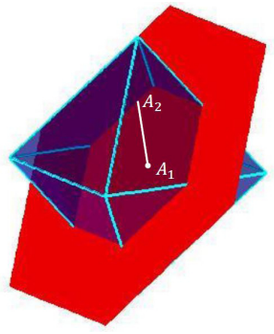

Figure 24.

It is clear that the plane and taxicab sphere intersect. The intersection of a plane and a taxicab sphere is a taxicab circle on plane E as the intersection of a plane and a Euclidean sphere is circle in $\mathbb{R}^3$. It is known that the measure of each interior angle of a regular $2n-$gon is $\frac{\pi(n-1)}{n}$ radians. It is obvious that $(n-1)$ line segments A_iA_{i+1}, $(2 \leq i \leq n)$, having the same taxicab length $d_T(A_1,A_2)$, can be drawn such that the measure of the angle between every two consecutive segments is $\frac{\pi(n-1)}{n}$ radians, by using the taxicab circles with center A_i and a radius of $d_T(A_1,A_2)$, as in Figure 25.

$\measuredangle A_2A_1A_{n+1} + \measuredangle A_nA_{n+1}A_1 = \frac{\pi(n-1)}{n}$. If we continue to draw line segments $A_i'A_{i+1}'$ which are symmetric to A_iA_{i+1}, $1 \leq i \leq n$, about the midpoint of A_1A_{n+1}, respectively, we get a $2n-$gon (see Figure 26). Since the symmetry to a point is taxicab isometry, both taxicab lengths and angle measures are preserved.

Thus, for $1 \leq i \leq n$,

$$d_T(A_i,A_{i+1}) = d_T(A_i',A_{i+1}') = d_T(A_1,A_2) \tag{31}$$

and

$$\begin{aligned}\measuredangle A_1A_2A_3 &= \measuredangle A_{n+1}A_2'A_1 = \ldots \\ &= \measuredangle A_{n-1}A_nA_{n+1} + \measuredangle A_{n-1}'A_n'A_1 = \frac{\pi(n-1)}{n}.\end{aligned} \tag{32}$$

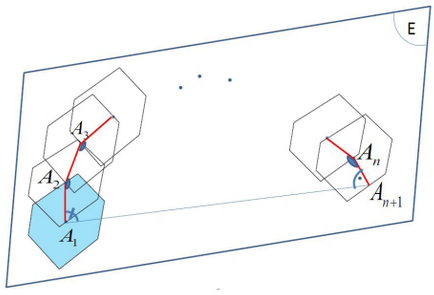

Figure 25.

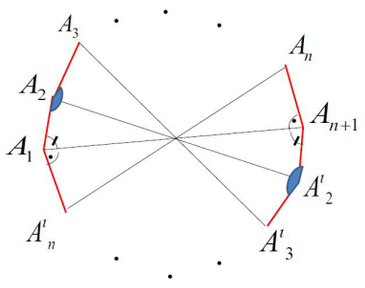

Figure 26.

Due to the equalities (31) and (32), this is a taxicab regular $2n-$gon. Since there are many planes which include the line segment, it is possible that many taxicab regular $2n-$gons can be drawn by using each plane. □

References

[1] Z. Akca, R. Kaya, On the Distance Formulae in Three Dimensional Space, *Hadronic Journal* **27** (2004), 521–532.

[2] Z. Akca, R. Kaya, On the norm in higher dimensional taxicab spaces, *Hadronic Journal Supplement* **19**(5) (2004), 491–501.

[3] H. B. Colakoglu, R. Kay, Regular Polygons in the Taxicab Plane, *KoG* **12** (2008), 27–33.

[4] B. Divjak, Notes on taxicab geometry, *KoG* **5** (2000), 5–9.

[5] C. Ekici, I. Kocayusufoglu, Z. Akca, The Norm in Taxicab Geometry, *Tr. J. of Mathematics* **22**(3) (1998), 295–307.

[6] Ö. Gelişgen, R. Kaya, The taxicab space group, *Acta Mathematica Hungarica* **122**(1–2) (2008), 187-200.

[7] E. F. Krause, *Taxicab Geometry*, Addision-Wesley, Menlo Park, California, 1975.

[8] K. Menger, *You Will Like Geometry*, Guildbook of the Illinois Institute of Technology Geometry Exhibit, Museum of Science and Industry, Chicago, III, 1952.

[9] H. Minkowski, *Gesammelte Abhandlungen*, Chelsa Publishing Co., New York, 1967.

[10] B. E. Reynolds, Taxicab Geometry, *Pi Mu Epsilon Journal* **7** (1980), 77–88.

Süleyman Yüksel
e-mail: suleymanyuksel@gazi.edu.tr
Gazi University, Polatli Arts and Sciences Faculty
Ankara, Turkey

Münevver Özcan
e-mail: mozcan@ogu.edu.tr
Osmangazi University, Department of Mathematics and Computer
Eskisehir, Turkey

Original scientific paper
Accepted 22. 12. 2015.

LÁSZLÓ NÉMETH

Sectrix Curves on the Sphere

Sectrix Curves on the Sphere

ABSTRACT

In this paper we introduce a class of curves derived from a geometrical construction. These planar curves are the generalization of the less-known sectrix of Ceva. We also present three variations of the sectrix curves on the sphere with using the geometrical construction on the sphere, with the stereographic projection and with a so-called "rolled" transformation.

Key words: sectrix, folium, Chebyshev polynomial, curves on sphere

MSC2010: 51N20

Sektrise na sferi

SAŽETAK

U ovom članku uvodimo klasu krivulja izvedenih geometrijskom konstrukcijom. Takve ravninske krivulje su generalizacija manje poznatih Cevinih sektrisa. Također, prikazujemo tri varijacije sektrisa na sferi, koristeći geometrijsku konstrukciju na sferi, stereografsku projekciju i takozvano "valjano" preslikavanje.

Ključne riječi: sektrisa, folium, Chebyshevjev polinom, krivulje na sferi

1 Sectrix on the plane

The Sectrix of Ceva is a less-known planar curve ([7, p. 314-315]), that is defined with the polar equation

$$\rho = a + 2a\frac{\sin k\varphi \cos(k+1)\varphi}{\sin\varphi}, \quad a > 0,\ k \in \mathbb{N},\ \varphi \in [0, 2\pi]. \tag{1}$$

Figure 1 shows its shape where $a = 1$ and $k = 2$. It has two perpendicular axes of symmetry. In this article we use this curve in case $a = 1$.

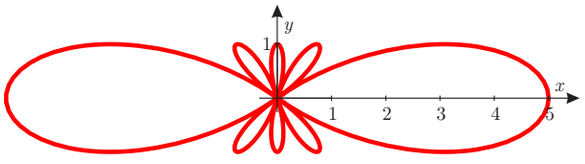

Figure 1: *Sectrix of Ceva ($k = 2$).*

If $k = 1$ then we get the so-called Ceva Cycloid (Figure 2). It was devised by Ceva, who termed it the cycloidum anomalarum ([2, p. 29], [8]). Its polar equation is

$$\rho = 1 + 2\cos 2\varphi,\ \varphi \in [0, 2\pi]. \tag{2}$$

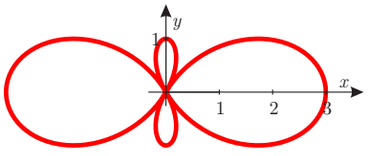

Figure 2: *Ceva Cycloid ($k = 1$ or $n = 2k+1 = 3$).*

In [3] a geometrical construction was defined from which a generalization of sectrix of Ceva comes. Let e be a line given by the origin O and angle α between axis x^+ and e, as the angle of polar coordinates of e (Figure 3). Let the point A_0 coincide with O. Let the point A_1 be given on e such that the distance between the points O and A_1 is 1. Let the point A_2 be on axis x such that the distance of A_1 and A_2 is equal also to 1 and $A_2 \neq O$ if it is possible. Then let the new point A_3 be on the line e again such that $A_2A_3 = 1$ and $A_3 \neq A_1$ if it is possible. Recursively, we can define the point A_i $(i \geq 2)$ on the line e or on axis x if i is odd or even, respectively, where $A_{i-1}A_i = 1$ and $A_i \neq A_{i-2}$ if it is possible. For all α the point A_i exists. Figure 3 shows the first six points. If α is small enough then A_i is between points O and A_{i+2}. Let angle $OA_{i+1}A_i$ be α_i, then $\alpha_i = i\alpha$ can be proved easily. If A_1 is on the axis x we obtain a similar geometric construction (Figure 4). These constructions gave a new proof for some trigonometric connections [5].

The parametric equation system of the orbits of the points in [3] is determined not only when the point A_1 is on line e, but also when it is on axis x. In case of vertices A_n $(n \geq 1)$ the parametric equation system of the curves is

$$\begin{aligned} x_n(\alpha) &= \cos\alpha\, U_{n-1}(\cos\alpha) \\ y_n(\alpha) &= \sin\alpha\, U_{n-1}(\cos\alpha), \end{aligned} \tag{3}$$

and the polar equation of the curves when $\alpha \in [0, 2\pi]$ is

$$\rho_n(\alpha) = U_{n-1}(\cos\alpha), \tag{4}$$

where $U_{n-1}(x)$ is the Chebyshev polynomial of the second kind. (Some orbits can be seen on Figure 3 and 4.) The recursive definition of the Chebyshev polynomials of the second kind $U_\ell(x)$ is

$$U_0(x) = 1,\ U_1(x) = 2x,\ U_{\ell+1}(x) = 2xU_\ell(x) - U_{\ell-1}(x),\ \ell \geq 1. \tag{5}$$

When $|x| \leq 1$ the substitution $x = \cos\varphi$ gives the expressions $\sin\ell\varphi = \sin\varphi\, U_{\ell-1}(\cos\varphi)$ [6].

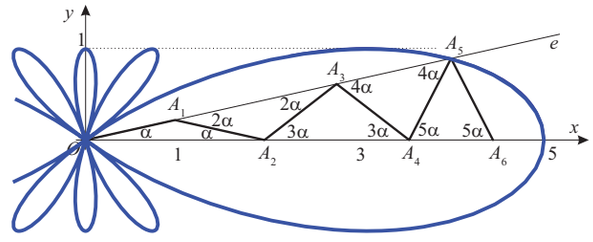

Figure 3: *Generalized sectrix of Ceva in case* $n = 5$.

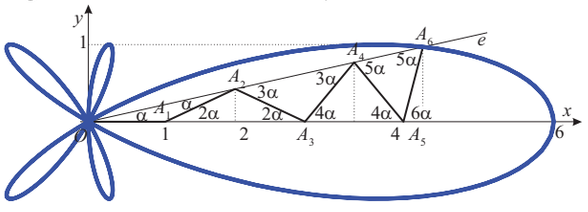

Figure 4: *Generalized sectrix of Ceva in case* $n = 6$.

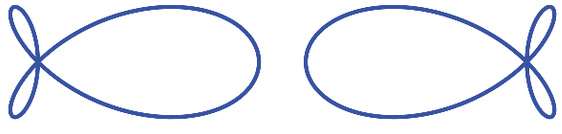

Figure 5: *Folium – curves in case* $n = 4$ and $n = -4$.

Lemma 1 *If* $n = 2k+1$ *the curves defined by equations* (4) *and* (1) *for* $a = 1$ *are the same.* (Compare the Figures 1 and 3.)

Proof. Since

$$\begin{aligned} \sin(2k+1)\alpha &= \sin(k+k+1)\alpha \\ &= \sin k\alpha\cos(k+1)\alpha + \cos k\alpha\sin(k+1)\alpha \\ &= \sin k\alpha\cos(k+1)\alpha \\ &\quad + \cos k\alpha\,(\sin k\alpha\cos\alpha + \cos k\alpha\sin\alpha) \\ &= \sin k\alpha\cos(k+1)\alpha \\ &\quad + \sin k\alpha\cos k\alpha\cos\alpha + \cos^2 k\alpha\sin\alpha \\ &= \sin k\alpha\cos(k+1)\alpha \\ &\quad + \sin k\alpha\,(\cos(k+1)\alpha + \sin\alpha\sin k\alpha) \\ &\quad + \cos^2 k\alpha\sin\alpha \\ &= 2\sin k\alpha\cos(k+1)\alpha + \sin^2 k\alpha\sin\alpha \\ &\quad + \cos^2 k\alpha\sin\alpha \\ &= 2\sin k\alpha\cos(k+1)\alpha + \sin\alpha, \end{aligned}$$

if $\varphi = \alpha$ then we have

$$\begin{aligned} U_{2k}(\cos\alpha) &= \frac{\sin(2k+1)\alpha}{\sin\alpha} = \frac{2\sin k\alpha\cos(k+1)\alpha + \sin\alpha}{\sin\alpha} \\ &= 1 + 2\frac{\sin k\alpha\cos(k+1)\alpha}{\sin\alpha}. \end{aligned}$$

□

The Cartesian equation of curves (without the point in the origin) defined with (3) or (4) is

$$x^2 + y^2 = U_{n-1}^2\left(\sqrt{\frac{x^2}{x^2+y^2}}\right), \tag{6}$$

where $x^2 + y^2 \neq 0$. We extend the equation (6) to negative values n. The definition of the Chebyshev-polynomials for negative indexes with definition (5) is

$$U_{\ell-1}(x) = 2xU_\ell(x) - U_{\ell+1}(x),\ \ell < 1. \tag{7}$$

Now, $U_{-1}(x) = 0$ and $U_m(x) = -U_{-m-2}(x)$, $(m \leq -2)$ and $x^2 + y^2 \neq 0$ implies $n \neq 0$. If $n = 2k+1$ then equation (6) gives the sectrix of Ceva. Otherwise, if $n = 2k$ we get the union of curves in case n and $-n$ (see Figure 5 and 6).

Figure 6: *Union of curves in case* $n = 4$ *and* $n = -4$.

Moreover, the polar equation of folium curve is

$$\rho = \cos\varphi\left(4a\sin^2\varphi - b\right), \quad \varphi \in [0, 2\pi], \tag{8}$$

and the curve defined by equations (4) is the folium curve if $n = -4$ and $a = 2$, $b = 4$, as $U_{-5}(\cos\alpha) = -U_3(\cos\alpha) = -8\cos^3\alpha + 4\cos\alpha = -4\cos\alpha(2\cos^2\alpha - 1) = \cos\alpha(8\sin^2\alpha - 4)$ (see Figure 5).

Here are some Cartesian equations from (6):

- $|n|=1$: $x^2+y^2=1$ (circle)
- $|n|=2$: $(x^2+y^2)^2=4x^2$ (two circles)
- $|n|=3$: $(x^2+y^2)^3=(3x^2-y^2)^2$ (Ceva cycloid, Figure 2)
- $|n|=4$: $(x^2+y^2)^4=16x^4(x^2-y^2)^2$ (union of foliums, Figure 6)
- $|n|=5$: $(x^2+y^2)^5=(5x^4-10x^2y^2+y^4)^2$ (sectrix of Ceva, Figure 1).

The two biggest loops are very similar to the loops of the lemniscates. In Figure 7 we can see that the angles between any two lines m_i $(i=1,\ldots,2n)$ are the multiples of $\pi/(2n)$, where m_i is a tangent line of the curve in the origin or a line goes through the origin and one of the extrema of the curve ($x=n$ or $y=\pm 1$). For some more details, for more figures and for a generalization see [3, 4]. These curves can also be considered as the generalizations of the well-known rose curves (see in [1]).

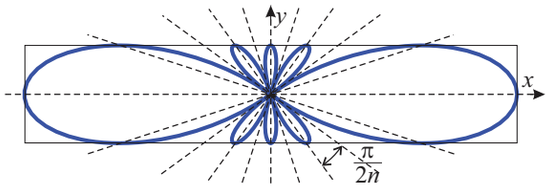

Figure 7: *Curve with some properties in case* $n=5$.

1.1 Sectrix on the sphere

In this subsection we determine the orbit of the point A_n $(n\geq 1)$ with similar conditions as in Section 1 on a sphere. We consider a sphere with radius 1 with equation $x^2+y^2+z^2=1$. Let the axes ξ and ψ of the coordinate system on it, with origin $K(1,0,0)$, be main circles according to Figure 8.

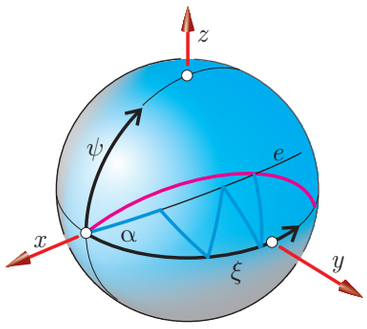

Figure 8: *Construction on the sphere.*

Let e also be a main circle through point K and let the rotation angle between the axis ξ and the "line" e be α, where $0\leq\alpha\leq 2\pi$. Moreover, let the distance between two consecutive points be d, where $0<d<\pi/2$.

Figure 9 demonstrates the construction in a plane with coordinate axes ξ and ψ. (Compare Figures 8 and 9.) Moreover, Figure 9 shows an odd case when A_1 lies on e and $n=5$. Let α_i $(i\geq 1)$ be the angles $A_iA_{i-1}A_{i+1}$ and $A_{i-1}A_{i+1}A_i$ and let $2\beta_i$ be the angle $A_{i-1}A_iA_{i+1}$. (If $\alpha_i<\pi/2$ then the point A_i $(i\geq 2)$ is further from the origin then A_{i-2}.)

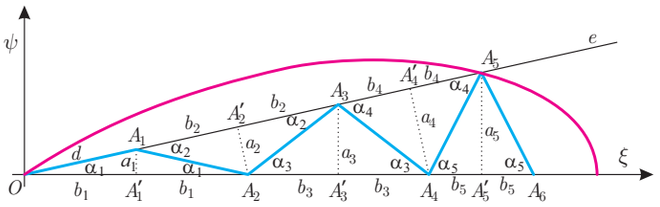

Figure 9: *Construction in the plane with coordinate axes* ξ *and* ψ.

Let the orthogonal projection of A_i to ξ or e in case if i is odd or even, respectively, be A'_i. We denote by b_i and a_i the spherical segments $A_{i-1}A'_i=A_{i+1}A'_i$ and $A_iA'_i$, respectively. Now we determine the angles α_i recursively.

Lemma 2 *If* $i\geq 2$ *then*

$$\alpha_i=\pi-2\beta_{i-1}-\alpha_{i-2},$$

where $\alpha_0=0$, $\alpha_1=\alpha$ *and* $\beta_{i-1}=\operatorname{arccot}(\cos d\tan\alpha_{i-1})$.

Proof: From the triangle $A_0A_1A_2$ we obtain at point A_1 that $\alpha_2=\pi-2\beta_1$ (see Figure 9). We suppose the lemma holds for any j from 2 up to $i-1$. From the triangle $A_{i-2}A_{i-1}A_i$ $(i\geq 3)$ we obtain at point A_{i-1} that $\alpha_{i-2}+\alpha_i=\pi-2\beta_{i-1}$ and by the use of the spherical trigonometric identity

$$\cot\alpha_{i-1}\cot\beta_{i-1}=\cos d$$

in the right angled triangle $A_{i-2}A_{i-1}A'_{i-1}$ we get the lemma. □

From the triangle $A_{i-1}A'_iA_i$ using the spherical trigonometry the next lemma holds.

Lemma 3

$$\begin{aligned}\sin a_i &= \sin d\cdot\sin\alpha_i,\\ \tan b_i &= \tan d\cdot\cos\alpha_i.\end{aligned}$$

Theorem 1 follows from the summation of the lemmas.

Theorem 1 *The equation system of the sectrix on the sphere is*

$$\begin{aligned} x_n(\alpha) &= \cos\psi_n(\alpha)\cos\xi_n(\alpha) \\ y_n(\alpha) &= \cos\psi_n(\alpha)\sin\xi_n(\alpha) \\ z_n(\alpha) &= \sin\psi_n(\alpha), \end{aligned}$$

where

$$\begin{aligned} \xi_n(\alpha) &= \begin{cases} 2(b_1+b_3+\cdots+b_{n-2})+b_n & \text{if} \quad n=2k+1, \\ 1+2(b_2+b_4+\cdots+b_{n-2})+b_n & \text{if} \quad n=2k, \end{cases} \\ \psi_n(\alpha) &= a_n. \end{aligned}$$

We mention that from the triangle OA'_nA_n the equation

$$\sin\xi_n(\alpha) = \cot\alpha\cdot\tan\psi_n(\alpha)$$

gives the implicit connection between the coordinates.

By using the parametric equations from Theorem 1, we obtain the visualizations of the curves in the software *Maple 17* (from *Maplesoft*). In this article, we improve the quality of Maple-graphics by re-rendering in the software *POV-Ray*.

Figures 10–12 show some curves on the sphere in case $n = 3$, 4 and 5.

Figure 10: *Sectrix curve on sphere in case* $n = 3$ *and* $d = \pi/6$.

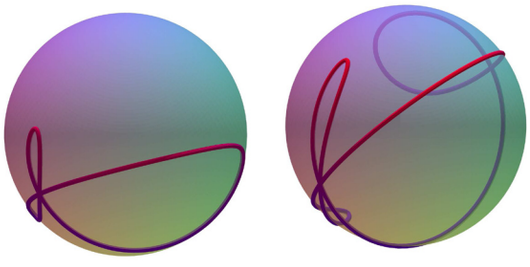

Figure 11: *Sectrix curves on sphere in case* $n = 4$, $d = \pi/6$ *and* $d = \pi/3$.

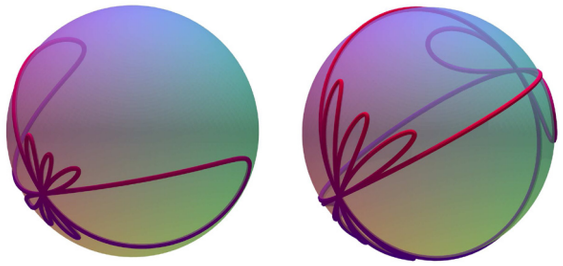

Figure 12: *Sectrix curves on sphere in case* $n = 5$, $d = \pi/8$ *and* $d = \pi/4$.

1.2 Sectrix curves with stereographic projection

We obtain similar curves on the surface of a sphere with the stereographic projection of the sectrix. Let the curve be in plane $z = -R$ and project it from point $N(0,0,R)$ into the sphere with centre $(0,0,0)$ and radius R (Figure 13).

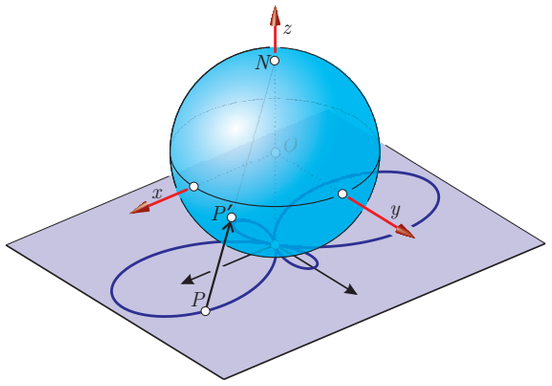

Figure 13: *Stereographic projection.*

In this case one can easily gain that the stereographic projection of a general point $P(x,y,-R)$ from the plane is $P'(cx,cy,1-2c)$, where $c = 4R^2/(x^2+y^2+4R^2)$.

Thus the stereographic projection of the curve with equation (3) is

$$\begin{aligned} x_n(\alpha) &= c(\alpha)\cos\alpha\, U_{n-1}(\cos\alpha), \\ y_n(\alpha) &= c(\alpha)\sin\alpha\, U_{n-1}(\cos\alpha), \\ z_n(\alpha) &= 1-2c(\alpha), \end{aligned} \tag{9}$$

where

$$c(\alpha) = \frac{4R^2}{U_{n-1}^2(\cos\alpha)+4R^2}, \qquad \alpha\in[0,2\pi].$$

Figures 14 and 15 give some examples in case $n = 3$, 4, 5, 6, 7 and 10 where $R = 1$ and in the figures we rotated the curves around axis z for better visualization.

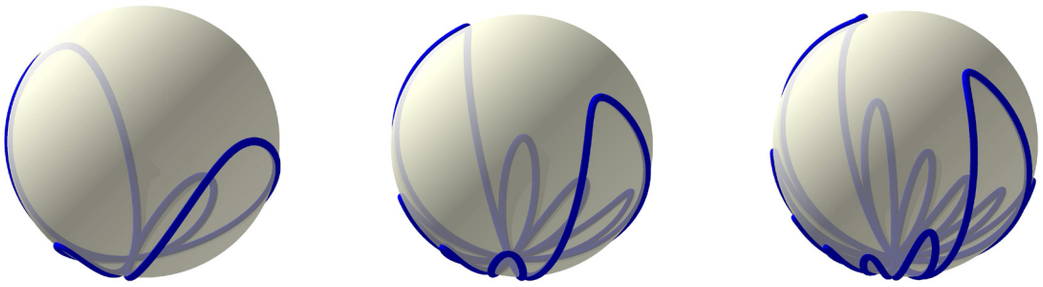

Figure 14: *Stereographic projection of sectrix in case* $n = 3$, 5 *and* 7.

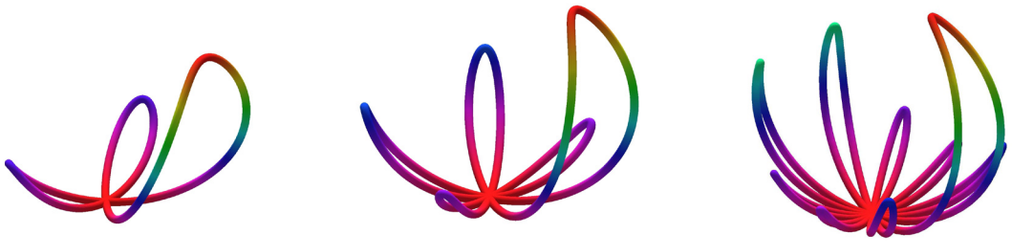

Figure 15: *Stereographic projection of sectrix in case* $n = 4$, 6 *and* 10.

1.3 Rolled sectrix on the sphere

In this subsection we give curves which are "rolled" to sphere. Let the radius of the sphere with centre $O(0,0,0)$ be R and let the plane of sectrix be the plane $z = -R$ (with point $S(0,0,-R)$) according to Figure 16.

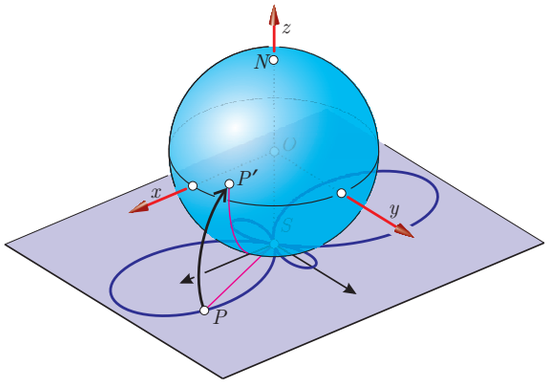

Figure 16: *Rolling of the sectrix onto sphere.*

Let P with parameter α be one of the points of the sectrix defined by (3), take the plane Π incident to the axis z and parallel to direction α (thus P is on Π) and let $P' \in \Pi$ be a point on the sphere so that the length of arc SP' be equal to $\rho_n(\alpha)$ from polar equation (4). In that way we project the point of the sectrix onto the sphere and the equation system of the curves ($\alpha \in [0, 2\pi]$) is

$$\begin{aligned} x_n(\alpha) &= R\cos(r(\alpha))\cos\alpha, \\ y_n(\alpha) &= R\cos(r(\alpha))\sin\alpha, \\ z_n(\alpha) &= R\sin(r(\alpha)), \end{aligned} \tag{10}$$

where

$$r(\alpha) = \frac{U_{n-1}(\cos\alpha)}{R} - \frac{\pi}{2}.$$

Figures 17 and 18 show some examples of the rolled sectrix curves, where the curves are rotated for better visualization.

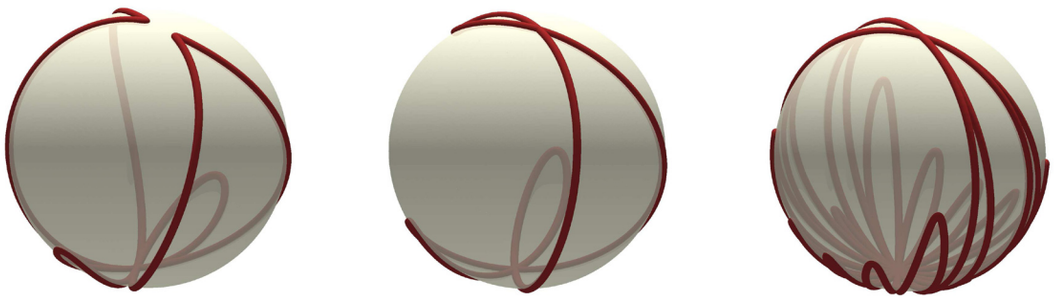

Figure 17: *Sectrix rolled onto sphere* ($n = 3,\ 4,\ 7$ *and* $R = 1$).

Figure 18: *Sectrix rolled onto sphere* ($n = 5,\ 6,\ 9$ *and* $R = 1,\ 2,\ 2$).

References

[1] S. GORJANC, Rose surfaces and their visualizations, *Journal for Geometry and Graphics*, **13**(1) (2010), 1–9.

[2] E. S. LOOMIS, The Cycloid of Ceva. §2.7 in *The Pythagorean Proposition: Its Demonstrations Analyzed and Classified and Bibliography of Sources for Data of the Four Kinds of Proofs*, 2nd ed. Reston, VA: National Council of Teachers of Mathematics, (1968), 29–30.

[3] L. NÉMETH, A new type of lemniscate, *NymE SEK Tudományos Közlemények XX.* Természettudományok 15. Szombathely, (2014), 9–16.

[4] L. NÉMETH, Rose curves with Chebyshev polynomials, *Journal for Geometry and Graphics*, **19**(2), (2015), 219–226.

[5] L. NÉMETH, A geometrical proof of sum of $\cos n\varphi$, *Studies of the University of Žilina, Mathematical Series*, **27** (2015), 63–66.

[6] T. J. RIVLIN, *Chebyshev polynomials*, New York Wiley (1990).

[7] E. V. SHINKIN, *Handbook and Atlas of Curves*, CRC Press (1995).

[8] E. W. WEISSTEIN, "Cycloid of Ceva". From MathWorld–A Wolfram Web Resource. `http://mathworld.wolfram.com/CycloidofCeva.html`

László Németh
e-mail: nemeth.laszlo@emk.nyme.hu

Institute of Mathematics
University of West Hungary
9400 Sopron, Ady E. u. 5, Hungary

Original scientific paper
Accepted 31. 12. 2015.

BLAŽENKA DIVJAK
MARCEL MARETIĆ

Geometry for Learning Analytics

Geometry for Learning Analytics

ABSTRACT

Learning analytics is focused on the educational challenge of optimizing opportunities for meaningful learning.

Assessment deeply influences learning, but at the same time data about assessment are rarely considered and utilized by learning analytics.

Current approaches to analysis and reasoning about peer-assessment lack rigor and appropriate measures of reliability assessment. Our paper addresses these issues with a geometrical model based on the taxicab geometry and the use of the scoring rubrics.

We propose and justify measures for calculation of the final grade in peer-assessment and related inter-rater and intra-rater reliability measures. We present and discuss a geometrical model for two important peer-assessment scenarios.

Key words: taxicab geometry, metrics, learning analytics

MSC2010: 53A35, 91E45, 97B10

Geometrija za analitike učenja

SAŽETAK

Analitike učenja usredotočene su na obrazovne izazove vezane uz postizanje svrsishodnog učenja. Vrednovanje postizanja ishoda učenja izrazito utječe na učenje. Međutim, podaci o procesu vrednovanja vrlo rijetko se koriste u postojećim analitikama učenja. Nadalje, postojeće implementacije i analize procesa istorazinskog (vršnjačkog) vrednovanja nisu zadovoljavajuće. Ovaj rad predstavlja izradu i upotrebu matematičkog modela za opis i računanje vezano uz istorazinsko vrednovanje. Razvijeni model zasniva se na Manhattan (taxicab) metrici te korištenju rubrika za vrednovanje ishoda učenja. U radu su opisane i opravdane metode računanja konačne ocjene vršnjačkog vrednovanja, mjere pouzdanosti takvog vrednovanja kao i ocjene za pojedine vrednovatelje. Razvijeni geometrijski model razmatran je u kontekstu dva važna scenarija istorazinskog vrednovanja.

Ključne riječi: taxicab geometrija, metrika, analitika učenja

1 Introduction and motivation for research

1.1 Learning analytics and related challenges

Learning analytics (LA) belongs to interdisciplinary scientific fields connected to educational sciences and technology enhanced learning that has emerged rapidly in last five years. The most cited definition of LA is "*Learning analytics is the measurement, collection, analysis and reporting of data about learners and their contexts, for the purposes of understanding and optimizing, learning and the environment in which it occurs*". In [8] it is stated that the definition comes from the first international Conference on Learning Analytics and Knowledge (LAK 2011) and adopted by the *Society for Learning Analytics Research* (SoLAR). Further, Ferguson in [8] states that LA is focused on the educational challenge: *How can we optimize opportunities for online learning?* Even better, we should look for opportunities for *meaningful* learning.

Research methods and methodology in LA are still very much under development. There is a great opportunity for mathematicians to contribute to development of various kind of measures and the research of mathematical models. There is a vocal support for broadening the scope and usefulness of LA and special issue in LA is research in student assessment (cf. [5]).

1.2 Assessment and reliability measures

Assessment is of fundamental importance to students. It deeply influences learning. At the same time assessment data are rarely utilized by learning analytics. One of the possible reasons is that available data is not granular enough. Fundamental issues of peer-assessment are reliability and validity (cf. [7]). Research on indicators and metrics to be potentially used in the context of reliability and validity of assessment, peer-assessment and self-assessment, is (currently) very limited.

1.2.1 MOOC, online learning context

Completely new playground for learning analytics the so called *networked learning* [14], e.g. Massive Open Online Courses (MOOCs), social learning platforms, online learning and e-learning in general. In networked learning the number of participants rapidly increases as well as the interactions between learners in the form of discussions and mutual learning. Dealing with tens of thousands of learners in one MOOC it is very natural/appropriate to use self-assessment for tasks leading to a certificate. This approach generates huge amount of assessment data but also asks for sound metrics for calculation of final grade and for estimates on the reliability of assessment. For our work in this paper it brings forwards challenging scenario when we have inexperienced evaluators (scenario A). In this case we will demand more peer-evaluations per assignment to attain sufficient reliability. The second discussed scenario corresponds to a situation with expert (or experienced) evaluators assessing a complex problem solving task. Here we must take into account that experts' time is expensive and their judgments, but their evaluations can be trusted (scenario B). A number of assessments per assignment can be lower in scenario B. Further, in scenario B we can anticipate for situations that some evaluators are experts for only some of the assessment criteria. For example, an expert in project management and scheduling can skip assessment for criteria on financial regulation if he/she lacks the required expertise.

1.2.2 Educational Rubrics

In order to increase transparency of assessment criteria and validity of assessment us of a scoring rubric is highly recommended (cf. [12]). Further, data from the rubric can be analyzed and utilized for estimation of reliability. Among several sets of assessment data, [5] mentions "*achievement mapped against explicit learning outcomes or assessment criteria (e.g. rubric results)*".

A widespread definition of the educational rubric describes it as *a scoring tool for qualitative rating of authentic or complex student work* [12]. A rubric consists of grading criteria and standards of attainment for those criteria (examples: [3, 4]).

Using rubrics provides several benefits such as increased consistency of assessment, attainment of the desired validity in assessment without sacrificing the need for reliability and promotion of learning [12].

Previous research claims that the use of rubrics in mathematics supports students' reflection and critical skills (deep learning) by clearly communicating what is asked from them [3].

Table 1 illustrates the scoring rubric for one criterium (whole scoring rubric is available in [3]). It refers to an assignment in a mathematics course where student had to relate a real world problem to the course material.

Rubrics are especially useful when more than one teacher/student is involved in the process of assessment. Grading can then be implemented as a combination of teacher's grading and automated grading. Rubrics are also vital in the case of a complex task assessment including problem-based learning, group work or peer-assessment that are authentic to the skills being tested (cf. [3]). Peer-assessment is a process where students grade assignments or tests of their peers based on teacher's benchmarks (cf. [16]).

Peer-assessment has several advantages over traditional (teacher) assessment and a few very strong disadvantages – comprehensively described and systematized in [4]. One known disadvantage is the so called "*reliability risk*" introduced by the fact that students are assessing their own peers – some of whom may be their friends. The teacher must be aware of the included risks and anonymize assessment tasks whenever possible (see [4]). Influential papers [12, 16] claim that the measurement of reliability is a problem for both peer-assessment *and* the use of scoring rubrics.

Table 1: *An example: Grading the "problem description"-criterium with a rubric (only one row of the rubric is shown)*

	0 points	1 points	2 points	3 points
problem description	*poor description, irrelevant context*	*problem is described but has no connection to the prescribed context*	*description of the problem is presented in a clear and interesting fashion but lacks the relevant context*	*problem is described in a clear and interesting fashion and is positioned/placed in a relevant real context*
⋮	...	...	...	...

We have to be aware that at this moment most teachers just use the available software (like Moodle Workshop) oblivious whether of the fact that the embedded metrics are not well justified or even missing (cf. [17]). Our paper addresses these problems with a geometrical model based on the taxicab geometry.

1.3 Research questions

We pose three research questions.

RQ1: How to model and implement the grading process for peer-assessment?

RQ2: How to calculate the grade in peer-assessment?

RQ3: What are the appropriate inter-rater (agreement among graders) and intra-rater (accuracy of a single grader for his several grading efforts) measures for peer-assessment?

In the following sections we are going to answer above-mentioned research questions.

2 RQ1 – Problem description and modeling

Let us assume that students' assignments are graded with the help of a scoring rubric with n criteria. Students participate in an activity for which they are graded by their peers. Each participant is asked to grade several (i.e. 3) assignments, and consequently each student should receive several gradings for his own assignment.
The set of participating students is enumerated and we speak of student k, or assignment k (instead of the assignment of student k).

A particular grading is represented as a point in an n-dimensional vector space. Let $\mathcal{S}_k = \{S_k^1, \ldots, S_k^m\}$ denote a set of gradings for assignment k where

$$\begin{aligned} S_k^1 &= (c_{k,1}^{(1)}, \ldots, c_{k,n}^{(1)}) \\ S_k^2 &= (c_{k,1}^{(2)}, \ldots, c_{k,n}^{(2)}) \\ &\vdots \\ S_k^m &= (c_{k,1}^{(m)}, \ldots, c_{k,n}^{(m)}). \end{aligned}$$

Optionally, some assignments receive teacher's grading

$$T_k = (c_{k,1}^T, \ldots, c_{k,n}^T).$$

It is expected to have the teachers grade only a selection of assignments. If present, teacher's grading T_k is taken as a proper (final) grade for assignment k. The intent is to have teachers intervene (providing T_k) only in cases where received peer-assessments for a task k are indicated/detected as unreliable.

Without the loss of generality we assume nonnegative grades $c_{i,j}^{(k)} \geq 0$. Ranges of points for criteria C_i are determined by the scoring rubric. We encode this as coordinates of a range vector

$$\mathbf{r} = (r_1, r_2, \ldots, r_n). \tag{1}$$

Values r_i communicate the relative weights of criteria C_i and must be carefully determined in advance during the design of the scoring rubric.

We need to calculate:

- the final grade for the assignment
- the measure for (inter-rater) reliability of gradings given for an assignment k (as deviation/divergence of the gradings)
- the assessment of the quality of gradings of a particular grader – (intra-rater, for "grading the grader").

Inter-rater reliability measures agreement among graders for grading the same assignment. Intra-rater reliability tells how good of a grader some is – it measures how k's performed gradings agree with other (final) grades for these assignments.

Remark 1. *A* 3*-dimensional array is needed for storing* $c_{i,j}^{(k)}$ *data. For example, data of* 2000 *records is needed if* $m = 4$ *(number of desired peer gradings),* $p = 100$ *(class size) and* $n = 5$ *(number of rubrics criteria).*
In a MOOC setting a reality is to have data of millions of record.

2.1 Taxicab geometry

Taxicab geometry is one of non-Euclidean geometries introduced by Hermann Minkowski (1864 – 1909) at the turn of the 20-th century.
H. Minkowski described a set of metrics that can be used to measure distance and which satisfies the axioms of the metric space. These metrics are induced by the so called p-norms defined for every $p \in \mathbb{R}$, $p \geq 1$ as real scalar functions in n-dimensional space.
Let $\mathbf{x}, \mathbf{y} \in \mathbb{R}^n$ with $\mathbf{x} = (x_1, x_2, \ldots, x_n)$, $\mathbf{y} = (y_1, \ldots, y_n)$.
p-norm for $p \geq 1$ is defined by

$$\|\mathbf{x}\|_p = \left(\sum_{i=1}^{n} |x_i| \right)^{\frac{1}{p}}, \tag{2}$$

which induces the associated p-metric

$$d_p(\mathbf{x}, \mathbf{y}) = |\mathbf{x} - \mathbf{y}|_p. \tag{3}$$

Specifically, for $p = 1$ the induced metric is

$$d_1(\mathbf{x},\mathbf{y}) = \sum_{i=1}^{n} |x_i - y_i| \ ,$$

better known as taxicab or Manhattan distance.

Taxicab geometry was named by Karl Menger in 1952. at the exhibit at the Museum of Science and Industry of Chicago. The justification for the name is straightforward – it measures distances traveled by a car in a city whose streets are laid out in a rectangular grid. Note that the shortest path in taxicab geometry is not unique (see Fig. 1).

For $\mathbf{x},\mathbf{y} \in \mathbb{R}^n$, $1 < r < p$, the following inequality holds

$$\|\mathbf{x}\|_p \leq \|\mathbf{x}\|_r \leq n^{\frac{1}{r}-\frac{1}{p}} \|\mathbf{x}\|_p \,, \tag{4}$$

meaning that p-norms are equivalent. Specifically, this gives

$$d_2(\mathbf{x},\mathbf{y}) \leq d_1(\mathbf{x},\mathbf{y}) \leq \sqrt{n} \cdot d_2(\mathbf{x},\mathbf{y}). \tag{5}$$

Euclidean distance to a taxicab driver represents air distance, e.g. it provides a lower bound for the length of a minimal trip between A and B. On the other hand, taxicab distance *is the exact* distance that needs to be traveled from A to B in a grid.

The taxicab metric d_1 will be denoted as d from now on.

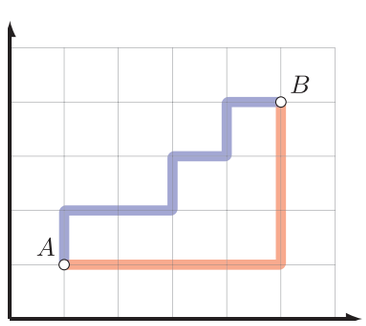

Figure 1: *2-dimensional illustration of shortest taxicab paths between A, B*

Hypersphere in the n-dimensional taxicab space with center $C(c_1, c_2, \ldots, c_n)$ and a radius r is a locus of points satisfying

$$\sum_{i=1}^{n} |x_i - c_i| = r \ . \tag{6}$$

A 2-dimensional taxicab circle is shown inscribed in the Euclidean circle of the same radius in the Fig. 2.

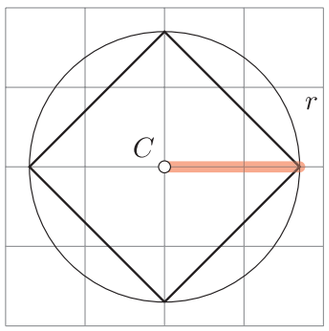

Figure 2: *Euclidean and taxicab 2-dimensional sphere with center C and radius r*

We argue that taxicab metric is adequate as a foundation for our model of LA of peer-assessment as possible rubric gradings are points laid out in hyper-rectangular grid. Taxicab metric is (topologically) equivalent to (but simpler than) Euclidean metrics. It is linear, e.g. distance on the criteria level contributes exactly the same amount to the total taxicab distance.

Finally, the total amount of points awarded for an assignment with a final grade $G = (g_1, \ldots, g_n)$ is exactly the 1-norm of G

$$|G| = g_1 + g_2 + \cdots + g_n \ , \qquad g_i \geq 0. \tag{7}$$

3 RQ2 – How to calculate the final grade in peer-assessment?

We propose and analyze two approaches for the calculation of the final grade. Let $\mathcal{S} = \{S_k^1, \ldots, S_k^m\}$ denote a set of peer gradings for assignment k.

3.1 Mean value final grade

Traditionally the final grade is calculated as an arithmetic mean of available gradings:

$$M(\mathcal{S}) = (a_1^f, \ldots, a_n^f), \quad \text{where} \quad a_i^f = \frac{1}{m}\left(\sum_{j=1}^{m} c_{k,i}^{(j)}\right). \tag{8}$$

$M(\mathcal{S})$ is a center of mass of the set $\mathcal{S}$. Mean value final grade is sensitive to all available data (gradings). We can say that it is mostly sensitive to quantity, and less sensitive to extremes (outliers). Mean value final grade "*respects the decision of the majority*". More data produces better results. We consider it appropriate for scenario A.

3.2 Optimal final grade

We define $W(\mathcal{S})$ and $B(\mathcal{S})$

$$W(\mathcal{S}) = (w_1, \ldots, w_n), \qquad w_i = \min_j c_{k,i}^{(j)},$$

$$B(\mathcal{S}) = (b_1, \ldots, b_n), \qquad b_i = \max_j c_{k,i}^{(j)},$$

as amalgamation of the worst received grades (W) and best received grades (B) respectively. We define the **optimal final grade**

$$O(\mathcal{S}) = (o_1^f, \ldots, o_n^f), \quad \text{where} \quad o_i^f = \frac{1}{2}\left(W(\mathcal{S}) + B(\mathcal{S})\right) . \tag{9}$$

Optimal final grade takes into consideration (is sensitive to) extremes: e.g. additional gradings within an axis-aligned hyperrectangle (box, see Fig. 3) encompassing the set $\mathcal{S}$ have no effect on a_k^f.

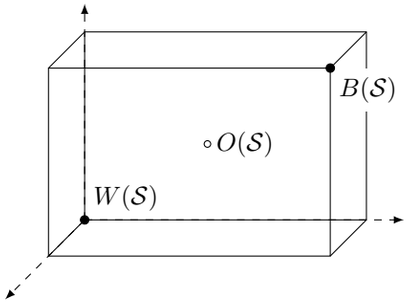

Figure 3: *A sketch of a 3-dimensional axis-aligned hyperrectangle*

Note that $W(\mathcal{S})$ and $B(\mathcal{S})$ as two juxtaposed vertices uniquely determine the hyperrectangle encompassing $\mathcal{S}$.

This approach is inspired by the TOPSIS method (*Technique for Order of Preference by Similarity to Ideal Solution*) in multi-criteria decision making (cf. [10]).

We find the optimal final grade approach adequate in situations where grading is performed by experts (i.e. several teachers), of whom abnormal/wild gradings are not expected (scenario B). After only a few expert gradings additional gradings should have little to no effect on the final grade. Expert's costs rise linearly, but benefits wane quickly. For this reason a balance must be struck to avoid overloading the experts with a workload that will have no effect.

3.2.1 Relative position of $M(\mathcal{S})$ and $O(\mathcal{S})$

$M(\mathcal{S})$ is positioned within the axis-aligned hyperrectangle encompassing $W(\mathcal{S})$, $B(\mathcal{S})$. Therefore

$$|M(\mathcal{S}) - O(\mathcal{S})| \leq \frac{1}{2}|B(\mathcal{S}) - W(\mathcal{S})| = \frac{1}{2}\left(|B(\mathcal{S})| - |W(\mathcal{S})|\right) \tag{10}$$

Relatively large $|M(\mathcal{S}) - O(\mathcal{S})|$ indicates a skewed data $\mathcal{S}$ with majority of data standing opposite to an outlier point.

The inequality

$$0 \leq \frac{2|M(\mathcal{S}) - O(\mathcal{S})|}{|B(\mathcal{S})| - |W(\mathcal{S})|} \leq 1 \tag{11}$$

resulting from (10) can be utilized for a normalized measure of skewness of the set $\mathcal{S}$.

Remark 2. *When teacher grading T_k is present, T_k is taken as a proper grade for assignment k.*

Example 1. *Grading set $\mathcal{S} = \{S_k^1, S_k^2, S_k^3\}$ for assignment k is given in the following table:*

	C_1	C_2	C_3	C_4	Σ
S_k^1	3	0	2	2	7
S_k^2	2	1	3	3	9
S_k^3	2	1	3	2	8

We can calculate the final grade for assignment k with (8) *and* (9)*:*

$$M(\mathcal{S}) = \frac{1}{3}(7,2,8,7), \quad |M(\mathcal{S})| = 8, \tag{12}$$

$$O(\mathcal{S}) = \frac{1}{2}\left((2,0,2,2) + (3,1,3,3)\right) = \frac{1}{2}(5,1,5,5), \quad |O(\mathcal{S})| = 8. \tag{13}$$

Note that looking at the total grade these assessment match, but they are far from agreement on granulated grades. Summative difference is 2*. Obviously, final grades can differ if calculated with mean and optimal value final grade. But, it can happen, as illustrated by this example, that agreement among evaluators is low.*

Suppose a teacher intervenes with

	C_1	C_2	C_3	C_4	Σ
T_k	2	1	2	2	7

.

Now T_k is a proper (final) grade for assignment k.

Gradings closer to the final grade (which is T_k in this case) are considered to be of better quality, and respective graders should be rewarded with more points for grading well. Here, for example, S_k^3 is the closest to the final grade T_k with $d(S_k^3, T_k) = 1$. S_k^1 and S_k^2 both have taxicab distance from T_k of 2 points.

4 RQ3 – What are the appropriate inter-rater and intra-rater measures for peer-assessment?

Main objectives regarding RQ3 are:

i. detection of inadequate grading set by measuring the agreement within a grading set,

ii. grading (rewarding) the grader proportionally to the measure quality of his effort.

4.1 The need for higher granularity of assessment data

We illustrate this with an example of "bad" grading that is visible only when analyzed at the higher level of detail.

Example 2. *Let's consider example gradings S_1 and S_2:*

	C_1	C_2	C_3	C_4	$\sum$	
S_1	3	0	2	2	7	summative
S_2	1	1	3	3	8	$\Delta = 1$
	granular					
	$d(S_1,S_2) = 5$					

Difference of totals (summative difference) for S_1 and S_2 is only 1 point, but the taxicab distance (sum of differences) is 5 points. Although gradings S_1 and S_2 seem coherent at the summative level, these gradings indicate a low quality of assessment(s) when observed at greater level of detail (criteria level).

We will use a set diameter as a measure for detection of inconsistent gradings. Grading set with a large diameter suggests inconsistent and possibly unreliable peer-assessment.
A **diameter** of a set of gradings $\mathcal{S} = \{S_1, \ldots, S_n\}$ is defined as
$\texttt{diam}\,\mathcal{S} = \max_{i,j} d(S_i, S_j)$.

$\texttt{diam}\,\mathcal{S}$ is also a diameter of a sphere encompassing $\mathcal{S}$. Note that, unlike in the Euclidean geometry, the encompassing sphere of the set $\mathcal{S}$ is *not* unique (see Fig. 4).
Any sphere of diameter $d(A,B)$ within the lightly shaded region of Fig. 4 is an encompassing sphere of $\{A,B\}$. This region is the intersection of two taxicab hyperspheres of radius $d(A,B)$ with centers A and B.

Let $e > 0$. A grading $\mathcal{S}$ is **acceptable** for an acceptable error e if the radius of the smallest encompassing sphere of $\mathcal{S}$ is smaller than e, i.e. if
$\texttt{diam}\,\mathcal{S} < 2e$.

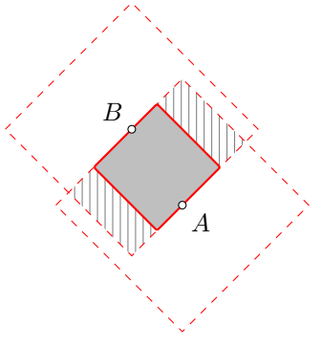

Figure 4: *Encompassing taxicab sphere for A, B*

4.2 Normalization

For the purpose of standardization (for comparison of results) and for easier application and interpretation of results by non-expert users (where acceptable error e can be set and recommended on a normalized $[0,1]$ scale) we introduce the normalization of the taxicab norm.
We define the norm $|\ |'$ for the points within the hyper-rectangle encompassing O and $\mathbf{r}$

$$|\mathbf{a}|' = \frac{1}{|\mathbf{r}|}\left(a_1, \ldots, a_n\right) , \tag{14}$$

where $\mathbf{r}$ is the range vector (see equation (1)). Both $|\ |'$ and the induced metric $|\mathbf{x}-\mathbf{y}|'$ map to $[0,1]$ on the $(O,\mathbf{r})$-hyper-rectangle.

Since relative weights of criteria have already been taken into account in the design phase of the scoring rubric the normalization is simple. Any concerns about disparate sizes of r_i in some rubrics have to be addressed during the design of the scoring rubric.

Now we can use the relative acceptable error $e' = \frac{e}{|\mathbf{r}|}$ instead of e.

5 Implementation of the grading process

5.1 Simple grading process

Let $e > 0$ be acceptable error. Let $\mathcal{S}$ be a grading set for assignment k. Let g be a grading method (mean value final grade or optimal final grade).
If $\mathcal{S}$ is acceptable, a final grade $g(\mathcal{S})$ is assigned for assignment k. If $\mathcal{S}$ is not acceptable, we ask for teacher's grading.

5.1.1 Advantages and disadvantages of the simple grading process

In a situation with a cluster of gradings of poor quality, a single grading of good quality can be enough to demand

supervision (and rectify the situation). Also, simple grading is computationally very simple (of linear complexity). On the other hand, one outlying grading is enough to "spoil" the grading set. Therefore, simple grading process demands supervision even when it would be easy to detect and eliminate an outlier.
Simple grading does not scale well. It can quickly become too work-intensive and overwhelming for the teacher even when the majority of gradings is performed by the peers and LMS. Simple grading is adequate for a face-to-face blended classroom and online classes of manageable size (scenario A).

5.2 Autonomous approach to grading

For scenario B we suggest a semi-autonomous approach – where we search for a maximal acceptable subset $\mathcal{S}'$ of $\mathcal{S}$ of minimal diameter. We must set the lower bound N (critical size) for $\#(\mathcal{S}')$ (number of assessments in $\mathcal{S}'$). Teacher's intervention will be asked for only if no such $\mathcal{S}'$ can be found.

This approach is described step-by-step in algorithm 1.

Algorithm 1: Semi-autonomous Grading Process

input : Set of gradings $\mathcal{S} = \{S^{(1)}, \ldots, S^{(m)}\}$,
acceptable error $e \geq 0$
grading calculation method g
critical size N (i.e. $N = 3$)

output: Final grade or indicate gradings $\mathcal{S}$ as invalid

find a maximal $\mathcal{S}' \subseteq \mathcal{S}$ with acceptable error
if $\#(\mathcal{S}') \geq N$ **then**
  find $\mathcal{S}''$ of minimal diameter such that $\#(\mathcal{S}'') = \#(\mathcal{S}')$
  return $g(\mathcal{S}'')$ as a proper grade for assignment k
else
  Ask for teacher intervention (grading)

5.2.1 Advantages and disadvantages of the semi-autonomous grading process

One outlying grading is not enough to "spoil" the computed grade. Discarding this grade can produce an acceptable set $\mathcal{S}'$ from which the final grade can be computed.
However, a cluster of bad gradings can prevail without demanding supervision, resulting in the wrong final grade being awarded. Additionally, as our intent is to reward good graders, in the case when good graders form a smaller cluster, they could even be unfairly "penalized" for their effort. Autonomous grading is somewhat computationally more intensive than the alternative method (`diam` for pairwise distances must be calculated for each subset tested).

Remark 3. *Note that $\mathcal{S}$ declared acceptable by the simple approach is also acceptable by algorithm 1. Therefore, we may consider that the simple method reflects the cautious approach to the grade calculation, whereas algorithm 1 attempts to be as autonomous as possible.*

Remark 4. *$\mathcal{S}$ with a tight cluster of gradings of poor quality passes as acceptable by both approaches. A good practice would be to give the student the opportunity to contest the received final grade as a safety net for catching errors.*

6 RQ3 –How to model the evaluation for peer-assessment?

Let $G_1, \ldots, G_m$ be gradings of different assignments performed by student k. Let F_i be a final grade for the task graded by G_i (F_i and G_i are grades for assignment i). Let $e > 0$ be radius of acceptable grading (acceptable error). Let $d_i = d(G_i, F_i)$.

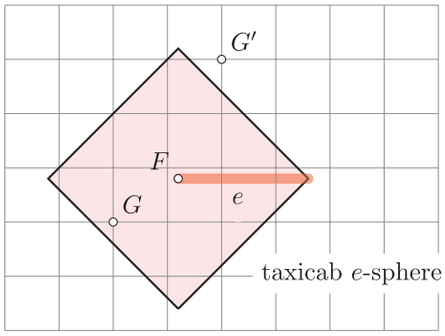

Figure 5

Fig. 5 shows an example of an e-sphere around F with two peer-assessments G i G'. The idea is to award the student who produced grading G that lies within the sphere proportional to $e - d(F,G)$. On the other hand, a student who produced grading G' will not receive points for his grading because G' lies outside of this sphere.

If we intend to award a maximum of A points for the task of peer-assessment grader k can be awarded A_i points for his grading G_i, where A_i is calculated by the following formula

$$A_i(d_i) := \begin{cases} \frac{A}{me}\left(e - d_i\right), & d_i < e \\ 0, & d_i \geq e \end{cases}.$$

If G_i is within the e-sphere around F_i, student k is rewarded an amount of points proportional to $(e - d_i)$ for each G_i for a maximum of A/m (see fig. 6).

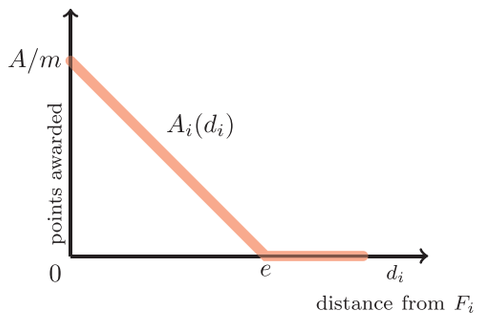

Figure 6: *Award A_i for grading G_i with $d_i = d(G_i, F)$*

Finally, grader k is awarded a total of $A(k)$ points for his effort with gradings $G_1, \ldots, G_m$ where $A(k) = \sum_{i=1}^{m} A_i(d_i)$.

6.1 Analysis of acceptable error

e must be set in advance (arbitrarily). But after all the data has been collected (after peer-assessment) we can analyze e to see how good was our aim for e. More precisely, we could analyze what would be the expected gain of "lazy" peer-assessment.

A good practice in general for addressing this issue is to ask for mandatory written argumentation/explanation along each grade in peer-assessment.

Remark 5. *We have analyzed data gathered in a course UPC at FOI, University of Zagreb. We argue that grading at the summative level is not granular enough for making judgments about the quality of the grade, as was illustrated in example 2.*

Calculated Pearson correlation of summative and granular difference for data in our case study is 0.57. This indicates that a significant proportion of gradings may seem reliable at the summative level, while being inconsistent at the criteria level (the exact proportion is 12/62 for the UPC course).

7 Conclusion and future research

Peer-assessment and its analysis present an interesting challenge in LA. It is an important topic in LA because peer-assessment actively enhances the learning process and contributes to deeper learning. Peer-assessment is becoming a necessity in a MOOC setting. The obvious appeal of peer-assessment is the delegation of assessment workload from teacher to students. In a MOOC traditional forms of teacher's assessment quickly become impractical because of the vast number of participants. However, even with peer-assessment teachers remain heavily involved as now they must conduct and supervise the assessment process.

The assessment of complex problem-solving tasks is the recommended application of the discussed peer-assessment model. Mechanical grading (easily performed by a computer or LMS) is not applicable in the context of complex problem solving. We have presented a well founded LA model of peer-assessment. Issues and concerns that arise in peer-assessment are dealt with and measured with a mathematical model based on the use of scoring rubric. Finally, a framework for rewarding the graders for their peer-grading effort is proposed. Measures regarding reliability in this mathematical model are based on the taxicab geometry.

We look forward to opportunities for the testing of our model. Also, we are interested in applicability of this model in other settings: i.e., a similar use case is evaluation of project applications and applicability of taxicab geometry in decision making. An interesting feature to consider would be to allow partial gradings, because even experts are not experts for assessing all criteria.

Also, we are currently working on a implementation of our model of peer-assessment. We intend to release it as a plug-in for the Moodle LMS.

References

[1] B. Divjak, Notes on Taxicab Geometry, *KoG* **5** (2000), 5–9.

[2] B. Divjak, Implementation of Learning Outcomes in Mathematics for Non-Mathematics Major by Using E-Learning, in *Teaching Mathematics Online: Emergent Technologies and Methodologies*, A. A. Juan, M. A. Huertas, S. Trenholm, C. Steegmann, Eds. IGI Global, 2012, 119–140.

[3] B. Divjak, Assessment of Complex, Non-Structured Mathematical Problems, *IMA International Conference on Barriers and Enablers to Learning Maths*, 2015.

[4] B. Divjak, M. Maretić, Learning Analytics for e-Assessment: The State of the Art and One Case Study, *Central European Conference on Information and Intelligent Systems*, 2015.

[5] C. Ellis, Broadening the scope and increasing the usefulness of learning analytics: The case for assessment analytics, *British Journal of Educational Technology* **44**(4) (2013), 662–664.

[6] N. J. ENTWISTLE, Approaches to studying and perceptions of university teaching-learning environments: concepts, inventory design and preliminary findings, *Powerful learning environments: Unravelling basic components*, 2003, 89–108.

[7] N. J. ENTWISTLE, *Teaching for understanding at university: deep approaches and distinctive ways of thinking*, Basingstoke, Hampshire, Palgrave Macmillan, 2009.

[8] R. FERGUSON *The state of learning analytics in 2012: a review and future challenges*, Technical Report KMI-12-01, vol. 4, March, 2012., 18.

[9] D. GAŠEVIĆ, S. DAWSON, G. SIEMENS, Let's not forget: Learning analytics are about learning, *TechTrends* **59**(1) (2015), 64–71.

[10] C. L. HWANG, K. YOON, *Multiple Attribute Decision Making and Applications*, New York, Springer Verlag, 1981.

[11] L. JOHNSON, S. ADAMS, V. ESTRADA, A. FREEMAN, *NMC Horizon Report: 2015 Higher Education Edition*, Austin, Texas, 2015.

[12] A. JONNSON, G. SVIGBY, *The use of scoring rubrics: Reliability, validity and educational consequences*, Educational Research Review, 2007.

[13] D. J. NICOL, D. MACFARLANE-DICK, Formative assessment and selfregulated learning: a model and seven principles of good feedback practice, *Studies in Higher Education* **31**(2) (2006), 199–218.

[14] Z. PAPAMITSIOU, A. A. ECONOMIDES, Learning Analytics and Educational Data Mining in Practice, *A Systematic Literature Review of Empirical Evidence, Educational Technology & Society* **17**(5) (2014), 49–64.

[15] C. REDECKER, Ø. JOHANNESSEN, Changing Assessment - Towards a New Assessment Paradigm Using ICT, *European Journal of Education*, **48**(1) (2013), 79–96.

[16] P. SADLER, E. GOOD, The impact of self-and peer grading on student learning, *Educational Assessment* **11**(1) (2006), 37–41.

[17] K. D. STRANG, Effectiveness of peer-assessment in a professionalism course using an online workshop, *Journal of Information Technology Education: Innovations in Practice* **14** (2015), 1–16.

Blaženka Divjak
e-mail: blazenka.divjak@foi.hr

Marcel Maretić
e-mail: marcel.maretic@foi.hr

Faculty of Organization and Informatics
University of Zagreb
Pavlinska 2, HR 42000 Varaždin, Croatia

Stručni rad
Prihvaćeno 15. 9. 2015.

IVA KODRNJA
ELIZABETA ŠAMEC

Familija ploha Heltocat

Family of Surfaces Heltocat

ABSTRACT

In this paper the Heltocat family of surfaces is defined according to [5]. It is shown that the surfaces defined by the family are minimal and form an isometric deformation from the helicoid to the catenoid. The visualizations and computations were made by using the programs *Sage* and *Mathematica*.

Key words: minimal surface, Gaussian curvature, mean curvature, Heltocat family of surfaces

MSC2010: 53A05, 53A10

Familija ploha Heltocat

SAŽETAK

U radu je prema [5] definirana familija ploha Heltocat. Za plohe iz definirane familije se pokazuje da su minimalne i da čine izometričnu deformaciju od helikoida do katenoida. Za vizualizaciju ploha i račune su korišteni programi *Sage* i *Mathematica*.

Ključne riječi: minimalna ploha, Gaussova zakrivljenost plohe, srednja zakrivljenost plohe, familija ploha Heltocat

Ovaj se članak temelji na seminarskom radu kojeg je pod voditeljstvom doc. dr. sc. Sonje Gorjanc, u okviru kolegija Diferencijalna geometrija na poslijediplomskom studiju Građevinskog fakulteta Sveučilišta u Zagrebu, izradila studentica Elizabeta Šamec.

1 Uvod

Neka je $U \subset \mathbb{R}^2$ otvoren i povezan skup te neka je vektorska funkcija $\vec{r} : U \to \mathbb{R}^3$ dana formulom:

$$\mathbf{r}(u,v) = x(u,v)\vec{i} + y(u,v)\vec{j} + z(u,v)\vec{k} \tag{1}$$

gdje su $x, y, z : U \to \mathbb{R}$ realne funkcije klase $C^1(U)$. Fiksirajmo $(u_0, v_0) \in U$. Krivulje $u \to \mathbf{r}(u, v_0)$ zovu se u-krivulje, dok se krivulje $v \to \mathbf{r}(u_0, v)$ zovu v-krivulje parametrizacije $\mathbf{r}$.

Skup točaka euklidskog prostora

$$\mathcal{M} = \{T \in \mathbb{R}^3 | T = (x(u,v), y(u,v), z(u,v)), (u,v) \in U\},$$

nazivamo *plohom*, a uređeni par $(U, \mathbf{r})$ *parametrizacijom plohe* $\mathcal{M}$. Ploha $\mathcal{M}$ može se zadati i s tri parametarske jednadžbe:

$$x = x(u,v), \quad y = y(u,v), \quad z = z(u,v), \tag{2}$$

gdje su $x, y, z : U \to \mathbb{R}$ diferencijabilne skalarne funkcije iz izraza (1), [8].

Točka plohe je *regularna* ako u njoj postoji jedinstvena dirna (tangencijalna) ravnina. Za regularnu točku $T \in \mathcal{M}$ tangencijalna ravnina sadrži tangente s diralištem u T svih onih krivulja koje leže na plohi $\mathcal{M}$ i prolaze točkom T. Točke plohe u kojima takve tangente ne formiraju ravninu nazivamo *singularnim* točkama plohe. *Normala* plohe $\mathcal{M}$ u njenoj regularnoj točki T je pravac kroz T koji je okomit na tangencijalnu ravninu plohe u točki T. Ravnine koje sadrže normalu n plohe $\mathcal{M}$ u regularnoj točki T nazivamo *ravninama normalnih presjeka* kroz T. Presjek ravnine normalnog presjeka s plohom je neka krivulja na plohi.

U točki T zakrivljenost krivulje normalnog presjeka određenog tangentom t nazivamo *normalnom zakrivljenošću* plohe u smjeru tangente t u točki T i označavamo ju K_t. Funkciju $K : [0, \pi] \to \mathbb{R}$, $K(\varphi) = K_t$, koja za točku $T \in \mathcal{M}$ svakom smjeru tangente pridružuje zakrivljenost odgovarajućeg normalnog presjeka nazivamo *funkcijom normalne zakrivljenosti* plohe $\mathcal{M}$ u regularnoj točki T. *Glavne zakrivljenosti* K_1 i K_2 plohe $\mathcal{M}$ u njenoj regularnoj točki T su minimum i maksimum funkcije $K(\varphi)$, [4].

Tangente u ravninama normalnog presjeka za koje je normalna zakrivljenost ekstremna nazivamo *glavnim smjerovima* plohe u točki T i označavamo p_1 i p_2, a krivulje koje su presjek njihovih ravnina normalnog presjeka i plohe nazivamo *glavne krivulje* u točki T. Primjer su meridijani i paralele rotacijskih ploha.

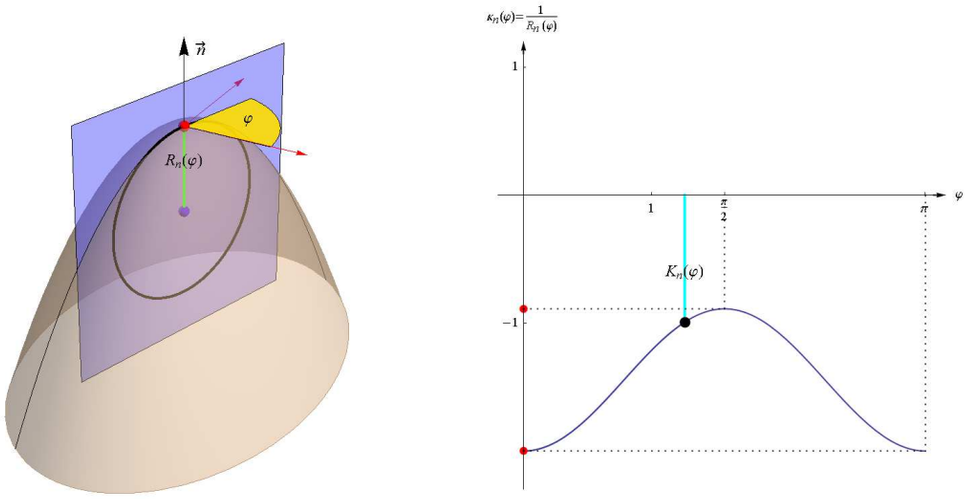

Slika 1: *Funkcija normalne zakrivljenosti* [10]

Za normalnu zakrivljenost u smjeru t vrijedi relacija

$$K(\varphi) = K_1 \cos^2 \varphi + K_2 \sin^2 \varphi,$$

gdje je φ kut između tangente t i glavnog smjera p_1 (vidi sliku 1).

Tangente u ravninama normalnog presjeka za koje je normalna zakrivljenost jednaka 0 nazivamo *asimptotski smjerovi* plohe. Asimptotske krivulje na plohi su one kojima su tangente asimptotski smjerovi. Primjer asimptotskih linija su pravci na plohama.

Srednja zakrivljenost plohe u njenoj točki T definirana je pomoću glavnih zakrivljenosti plohe K_1 i K_2 sljedećom formulom

$$H(T) = \frac{1}{2}(K_1(T) + K_2(T)). \tag{3}$$

U singularnim točkama srednja zakrivljenost nije definirana.

Gaussova (*potpuna* ili *totalna*) zakrivljenost plohe u točki T odgovara produktu glavnih zakrivljenosti,

$$G(T) = K_1(T) \cdot K_2(T).$$

Ploha je u prostoru jednoznačno određena lokalnim invarijantnim veličinama koje se zovu *prva* i *druga diferencijalna forma*. Prva diferencijalna forma služi za mjerenja na plohi kao što su duljina luka, kut između dviju krivulja plohe, površina omeđenog dijela plohe i sl. Prema [1], prvu diferencijalnu formu možemo preko duljine luka definirati s

$$I = ds^2 = (d\mathbf{r})^2 = Edu^2 + 2Fdudv + Gdv^2,$$

gdje je $\mathbf{r}(u,v)$ vektorska funkcija koja određuje plohu, a koeficijenti prve diferencijalne plohe tj. Gaussove osnovne veličine prvog reda su određene s

$$\begin{aligned} E &= \mathbf{r}_u^2 = \mathbf{r}_u \cdot \mathbf{r}_u, \\ F &= \mathbf{r}_u \cdot \mathbf{r}_v, \\ G &= \mathbf{r}_v^2 = \mathbf{r}_v \cdot \mathbf{r}_v. \end{aligned} \tag{4}$$

Druga diferencijalna ploha može nam dati odgovor na pitanje kakvog je oblika ploha u okolini neke točke na njenoj površini proučavanjem svojstava krivulja na plohi koje prolaze tom točkom. Definirana je s

$$II = Ldu^2 + 2Mdudv + Ndv^2.$$

Koeficijenti druge diferencijalne plohe tj. Gaussove osnovne veličine drugog reda određeni su preko Weingartenove funkcije W koja je prema uvjetu regularnosti u svakoj točki različita od 0, pa slijedi

$$\begin{aligned} L &= \frac{1}{W}\left[\mathbf{r}_u, \mathbf{r}_v, \mathbf{r}_{uu}\right], \\ M &= \frac{1}{W}\left[\mathbf{r}_u, \mathbf{r}_v, \mathbf{r}_{uv}\right], \\ N &= \frac{1}{W}\left[\mathbf{r}_u, \mathbf{r}_v, \mathbf{r}_{vv}\right], \qquad W = \sqrt{EG - F^2}, \end{aligned} \tag{5}$$

gdje $[\mathbf{a}, \mathbf{b}, \mathbf{c}]$ označava mješoviti produkt vektora $\mathbf{a}$, $\mathbf{b}$ i $\mathbf{c}$.

Znajući kako su definirani koeficijenti prve i druge diferencijalne forme, srednju zakrivljenost plohe H zapisujemo kao

$$H(T) = \frac{EN - 2FM + GL}{2(EG - F^2)}. \tag{6}$$

Gaussovu zakrivljenost preko koeficijenata prve i druge diferencijalne forme možemo zapisati

$$G(T) = \frac{LN - M^2}{EG - F^2}.$$

Lokalna izometrija $f : \mathcal{M} \to \overline{\mathcal{M}}$ je preslikavanje među plohama koje čuva mjerenja na plohama. Lokalnu izometriju zamišljamo kao preslikavanje koje savija plohe, ali pritom čuva unutarnju udaljenost između točaka. Lokalna izometrija čuva skalarni produkt i normu tangencijalnih vektora, odnosno Gaussove osnovne veličine prvog reda [11]. Vrijedi i obrat. Ako je $\mathbf{r} : U \to \mathbb{R}^3$ regularna injektivna parametrizacija od $\mathcal{M}$ i $\overline{\mathbf{r}} : U \to \mathbb{R}^3$ parametrizacija od $\overline{\mathcal{M}}$, tada je preslikavanje $f = \overline{\mathbf{r}} \circ \mathbf{r}^{-1}$ lokalna izometrija ako i samo ako vrijedi

$$E = \overline{E}, \quad F = \overline{F}, \quad G = \overline{G}. \tag{7}$$

2 Minimalna ploha

Ukoliko je srednja zakrivljenost plohe jednaka nuli ($H = 0$) plohu nazivamo *minimalnom* plohom. Za minimalnu plohu vrijedi da je $K_1 = -K_2$. Minimalna ploha, parametrizirana u obliku $(x, y, f(x, y))$, zadovoljava Lagrangeovu nelinearnu parcijalnu diferencijalnu jednadžbu

$$(1 + f_y^2) f_{xx} - 2 f_x f_y f_{xy} + (1 + f_x^2) f_{yy} = 0.$$

Rješavanjem Langrangeove jednadžbe možemo dobiti ravninu kao trivijalno rješenje (najjednostavniju minimalnu plohu) ili neko od netrivijalnih rješenja. Prva netrivijalna rješenja, katenoid i helikoid, dobivena su u 18. stoljeću. Danas pomoću računala i simboličkih matematičkih programa možemo dobiti niz analitički definiranih minimalnih ploha odnosno rješenja Lagrangeove jednadžbe. Kao pojednostavljenje, za plitke plohe, Lagrangeova se jednadžba može aproksimirati linearnom, Laplaceovom jednadžbom

$$f_{xx} + f_{yy} = 0.$$

Ipak, u građevinarstvu se takve plohe rijetko koriste zbog minimalnog odstupanja od ravnine uslijed kojeg nemaju dovoljnu zakrivljenost ni geometrijsku krutost u smjeru okomitom na plohu. Minimalne plohe koje koristimo u građevinarstvu, u prirodi se javljaju kao oblici koje poprima opna od sapunice razapeta na žicu savijenu u zadanu prostornu krivulju. Opna će uvijek poprimiti najmanju površinu od svih ploha koje zadovoljavaju iste rubne uvjete. Prije nego što je numerička analiza postala moguća razvojem računala, ova se pojava koristila u izradi fizikalnih modela.

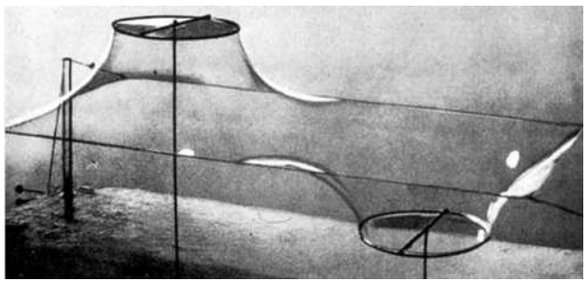

Slika 2: *Fizikalni model konstrukcije od sapunice*
(slika preuzeta sa stranice [12])

Na minimalnoj su plohi naprezanja jednaka u svakoj točki i u svim smjerovima tangencijalne ravnine uslijed čega je i nosivost materijala svuda jednoliko iskorištena [6].

3 Helikoid

Ako zamislimo točku na uspravnom kružnom valjku kako jednoliko kruži oko njegove osi, a istovremeno se jednoliko giba u smjeru te osi dobit ćemo krivulju koju nazivamo *kružna zavojnica*, a u parametarskom obliku možemo ju zapisati

$$x(u) = a\cos u, \quad y(u) = a\sin u, \quad z(u) = bu,$$
$$u \in \mathbb{R}, a > 0, b \neq 0,$$

gdje je a polumjer zavojnice (polumjer valjka), a $2b\pi$ korak zavojnice. *Korak* ili *visina hoda* zavojnice je visinska razlika dviju njezinih točaka koje leže na istoj izvodnici valjka, a parametri u im se razlikuju za 2π.

Zavojnica je *geodetska linija* valjka tj. ona je najkraća linija na valjku koja spaja njegove dvije točke, ukoliko te točke ne leže na istoj izvodnici valjka.

Normale zavojnice koje ortogonalno sijeku zavojnu os (glavne normale) tvore uspravnu pravčastu plohu koju nazivamo *helikoid*. Helikoid je uz ravninu jedina pravčasta minimalna ploha, [5]. Pravci koji leže na helikoidu su asimptotske linije te plohe - linije duž kojih je normalna zakrivljenost jednaka 0. Parametarske jednadžbe ove plohe su

$$x(u, v) = av\cos u, \quad y(u, v) = av\sin u, \quad z(u, v) = bu, \tag{8}$$
$$(u, v) \in \mathbb{R}^2, a > 0, b \neq 0.$$

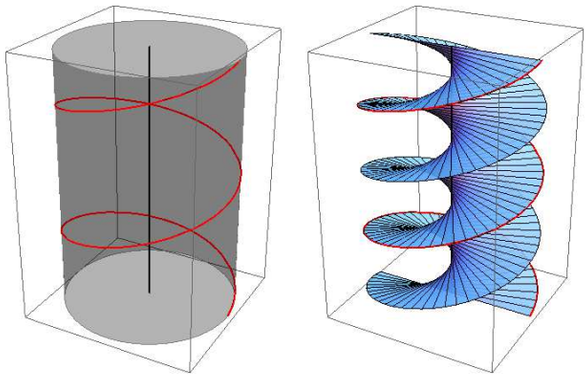

a b

Slika 3: *Zavojnica na valjku* (a) *i toj zavojnici pridružen helikoid* (b)

Za točku (u_0, v_0), zavojnica polumjera av_0 je u-linija helikoida, dok su v-linije helikoida pravci.

Pomoću formula (4) i (5) možemo za helikoid određen jednadžbama (8) izračunati Gaussove osnovne veličine prvog i drugog reda

$$E = a^2v^2 + b^2, \quad F = 0, \quad G = a^2,$$
$$L = 0, \quad M = \frac{a^2 b}{\sqrt{a^4v^2 + a^2b^2}}, \quad N = 0. \tag{9}$$

Prema izrazu (6) slijedi da je srednja zakrivljenost jednaka nuli čime je dokazano da je helikoid minimalna ploha.

Glavne zakrivljenosti K_1 i K_2 helikoida u točki $T(u,v)$ su suprotnih vrijednosti i iznose

$$K_1, K_2 = \pm\frac{a}{a^2 + u^2}.$$

4 Katenoid

Nit ovješena o dvije nepomične točke na horizontalnom razmaku i opterećena vertikalnim raspodijeljenim opterećenjem po cijeloj duljini u ravnotežnom položaju zauzima zakrivljeni oblik koji nazivamo *lančanica*, [9]. Jedan od klasičnih zadataka računa varijacija je traženje krivulje koja spaja dvije zadane točke i čijom se rotacijom oko danog pravca dobije ploha minimalne površine. Euler je 1744. pokazao da je ta krivulja lančanica, a rotacijska ploha koja nastaje naziva se *katenoid*. Ako u ravnini yz lančanicu zadamo parametarskim jednadžbama

$$y(v) = a\cosh\frac{v}{a}, \quad z(v) = v, \quad v \in \mathbb{R}, \quad a > 0,$$

njezinom rotacijom oko osi z nastat će katenoid dan sljedećim parametarskim jednadžbama:

$$x(u,v) = a\cosh\frac{v}{a}\cos u$$
$$y(u,v) = a\cosh\frac{v}{a}\sin u \tag{10}$$
$$z(u,v) = v, \quad (u,v) \in [-\pi,\pi] \times \mathbb{R}, \quad a \neq 0.$$

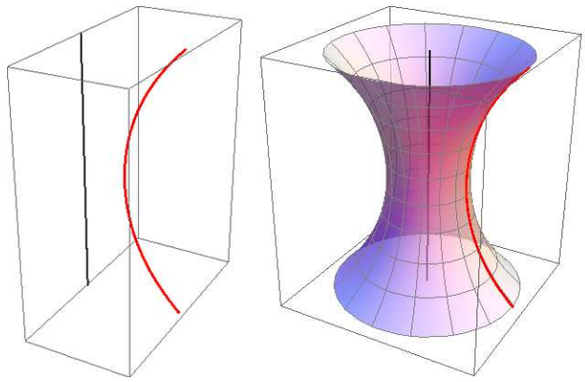

Slika 4: *Katenoid nastaje rotacijom lančanice*

Katenoid je rotacijska ploha, njegovi meridijani (lančanice) te paralele (kružnice) su glavne krivulje te plohe - krivulje duž kojih je normalna zakrivljenost ekstremna. One su ujedno i u-linije odnosno v-linije plohe, a to znači da je parametrizacija (10) takozvana glavna parametrizacija.

Ukoliko je parametrizacija katenoida zadana jednadžbom (10), osnovne veličine prvog reda mogu se izračunati kako je prikazano u uvodu i iznose:

$$E = a^2\cosh^2\frac{v}{a}, \quad F = 0, \quad G = \cosh^2\frac{v}{a}, \tag{11}$$
$$L = \frac{1}{a}, \quad M = 0, \quad N = -a\cosh^2\frac{v}{a}\operatorname{sech}^2\frac{v}{a}.$$

Vrijedi $H = 0$, odnosno katenoid je minimalna ploha. Katenoid je, uz ravninu, jedina rotacijska ploha koja je minimalna, [5].

5 Pridružena familija minimalne plohe

Poznat je rezultat da svaka ploha konstantne srednje zakrivljenosti dopušta izometričnu deformaciju, tj. postoji familija izometričnih ploha u koju je uključena takva ploha kao što se može naći u [3]. Plohe konstantne srednje zakrivljenosti (posebno su tu uključene minimalne plohe) spadaju u kategoriju takozvanih *Bonnetovih ploha* koje su proučavane još u 19. stoljeću, [2]. Prateći [5], poglavlje 31, opisat ćemo metodu kojom se svaka minimalna ploha

ulaže u familiju izometričnih minimalnih ploha, njoj pridruženu familiju i pogledati kako ta familija izgleda za helikoid odnosno katenoid.

Za parametrizaciju $\mathbf{r} : U \to \mathbb{R}^3, U \subset \mathbb{R}^2$ definiramo sljedeće:

1. $\mathbf{r}$ je *izotermalna* parametrizacija ako vrijedi

   $$\mathbf{r}_u\mathbf{r}_u = \mathbf{r}_v\mathbf{r}_v = \lambda^2, \quad \mathbf{r}_u\mathbf{r}_v = 0,$$

   pri čemu je $\lambda : U \to \mathbb{R}$ diferencijabilna funkcija.

2. $\mathbf{r}$ je *harmonička* parametrizacija ako vrijedi

   $$\mathbf{r}_{uu} + \mathbf{r}_{vv} = 0.$$

3. Harmoničku izotermalnu parametrizaciju nazivmo *minimalna izotermalna parametrizacija*. Regularna minimalna izotermalna parametrizacija definira minimalnu plohu i svaka minimalna ploha ima minimalnu izotermalnu parametrizaciju.

Primjer regularne izotermalne parametrizacije je parametrizacija katenonida (10) za $a = 1$ (označimo ju s $\mathbf{k}$), budući da vrijedi

$$\mathbf{k}_u\mathbf{k}_u = \mathbf{k}_v\mathbf{k}_v = \cosh^2 v, \quad \mathbf{k}_u\mathbf{k}_v = 0.$$

Parametrizacija helikoida (8) nije niti izotermalna niti harmonička. No, znamo da je helikoid minimalna ploha, prema tome postoji minimalna izotermalna parametrizacija. Ako uvedemo zamjenu varijabli

$$\overline{u} = u, \quad \overline{v} = a\sinh v$$

u (8) dobivamo novu parametrizaciju helikoida:

$$\overline{\mathbf{h}}(u,v) = (a\sinh v\cos u, a\sinh v\sin u, bu), \quad b \neq 0. \qquad (12)$$

Ova parametrizacija je minimalna izotermalna za $a^2 = b^2$ i vrijedi

$$\overline{\mathbf{h}}_u\overline{\mathbf{h}}_u = \overline{\mathbf{h}}_v\overline{\mathbf{h}}_v = a^2\cosh^2 v, \quad \overline{\mathbf{h}}_u\overline{\mathbf{h}}_v = 0.$$

Parametrizacije $\mathbf{r}$ i $\mathbf{s}$ zadovoljavaju *Cauchy-Riemannove uvjete* ako vrijedi

$$\mathbf{r}_u = \mathbf{s}_v \quad \text{i} \quad \mathbf{r}_v = -\mathbf{s}_u,$$

a takve parametrizacije nazivamo *konjugirano harmoničke*.

Ukoliko reparametrizirani helikoid (12) rotiramo za $\frac{\pi}{2}$ primjenom matrice transformacije

$$R = \begin{pmatrix} \cos\theta & -\sin\theta & 0 \\ \sin\theta & \cos\theta & 0 \\ 0 & 0 & 1 \end{pmatrix},$$

dobit ćemo parametrizaciju rotiranog helikoida:

$$\overline{\mathbf{h}}^R(u,v) = (a\sin u\sinh v, -\cos u\sinh v, bu), \quad b \neq 0. \qquad (13)$$

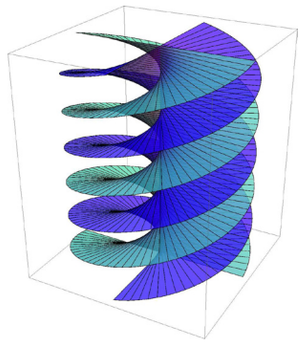

Slika 5: *Svijetloplavi helikoid (8) i tamnoplavi rotirani reparametrizirani helikoid (13)*

Parametrizacija (13) i parametrizacija $\mathbf{k}$ katenoida (10) za $a = 1$ su konjugirano harmoničke parametrizacije budući da vrijedi

$$\overline{\mathbf{h}}_u^R = \mathbf{k}_v = (\cos u\sinh v, \sin u\sinh v, 1),$$
$$\overline{\mathbf{h}}_v^R = -\mathbf{k}_u = (\sin u\cosh v, -\cos u\cosh v, 0).$$

U [5] je opisana metoda koja bilo kojoj minimalnoj izotermalnoj parametrizaciji nalazi njoj konjugirano harmoničku. Za parametrizaciju (10) tom metodom se dobiva točno parametrizacija (13).

Ako su $\mathbf{r}$ i $\mathbf{s}$ konjugirano harmoničke izotermalne parametrizacije, tada definiramo 1-parametarsku familiju ploha $t \to \mathcal{R}(t)$ s parametrizacijama

$$\mathcal{R}(t) = \cos t\mathbf{r} + \sin t\mathbf{s} \qquad (14)$$

koju nazivamo *pridružena familija ploha*. Preslikavanje $t \to \mathcal{R}(t)$ je izometrička deformacija - sve plohe u familiji $\mathcal{R}(t)$ su minimalne i imaju istu prvu fundamentalnu formu, tj. lokalno su izomorfne.

6 Familija Heltocat

Heltocat je uređena familija ploha $\mathcal{H}(t)$, $t \in [0, \frac{\pi}{2}]$ danih sljedećim parametarskim jednadžbama:

$$\begin{aligned} x(u,v) &= \cos t\sinh v\sin u + \sin t\cosh v\cos u, \\ y(u,v) &= -\cos t\sinh v\cos u + \sin t\cosh v\sin u, \\ z(u,v) &= \cos tu + \sin tv, \quad (u,v) \in \mathbb{R}\times\mathbb{R}. \end{aligned} \qquad (15)$$

Ukoliko varijablu t izjednačimo s 0, funkcija *heltocat* daje helikoid koji odgovara rotiranom reparametriziranom helikoidu $(a = 1, b = 1)$ definiranom izrazom (12). Za $t = \frac{\pi}{2}$ *heltocat* prelazi u katenoid $(a = 1)$ definiran izrazom

(10). (Time je objašnjen naziv ove familije - **hel**icoid **to cat**enoid). Ova familija je pridružena familija helikoida odnosno katenoida u smislu definicije (14).

Osnovne veličine prvog i drugog reda za $\mathcal{H}(t)$ su

$$E = \cosh^2 v, \quad F = 0, \quad G = \cosh^2 v,$$
$$L = -\cosh^2 v \operatorname{sech}^2 v \sin t, \quad M = \cosh^2 v \operatorname{sech}^2 v \cos t,$$
$$N = \cosh^2 v \operatorname{sech}^2 v \sin t.$$

Glavne zakrivljenosti K_1 i K_2 plohe $\mathcal{H}(t)$ u točki $T(u,v)$ su

$$K_1, K_2 = \pm \operatorname{sech}^2 v, \quad \forall t,$$

stoga su sve plohe ove familije minimalne.

Prva diferencijalna forma i glavne zakrivljenosti jednake su za sve plohe u familiji *Heltocat* (ne ovise o varijabli t) što potvrđuje da su sve plohe minimalne i lokalno izometrične.

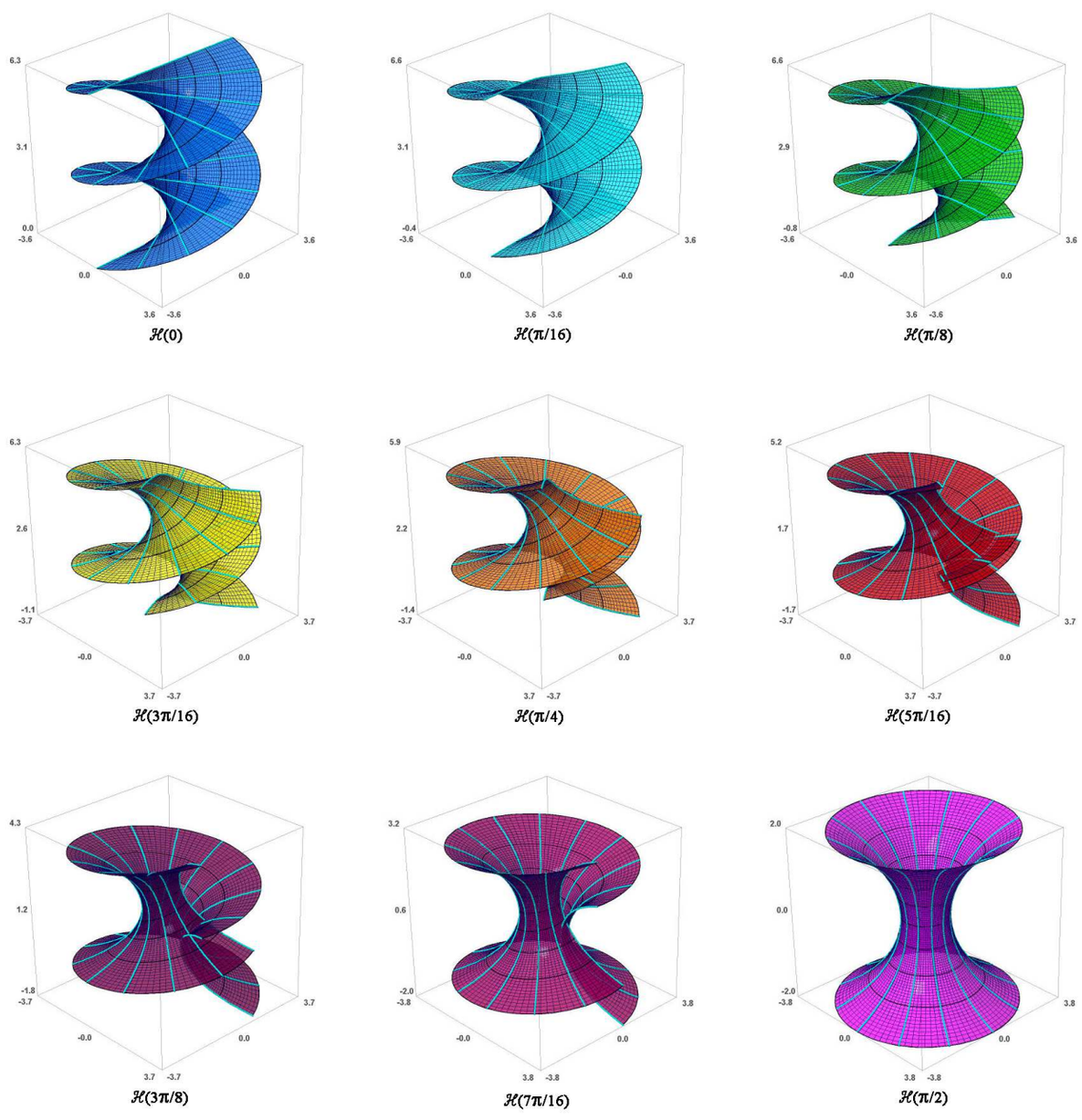

Slika 6: *Transformacija helikoida u katenoid*

Slika 6 prikazuje plohe $\mathcal{H}(t)$ za $t = n\pi/16$, $n = 0,1,\ldots,8$, a $(u,v) \in [0,2\pi] \times [-2,2]$. Crnom bojom istaknute su u-krivulje, a bojom cijan v-krivulje ploha. Vidimo da se asimptotske linije helikoida preslikavaju u glavne linije katenoida (zavojnice u kružnice, pravci u lančanice).

Pogledajmo u-linije plohe $\mathcal{H}(t)$ i pokažimo da su one zavojnice. Za fiksirane $t = t_0$ i $v = v_0$ u-linija plohe $\mathcal{H}(t_0)$ ima parametarske jedandžbe u sljedećem obliku:

$$\begin{aligned} x(u) &= a\cos u + b\sin u, \\ y(u) &= a\sin u - b\cos u, \\ z(u) &= cu + d, \quad u \in [-\pi,\pi], a,b,c,d \in \mathbb{R}. \end{aligned} \tag{16}$$

Zavojnica je karakterizirana činjenicom da leži na valjku te činjenicom da ima konstantan kut nagiba prema osi tog valjka. Uspravni valjak kojem je os z i polumjer r ima jednadžbu $x^2 + y^2 = r^2$, pa uvrštavanjem vrijednosti iz (16) dobivamo

$$x^2(u) + y^2(u) = a^2 + b^2 = \sin^2 t_0 + \sinh^2 v_0,$$

te zaključujemo da ova u-linija leži na valjku polumjera $\sqrt{\sin^2 t_0 + \sinh^2 v_0}$. Tangenta u-linije u točki (u_0, v_0) ima vektor smjera jednak

$$\mathbf{t} = (-a\sin u_0 + b\cos u_0, a\cos u_0 + b\sin u_0, c),$$

dok os z ima vektor smjera $\mathbf{z} = (0,0,1)$. Računamo kut nagiba između osi z i tangente t u točki (u_0, v_0)

$$\cos\varphi = \frac{|\mathbf{tz}|}{|\mathbf{t}||\mathbf{z}|} = \frac{c}{\sqrt{(a^2+b^2+c^2)}},$$

a ta je vrijednost konstantna s obzirom na u. Zaključujemo da je svaka u-linija plohe $\mathcal{H}(t)$ zavojnica polumjera $\sqrt{\sin^2 t_0 + \sinh^2 v_0}$, a budući da je $c = \cos t$ korak te zavojnice je $2\pi\cos t$.

7 Samopresjeci ploha $\mathcal{H}(t)$, $0 < t < \pi/2$

U [5] je spomenuto (bez dokaza i objašnjenja) da svaka ploha $\mathcal{H}(t)$, $0 < t < \pi/2$, ima krivulje samopresjeka čiji se dijelovi jasno uočavaju na tri plohe sa slike 6.

Za plohu danu parametrizacijom $\mathbf{r} : U \to \mathbb{R}^3$, $U \subset \mathbb{R}^2$, točke samopresjeka su one za koje je zadovoljeno:

$$\begin{aligned} &\mathbf{r}(u_1,v_1) = \mathbf{r}(u_2,v_2), \\ &(u_1,v_1) \neq (u_2,v_2), \quad (u_1,v_1),(u_2,v_2) \in U, \end{aligned} \tag{17}$$

tj. to su one točke za koje parametrizacija nije injektivna.

Računanje samopresjeka ploha je bitno kod CAD programa i računalnog 3D modeliranja ploha, posebno kod modeliranja offset ploha. Taj problem nije jednostavan i razvijene su numeričke i algebarske metode za traženje samopresjeka ploha s racionalnom parametrizacijom, [7]. Nažalost, kako plohe promatrane familije nisu racionalne, nije bilo moguće primijeniti neku od gore spomenutih metoda. Stoga rješavanje ovog problema ostavljamo za neki budući rad.

U pokušaju da odredimo krivulje samopresjeka, nismo mogli koristiti uvjet singularnosti plohe ($\mathbf{r}_u(u,v) \times \mathbf{r}_v(u,v) = 0$). Njegova primjena na plohe (15) daje kompleksna rješenja (npr. $\sinh v = \pm i$).

Pregledavanje velikog broja grafičkih prikaza navelo nas je na sljedeće hipoteze:

- Samopresjeci ploha $\mathcal{H}(t)$, $0 < t < \pi/2$, su neke njihove u-linije i ima ih prebrojivo mnogo na svakoj plohi.
- To su one u- linije ploha za koje vrijedi $\mathbf{r}(u_1,v) = \mathbf{r}(u_2,-v)$.

Iz jednadžbi $\mathbf{r}(u,v) = \mathbf{r}(u+x,-v)$ dobili smo sljedeće relacije za varijable x i v na linijama samopresjeka:

$$\begin{aligned} x &= 2v\tan t, \\ \sin x &= \frac{2\sin 2t \sinh v \cosh v}{\cosh 2v - \cos 2t}. \end{aligned} \tag{18}$$

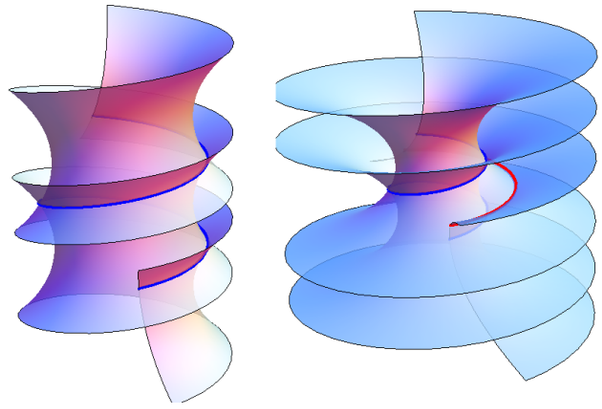

a b

Slika 7: *Ploha* $\mathcal{H}(7\pi/16)$ *nad područjima* $[-4\pi,\pi] \times [-1,1]$ *i* $[-4\pi,\pi] \times [-2,2]$, *s istaknutim u-linijama za* $v = 0.625$ *(plavo) i* $v = 1.25$ *(crveno).*

Literatura

[1] J. BEBAN-BRKIĆ, *Diferencijalna geometrija*, web skripta, 2012. `http://www.grad.hr/geomteh3d/DG_projekt/DG_sadrzaj_web.html` (pristupljeno 15. 7. 2015.)

[2] O. BONNET, Mémoire sur la théorie des surfaces applicables, *J. Ec. Polyt.*, **42** (1867), 72–92.

[3] A. G. COLARES, K. KENMOTSU, Isometric Deformation of Surfaces in $\mathbb{R}^3$ Preserving the Mean Curvature Function, *Pacific Journal of Mathematics* **136**(1) (1989).

[4] S. GORJANC, *Normalna, Gaussova i srednja zakrivljenost u regularnoj točki plohe*, web skripta, 2003. http://www.grad.hr/itproject_math/Links/sonja/gauss/gauss.html (pristupljeno 15. 7. 2015.)

[5] A. GRAY, *Modern Differential Geometry of Curves and Surfaces with Mathematica*, CRC Press, Boca Raton, 1998.

[6] S. HAK, M. UROŠ, *Gaussova i srednja zakrivljenost ploha- vizualizacije u programu Mathmatica*, studenski rad nagrađen Rektorovom nagradom, Građevinski fakultet u Sveučilišta u Zagrebu, 2004. http://www.grad.hr/sgorjanc/Links/sanjaimario.pdf (pristupljeno 15. 7. 2015.)

[7] Y. HUANG, D. WANG, Computing Self-intersection Loci of Parametrized Surfaces Using Regular Systems and Gröbner Bases, *11th International Symposium on Symbolic and Numeric Algorithms for Scientific Computing*, Timisoara, Romania, 2009.

[8] Ž. MARKOVIĆ, *Uvod u višu analizu*, II dio, Školska knjiga, Zagreb, 1952.

[9] V. SIMOVIĆ, *Leksikon građevinarstva*, Masmedia, Zagreb, 2002.

[10] D. ŠTAMBUK, "Normal Curvature at a Regular Point of a Surface" from the Wolfram Demonstrations Project http://demonstrations.wolfram.com/NormalCurvatureAtARegularPointOfASurface/ (pristupljeno 15. 7. 2015.)

[11] Nastavni materijal kolegija *Uvod u diferencijalnu geometriju*, Prirodoslovno-matematički fakultet u Zagrebu http://web.math.pmf.unizg.hr/nastava/udg/dio10.pdf (pristupljeno 15. 7. 2015.)

[12] https://www.pinterest.com/pin/329185053987707692/ (pristupljeno 15.7.2015.)

Iva Kodrnja
ikodrnja@grad.hr

Elizabeta Šamec
elizabeta.samec@gmail.com

Građevinski fakultet Sveučilišta u Zagrebu
Kačićeva 26, 10000 Zagreb

Professional paper
Accepted 27. 11. 2015.

LUIGI COCCHIARELLA

When Image sets Reality Perspectival alchemy in Velázquez's *Las Meninas*

When Image sets Reality
Perspectival alchemy in Velázquez's *Las Meninas*

ABSTRACT

There are images in History of Art, Science, Technique, Humanities, which are milestones. *Las Meninas* is one of these. Several levels of reading and deepening have been proposed by historians and theoreticians, and many interpretations have been made. Yet the very sophisticated construction of this masterpiece seems to escape any univocal hypothesis, making it as well astonishing as enigmatic.

Our interest in this extraordinary opera stems from the fact that it belongs to that special category of paintings whose meaning is inextricably based on and linked to their projective structure; therefore, aware of the wideness of the implications, we will mainly focus on its geometric and graphic feature.

Key words: Diego Velázquez, Alcázar de Madrid, perspective, geometry and graphics, photogrammetry, projective geometry, descriptive geometry, optics, catoptrics

MSC2010: 00A05, 00A66, 01A05, 51N05, 97U99

Kad slike postavljaju stvarnost
Perspektivna alkemija u Velázquezijevoj *Las Meninas*

SAŽETAK

Postoje djela prekretnice u povijesti umjetnosti, znanosti, tehnici i humanistici. Takvo djelo je i slika *Las Meninas*. Povjesničari i teoretičari su predložili nekoliko razina "čitanja" i istraživanja djela te su se pojavila brojna tumačenja. Izgleda da još uvijek vrlo sofisticirana konstrukcija ovog remek djela nije pod jednoznačnom hipotezom što ga čini jednako zadivljujućim koliko i zagonetnim.

Naše zanimajnje za ovo izvanredno remek djelo proizlazi iz činjenice da slika pripada posebnoj kategoriji djela čije se značenje temelji i neraskidivo je povezano s njihovom projektivnom strukturom. Stoga, svjesni opsežnosti implikacija mi ćemo se fokusirati na njezin geometrijski i grafički značaj.

Ključne riječi: Diego Velázquez, Alcázar de Madrid, perspektiva, geometrija i grafika, fotogrametrija, projektivna geometrija, deskriptivna geometrija, optika, katoptrika

1 Introduction

Painted by Diego Rodríguez de Silva y Velázquez in 1656, this imposing painting (318 x 276 cm) shows an intriguing scene taking place in a lazy afternoon in the *Galería de Mediodía of the Alcázar de Madrid*. Strangely enough we basically see the painter in person at work beyond a large canvas, the Infanta Margarita Theresa of Spain, her Maids of Honour and other members of the Royal entourage, including a dwarf, a midget and a dog. Apart from the last two, all the characters are looking fixedly at us with curiosity, while we are looking into their space, that is, quite unusually, the studio of the painter. In this dialog of glances, looking more closely and attentively we surprisingly discover the image of the King Felipe IV and Queen Mariana de Austria, which is reflected in a small mirror hanging in the middle of the rear wall, also they looking towards us. Above, two big mythological paintings appear, showing the hard punishments that await those who dare to challenge gods.

Any attempt to undertake a philological reconstruction of the geometric space of the scene has to deal with at least two issues. On the one hand the sophisticated perspective pattern of the painting, including the representation of mirror and reflection effects, and the crucial fact that the large canvas appearing in the painting, slightly rotated and tilted,

faces the artist, therefore its figurative content remains a secret. On the other hand, the fact that the real room represented in the painting was located in the south western wing of the castle, known as Cuarto del Príncipe Major, which burned during the big fire of Christmas Eve in the year 1734. On the bases of the available information, we aim to compare the presumable shape of the painted room as it results from the perspective reconstruction based on the *depicted space*, with the presumable shape of the *real space* hypothesized on the base of some historical plans, especially that of Juan Gómez de Mora date back to 1626, and some information about other important changes supervised by the same Velázquez afterwards. In this process, the reflection in the mirror will provide a valuable aid for the geometrical reconstruction, but at the same time it will set a limit to the investigation.

2 A glance at the painting

Based on the available information, mainly coming from the book *El Museo Pictórico, y Escala Óptica* by Acisclo Antonio Palomino de Castro y Velasco, the painting has been painted in 1656. It is a big oil on canvas, 2,76 meters wide and 3,18 high, nowadays placed at the Prado Museum in Madrid [12]. At its time, it was known as *La Familia* (The Family) and hung in the Royal Alcazar de Madrid for about eighty years, until 1734 when the castle burned during Christmas Eve. Due to the fire both left and right edges were damaged and consequently these marginal areas were cut and removed, while the high temperature caused the loss of pigment in some parts, including one cheek of the Infanta Margarita, as well as some diffused alterations of the original colours. It was soon restored and cleaned by the painter Juan Garcia de Miranda and included in the royal collection in 1748. In 1772 it was in the new Royal Palace of Madrid with the title *La Familia de Felipe IV* (The Family of Philip IV). Half a century later, in 1819 it was finally included in the collection of the Prado Museum, where it received his final name, *Las Meninas*, about twenty years later, in 1843. The last restoration took place on 1984 and nowadays it is still visible at the Prado Museum (Figure 1) [13].

Curiously, the present name takes its origin from two secondary characters, namely the two young Maids of Honour, that is, *Las Meninas*, who appear in the painting at the two sides of the Infanta Margarita (1651-1673), at the time aging five, the young daughter of King Felipe IV (1605-1665) and Queen Mariana de Austria (1634-1696), who stands shiningly at the centre of the scene, blond and white dressed. Thanks to Palomino, who had the opportunity to talk with persons that had been in touch or that simply had known the members of the royal court, and based on other

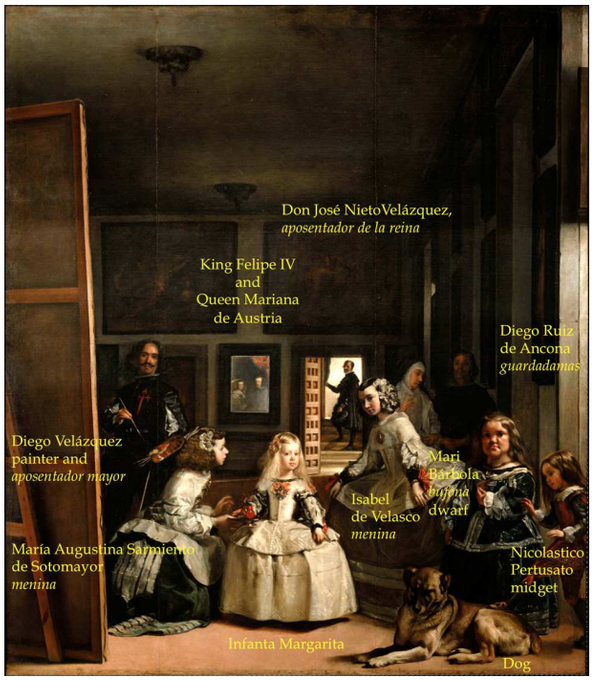

Figure 1: *Las Meninas, 1656: space and scene (source of image* [12]*, text by author)*

historical sources, we have information about all the persons portrayed in the painting, which makes understandable the situation and helps us to get the feeling of the scene. The maid on the left is María Augustina Sarmiento de Sotomayor, who is offering the Infanta a red cup on a silver plate, the one on the right is Isabel de Velasco. The two young girls are attending the young princess. Beyond them, almost in the shadow, close to the balconies, we see Marcela de Ulloa and Diego Ruiz de Ancona, enrolled as *guardadamas*, that is, in charge for the surveillance of the maids, silently discussing with each other, in a way that contributes to giving the scene the special atmosphere of a private family meeting. On the foreground we see another group composed by the German dwarf Mari Bárbola, and the Italian midget Nicolastico Pertusato, who is joking with a big indolent dozy dog. Dwarfs and midgets were very familiar at royal court at that time. They were considered as fool of God and had the task to cheer up court and guests, but they were also considered talented with a supernatural wisdom, symbols of divine mercy, then they were among the fewest allowed to tell the King truth, no matter how much unwelcome it could be, without any consequence. In the very foreground the dog, symbolizes loyalty and devotion, he is growing drowsy but he is also garrisoning the threshold of the gate to the painted space. On the left side, just beyond the kneeling maid, we see the painter, Diego Velázquez (1599-1660), standing, imperious and attentive, at work in front of the huge canvas, whose pictorial

surface we can not see directly. It shows in a key moment of pause, looking in our direction as he was taking information about his subject in order to proceed or complete his work. At that time he was *aposentador major*, a kind of Marshal and Master of Ceremonies of the castle, at the service of King, the highest grade in this role. We will know a bit more about him in the following paragraph. On the opposite side, beyond the door of the rear wall, another *aposentador* is on the mid steps of a short staircase. He is Don José Nieto Velázquez, who apart from the name did not have any family ties with Diego Velázquez. He was the person in charge of staying at hand of the Queen, opening and closing the doors to give her way. Since he is managing with a drapery, it has been written that he was preparing the way to the Queen, who was on the point of leaving the room, consequently what we see in the painting might be the end of the painting session. But it is also possible, on our opinion, that he was just coming to see the advancement of the session, or just leaving before the session started. These latter hypotheses seem quite convincing if we look at the sense of waiting pervading the space, emphasized by the bowing maid on the right, as well as by the attentive glances of the bystanders gazing into our space. The last two members of the group, smaller than one could expect, appear as busts in a frame located in the middle of the rear wall. They are King Felipe IV and Queen Mariana. The boundary of the rectangular area from which their profiles arise, and the less sharp outlines and colours, tell us that they appear in a mirror, which is one of the most interesting aspects and one of the most discussed points of this masterpiece, besides being one of the major focuses of our projective investigation.

3 The painter

As widely recognized, Diego Velázquez is considered as the leading artist of the Spanish "Golden Age" (Figure 2). His curriculum includes not only pictorial masterpieces but also a relevant number of public offices and appointments under the kingdom of Felipe IV. Born in Seville on June 1599, he was at the royal court since 1623, at his twenties, having a special feeling with the King since the beginning. It is told that, especially in the old age, he used to visit the painter in his studio, frequently waiting there for long hours looking at him painting. When Velázquez died at the beginning of August 1660, Felipe wrote moving words expressing his solitude and grief for the loss of the esteemed artist, adviser and confident. Velázquez was, indeed, a deeply cultured artist, at same time very brilliant in political, administrative stuffs, and management. His library was very rich and full of international books and treatises. Thanks to his sensibility and active efforts, the royal

Figure 2: *Diego Rodríguez de Silva y Velázquez. Self portrait, about 1640 (left, source of image* [13]*). In Las Meninas, 1656 (right, source of image* [12]*) (Images cropped by author)*

collection of art masterpieces had a significant increase under his tutorship. He was in touch with great artists, especially Pieter Paul Rubens, getting from him a deep pictorial influence and important works for the archives of Spain. To further enrich the art collection Diego Velázquez also visited Italy twice, selecting and importing in Madrid important sculptures, paintings and documents. Again Palomino, the official biographer of the Spanish artist of that time, whose contribution is often compared with the one offered by Vasari for Italian Renaissance, helps us to know detailed information about him, especially in the period from 1650 and 1660. Palomino completed the biography in 1724, only six decades after the death of the artist, therefore he could get direct information about the painter from people who had the opportunity to meet him in person, including Juan de Alfaro y Gámez, one of his artistic disciples [4]. There are not so many other words to spend about Velázquez's universally recognized outstanding career as a painter. Instead, here we would look at a special part of his story as a public man, which is related to the red cross appearing on his chest in *Las Meninas*. At the time when he painted *Las Meninas*, he was at the apex of his public career, attending several royal offices. He was, indeed, *Pintor de camera*, kind of personal painter of the King, *Ayuda de camera*, that is a kind of personal counsellor and assistant of the King, *Aposentador de palacio*, or the marshal of the Alcazar de Madrid, that is, the castle of the King of Spain, and from 1652 *Superintendente de obras particulares*, or superintendent to special works, like managing royal art collections and architectural works in the castle. In short, he was also a kind of artistic supervisor and managing director of the King.

Nevertheless, his biggest ambition was not yet been satisfied. At that time indeed, he was struggling in the middle of a personal fight to become a member of the *Orden de Santiago*, which was the most prestigious monastic-military order, whose reputation was echoing since its foundation in

XII century. Symbol of the members was, precisely, a red cross on the chest. Well, almost incredible the sequence of facts concerning Velázquez's admission to this Order, which also demonstrates the tenaciousness of the painter. The story starts in 1650, six years before *Las Meninas* was painted and before the birth of the Infanta Margarita, when, after the death of his first wife Isabel de Borbón (1602-1644) and of his young son Balthasar Carlos (1629-1646), Felipe IV was starting forming a new family with Mariana de Austria. In this year, Velázquez obtained the support from the Secretary of State of the Pope. From that moment, it will have taken other eight years to obtain the royal nomination, the document with which the King tried to solve the pending suit. *Las Meninas* was painted during the wait for this royal document. But once obtained the royal paper, the request was reviewed and rejected by the Council of Military Orders, after investigation about painter's genealogy and social condition. To deny the admission, they highlighted the basic contradiction between the painter's "God-given talent" and his "man-made hierarchy of court". Obstinate as never before, Diego Velázquez brought a legal action against this result, and a big trial started up involving 148 witnesses. The main point was about nobility. In order to demonstrate his noble origin, he pushed many witnesses to affirm that he had never worked for money, since he did not need it because of his aristocratic genealogy. At the end, it was not difficult to discover the falseness of these proofs, which made the situation even worse. At this point, in a short time between 1658 and 1659, a new endorsement by Pope and, to redundantly reinforce it, the ennoblement by King, removed the obstacle once and forever. In the same year of 1659, on November 28, Diego Rodríguez de Silva y Velázquez was finally admitted to the *Orden de Santiago*, eight months before he passed away [4]. Thus, what about the red cross depicted on his chest in *Las Meninas*? Legend tells that it should have added by direct hand of King Felipe IV after the death of his beloved "painter and courtier".

4 Architectural set

The room we see in the painting is no longer an existing room. It was destroyed in the fire of that fatal night during the Christmas Eve of 1734, which just started from the south-western wing of the Castle (Figure 3), where the room was located as a part of the *Cuarto Bajo del Principe*, that is, an apartment at the ground floor belonging to the *Cuarto del Rey*, the western part of the Castle in use by the King and for his private activities and public ceremonies. This room, also known as *Galería de Mediodía*, which means southern gallery, was pleasantly warm, especially during winter time, then kings since Felipe II liked to spend time there during the most freezing days of the year

Figure 3: *Alcázar de Madrid, XVII century, by anonymus (source of image* [13]*, cropped by author)*

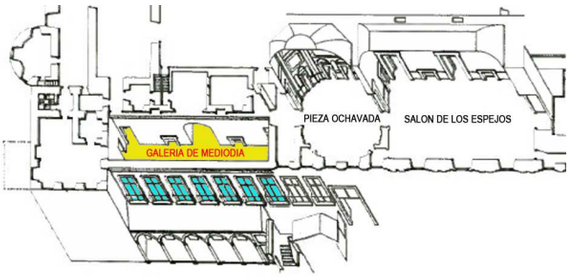

Figure 4: *Galería de Mediodía, axonometry (source of image* [2]*, cropped and coloured by author)*

(Figure 4). Since 1646 the room was also the *atelier* of the painter, as the paintings represented in the canvas testify. The Alcázar de Madrid was founded in IX Century as a Muslim fortress and had done several significant transformations over time. One of the most impressive transformations took place between 1640 and 1650, in part under Velazquez's direction, when the great royal gallery at the first floor decorated with mirrors and named *Salón de los Espejos* was realized, together with the contiguous *Sala Ochavada*, an octagonal room adorned with precious statues, some of them coming from Italy, and directly connected by a staircase with the *Galería de Mediodía* at the lower floor [2]. There are no evidences of this staircase in the coeval maps, but only in *Las Meninas*, which shows a view of a stepped ramp beyond the rear wall, where José Nieto stands on looking at the scene and preparing the way to the Queen. The reason why *Las Meninas* is also one of the historical sources taken into account by the scholars in relation to the history of Alcazar.

The main iconographic sources basically consist of a plan by Juan Gomez de Mora, date back to 1626, thirty years

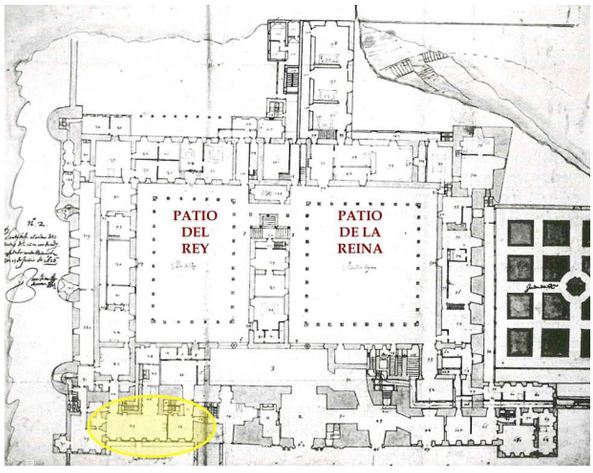

Figure 5: *Galería de Mediodía (yellow area) in the Alcázar de Madrid, by Juan Gomez de Mora, 1626 (source of image* [1]*, cropped by author)*

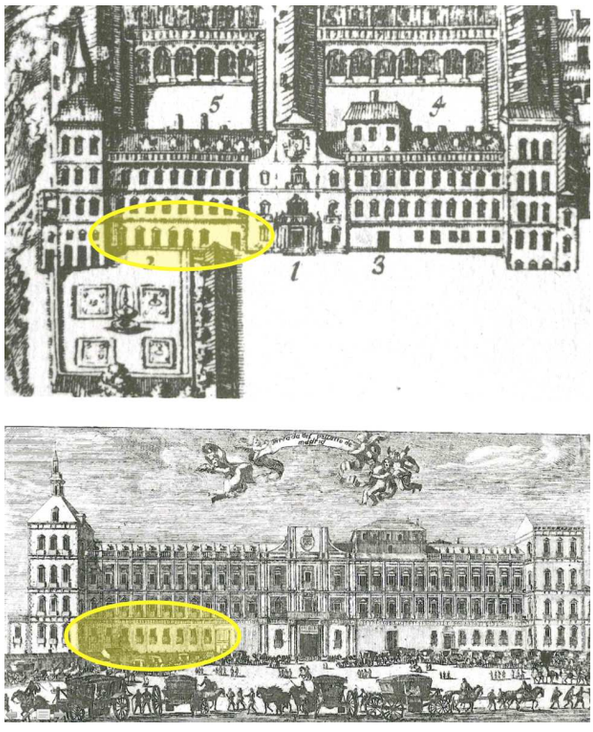

Figure 6: *Front of the Galería de Mediodía (yellow area), southern wing of Alcázar de Madrid (source of images* [1]*, both cropped by author). Views by Pedro Texeira Albernaz, 1656 (above), and Luis Meunier, 1666 (below)*

before the painting (Figure 5), and a plan by Teodoro Ardemans, realized in 1705. They are both quite far from the time of the painting here discussed, but they are anyway helpful to understand architectural structure and proportions of the room. A view from 1656 by the cartographer

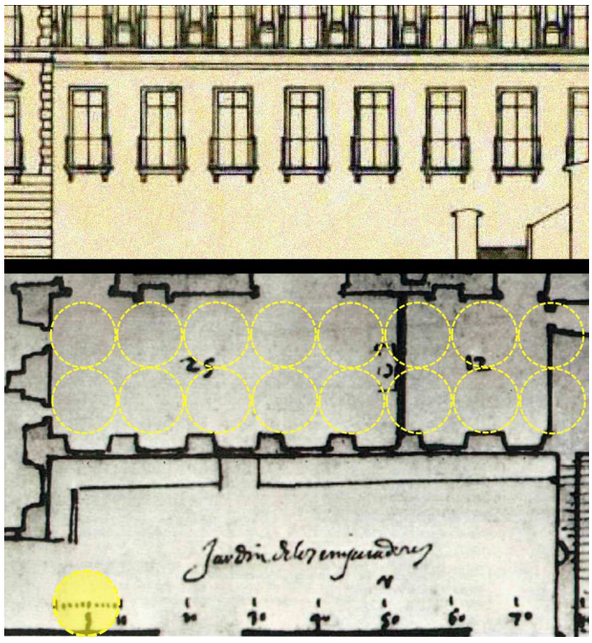

Figure 7: *Galería de Mediodía, the geometrical set. Detail of the plan (source of image* [3]*) and front (source of image* [1]*). Unit: pie castellano,* 1 *pie* = 27.86 *cm (composition and diagram by author)*

Pedro Texeira Albernaz and a view from 1666 by Luis Meunier help us to complete the picture, being useful to analyse the consistency between the faade and the interiors (Figure 6). There are also maquettes of the castle, the most well-known realized after 1630 and now at the Museo Municipal, in Madrid. A recent, complete and detailed historical reconstruction of the castle and its transformations is nowadays available, thanks to the book *Alcázar de Madrid*, by José Manuel Barbeito, published in 1992 [1].

The geometry of the room appearing in *Las Meninas* is clear from the mentioned map of Juan Gómez de Mora. It shows a long room with seven balconies along the southern wall, the one appearing on the right in the painting (Figure 7). At the time when the plan was drawn a thin partition divided the room in two parts, marked in the plan with numbers 25 and 12, the latter included in the apartment of Prince Balthasar Carlos, also said *El Cardenal Infante*. When the young Prince died, the partition was removed and the room became the studio of Diego Velázquez. The eastern wall, corresponding to the rear wall appearing in the painting, only shows one gate to a gallery in a massive wall, but not the other gate, where José Nieto appears in *Las Meninas*, neither the staircase on which he is standing (Figure 8). Gate and staircase could have been realized during the big transformation occurred between 1630 and 1650, when the *Torre del Sumiller*, that is, the huge tower connected to the room and its massive wall, were

demolished. The western wall represented in the 1626's map, shows two gates, one of them close to the wall with balconies and almost specular to the Nieto's gate visible in the painting, for this reason supposed to hold the viewpoint from which the scene was depicted. Northern wall does not appear in the painting, but it has been useful to understand the symmetry of the room, which has been helpful in reconstructing the sequence of the balconies in spite of the graphic approximations in the map.

Concerning metrics, we had to refer to the unit in use at the time, clearly indicated in the drawing, which is *pie castellano*, or the castilian foot, so that 1 *pie* $= 27.86$ *cm*. The size of the room is 75×20 *pies*, which means about 20.90×5.57 *mt*. Taking advantage from the fact that width and height of one of the walls, namely the eastern wall, appear frontally in the painting, the height of the room has been deduced by a simple proportion, and then compared with the available drawings of the façade. Other important information comes from an *Inventory* of the paintings recorded in 1686 [3]. Starting from the ceiling, this list describes all the paintings hanging above and in between the balconies (Figure 9), including precise information about their sizes. All the paintings are by Juan Baptista del Mazo, the Velázquez's son in law, some original, mostly are copies of Rubens. In *Las Meninas* they appear strongly foreshortened by the effect of perspective distortion, which affects the representation of that side of the room. As the inventory includes the description of the frames, we considered the metrical information as related to the outline of the frames and not to the real dimensions of the canvases, about which there are no explicit information. New multiple units are mentioned in the inventory, namely 1 *vara* $= 83.5$ *cm*, 1 *tercia* $= 27.5$ *cm*, 1 *quarta* $= 20.5$ *cm*. In total, four types of frames are mentioned. Above the balconies, seven long frames measuring 3 *varas* $\times$ 3 *quartas*, copies of Rubens, showing images of birds, animals and landscapes. In between, five small original paintings by Mazo measuring $\frac{1}{2}$ *vara* $\times$ 3 *quartas*, displaying wild boar, small dogs, and again animals and landscapes. Below, other six smaller copies by Rubens, measuring $\frac{1}{2}$ *varas* $\times$ 2 *tercias*, with the Labor of Hercules. Below these and finally, six higher copies of Rubens, measuring 2 *tercias* $\times 1 + \frac{1}{2}$ *varas*, showing the philosophers Heraclitus and Democritus, Hercules slaying the seven-headed Hydra, Mercury, Saturn, and Diana. Magnified by the frontal view, hanging up on the rear wall under the ceiling, are two big copies of Rubens realized by Mazo, telling mythological stories. The one on the left, burned during the fire, is about *Minerva Punishing Arachne*, the other is about *Apollo's victory over Marsyas*. Besides the mentioned works, the framed mirror between the two doors and the big canvas on which Velázquez is at work, complete the set. On the ceiling, two lamps appear, and some evident

Figure 8: *South eastern entrance and staircase (source of image* [12]*, cropped by author)*

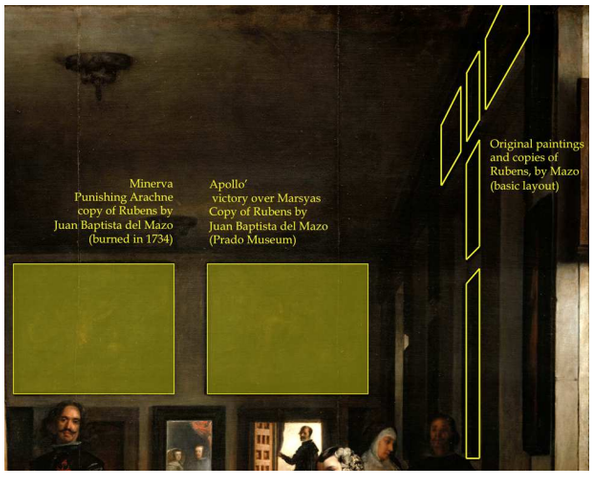

Figure 9: *Distribution of paintings on the walls (source of image* [12]*, cuts and diagrams by author)*

humidity stains, a clear proof of one of the major persisting problems that Alcázar had to face during its existence, well documented in the archives and often cause of restoration as well as of profound architectural transformations [1]. Nowadays the Royal Palace of Madrid stands on the same place of the Alcázar de Madrid.

5 Graphics, or, "the truth of tone"

Talking about painting necessarily implies to take into account the primary role of Graphics. No matter what subject and story are, and what the organization of shapes is, at the end a painting is made of pigments on a canvas, and these pigments makes the story alive. Discussing about graphic aspects is not the main purpose of this work, anyway we could not avoid to note how much they are in a masterly manner interlinked with geometry of space, spatial perception, location of characters, and symbolism in this art masterpiece. Besides how the scene is shaped and its proportions on the canvas, the whole atmosphere of the event is here dominant, based on a refined chromatic combination of factors [7]. First of all the dimension of the room is emphasized thanks to a wide use of dim light effects, and of their contrast with brighter areas and silhouettes. The soft colour of the ground and the absence of any flooring, drive the attention on the human characters and the space around, far from the traditional iconography of tiled perspective grounds, which in this case would have interfered with the contemplation of the very points of the scene. Velázquez pushes our sight up to the space in front of us instead of on graphic nets under our feet. We can then appreciate the illuminated foreground, as if we also were invested by the light incoming through the opened shutters of the balcony on the right. The opposite happens on the left, due to the huge brown back side of the canvas where the painter's work is supposed to be in progress. Then a dark *penumbra* pervades the whole depth of the room. This area is really wide, if we consider that the entire upper half of the painting is shown as an empty space (Figure 10). It has been a really superb choice to take this risk, but in a way it seems this upper half part is the space of Art and Myth, indeed, almost the total amount of paintings lay in this superior area. It is remarkable that almost all these paintings are perfectly recognizable, being masterly reproductions of those that hung in the room. The lower half of the painting is where the scene with people takes place (Figure 11). Then, in the dark rear wall darkness is again broken, firstly by the reflected image of the royal couple in the mirror, mid of the wall, and most of all by the very bright spot of light filtering through the door where José Nieto stands, light coming from an undefined space beyond the room. These oases of light work as a tonal balance in the painting, the latter being located exactly in front of the supposed designated location for the perspectival viewpoint. Great attention is paid on graphic resolution and tones according to the distances, as explicitly recommended since the Leonardo da Vinci's *perspectiva aerea*. Compared with the figures of the persons in the foreground, the silhouette of José Nieto, as well as those of King and Queen, appearing under the red drapery of a gate, are less defined. This latter could also have been a strategy, either due to a certain reluctance of the King to show in sharp portraits during his mature age, reasonable also in consideration of the very young age of his wife, or and at the same time to affirm the minor role of the attendant of Queen in comparison with the role of the painter himself as an attendant of King. Light and colours also help to recognize hierarchies among the portrayed persons (Figure 12). Fully direct light, indeed, only reaches the Infanta Margarita, at the time aging five and being the only daughter of the royal house still alive, first descendant for Felipe IV and Queen Mariana. Shining as the hope of the reign, she is blond and white dressed, while vivid red details, like the round big brown eyes, brooches in the hear and on the corset, as well as the red cup, exalt her bright figure even more. Not by chance, she is at the centre of the scene. Other characters, although showing faces, are never

Figure 10: *Las Meninas, upper pictorial area (source* [12]*, cropped by author)*

Figure 11: *Las Meninas, lower pictorial area (source* [12]*, cropped by author)*

Figure 12: *Las Meninas, graphic features of characters (source* [12]*, cropped and composed by author)*

fully illuminated, like in the case of the dwarf, or in the light but only showing a profile, like in the case of the maids of honour. Very secondary characters are even more far from light, like the two tutors of the maids. The midget and the dog show detailed feature because they are in the very foreground, but not so much in the light, which comes from the upper area of the balcony. Velázquez's silhouette is definitely imposing in the composition. Not as much important as the Royal Family, the pictorial feature makes anyway impossible not to be attracted by his image. Apart from the proud and aristocratic pose, his location in a uniform *penumbra* weakens the light contrasts on his face, which is clear and defined, together with his hands. This kind of fore-ground effect achieved in a mid-ground position is also emphasized by the total black uniform he dresses, since this black area makes the image of his face and hands emerging from the shady atmosphere around. Of course much other could be told about the expressiveness of the characters, or on the chromatic techniques adopted and developed by Velázquez, including the special blue pigment used in this painting, but all this is beyond our specific task and competences. Only one thing more about light and shadows: what time is it? Although we will not go in search for the sunlight angles of incidence, considering that the balconies on the right were oriented towards South, and that light runs towards the scene, the depicted event might have taken place in an early afternoon. On our opinion the light blade casting on the floor from an apparently opposite direction through the gate in the rear room does not contradict this hypothesis, being the normal effect of light in the space beyond the wall, entering the darkest part of the room, something we are quite familiar with in our real life. Because of all this and much other that we will not tell in this paper, this painting has been considered one of the best examples of "truth of tones", using Kenneth Clark's words, ever realized in the history of painting [5].

6 Geometry, or, "the bones of truth"

Talking about painting also implies Geometry, at different levels of investigation. In our case, at least two levels: topology of composition, and projective structure. Concerning composition, a dynamic equilibrium emerges from position and orientation of the static images on the canvas (Figure 13). The wide empty part of the room represented in the upper half part of the canvas, where we see the gallery of paintings on the walls symbolizes, have we already mentioned, the higher level of Art, giving at the same time gravity and weight to the human characters in the lower part, pushing them firmly on the floor, balancing the absence of visual references on this horizontal plane. Primary and secondary characters can be identified, related in various ways one another. Infanta, mirrored images of King and Queen, and painter at work, define a first primary group. Without these members of the royal family the painting would not make sense, without the painter it could not have been made. Infanta and the two maids form another group, a wing dynamically growing up and bearing anti-clockwise from left to right, where genuflexion and courtesy of maids suggest a balanced rotational motion about the Infanta, and the sloping axes of their busts form an ideal protective triangular shelter above the young princess. Velázquez and José Nieto are corresponding figures garrisoning the beginning and the end of the space of the room, keeping King and Queen between them, similarly to what Maids of Honour do with the princess. Moreover, Velázquez, José Nieto, and the dog, are the endpoints of an ideal triangle around the Infanta, meaning again a sense of protection and defence. It is important to highlight the role of these three figures in emphasizing the perspective effect and in helping to appreciate the long extension of the room. Velázquez and dog's heads are also the endpoints of a line touching the Infanta's head. Two dynamic crossing curves are formed, the first including maids, princess and *guardadamas*, the second including Velázquez, the maid on the right and the group of dwarf, midget, and dog. This latter group contributes to stabilizing the lower right area of the painting, balancing the visual weight of the huge canvas on the left. The gesture of distraction played by the midget Nicolastico joking with the dog, releases a little the brake of tension, working in favour of a familiar atmosphere. The dozy dog would also tell about the serene security of the place, and by extension,

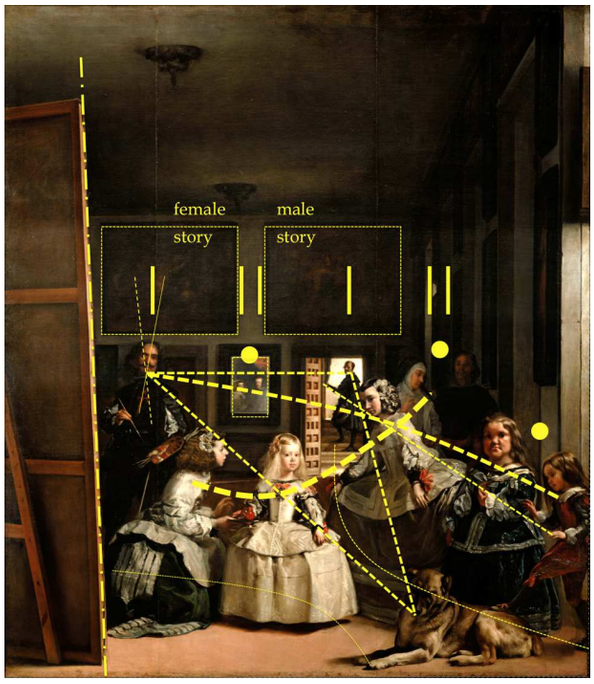

Figure 13: *Las Meninas, rhythm and composition (source of image* [12]*, diagrams by author)*

Figure 14: *Las Meninas, a special framing into the whole frame (source of image* [12]*, cropped by author)*

of the kingdom. Once one look at this very close zone, some details drive the sight again in opposite directions, like the position of the Nicolastico's leg towards left, and his inclined arm, aligned with and echoed by the Nieto's arm keeping the drapery at the end of the room, so recalling the main perspective direction. X-ray analysis of the painting also revealed an afterthought in the inclination of painter's head, which was leftwards in the first version. Maybe this change is also in order to keep the dynamism of the composition, either in relation to the opposite inclined outline of the canvas in front of him, or in relation to the inclinations of the other figures. Moreover, much other could be said about the geometry of glances looking at the eyes of each member in the scene, and mainly in relation with our direction of sight. Other interesting relationship is in the alternation of single figures and couples in the sequence from left to right from Velázquez to King and Queen, Nieto, and the *guardadamas*, a kind of horizontal rhythm reducing the strong effect of perspective. Another significant fact we noticed is that Velázquez, Infanta Margarita, Royal Couple in the mirror, the Maids of Honour and Nieto, together with the two big paintings above the doors and their legendary stories, and in part the canvas on which Velázquez is at work, lay inside the boundaries of the rear wall, whose ideal frame works as a picture apart in the whole picture (Figure 14).

Concerning projective structure, the main vanishing point, and consequently the viewpoint, is eccentric and laid in the surrounding of the right arm of Nieto, emphasizing the southern area of the room, closer to the sun light. The eccentric effect is reinforced by the diagonal foreshortenings of the lamps on the ceiling. Consistently with the other aspects here discussed, this choice also contributes to giving a dynamic impact to the image. The spatial depth of the room can be subdivided in three main stages (Figure 15). The very background beyond the rear wall, or the space in which the staircase and Nieto appear, illuminated by a dazzling light. Hypotheses on this space have been formulated, supposing that a monumental staircase to the main floor would be there, connecting the room with the main floor upstairs [11]. In relation to our purposes, we see that this undefined space tells us that there is something else, something shining, beyond the room, therefore it either works as a perspective safety-valve avoiding claustrophobic effects, or metaphorically, suggesting the idea of the depicted room as a small space in a wider reign. A "poetic" projective licence, maybe the only deviation from the purely perspective rules in order to have a better picture, is in the upper side of door, which is not visible as it should be (Figure 16). Another stage can be recognized between the rear wall and about half of the visible part of the room, more or less until the position of the two *guardadamas*. This mid-ground is totally empty. Closer to us is the foreground, where eight out of eleven depicted people show, together with the dog. Here the big canvas introduces an oblique perspective, avoiding the risk of a motionlessness perception of the gallery. The distribution of the three couples, that is, sovereigns, *guardadamas*, dwarf and midget, also helps to visually mark the three foreshortening stages of the space, again fostering a dynamic perception. As we can see, a very sophisticated system of topologic and projective aspects has been build up in this painting, perfectly

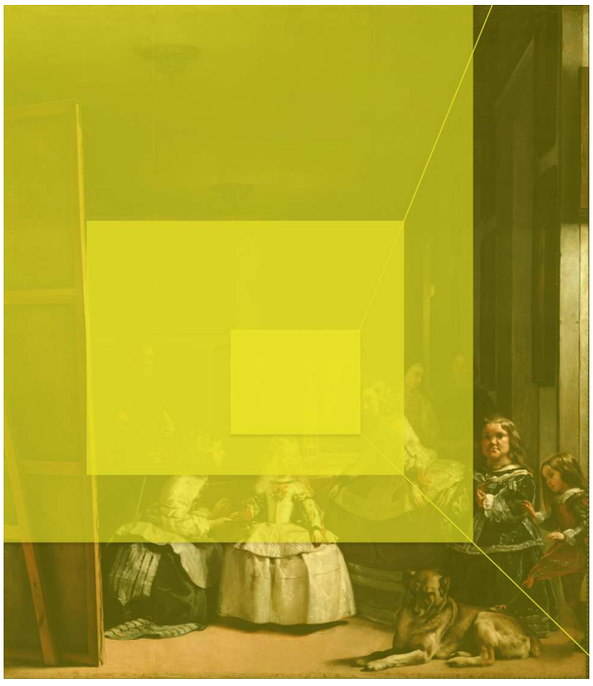

Figure 15: *Las Meninas, perspective stages in the pictorial space (source of image* [12]*, diagram by author)*

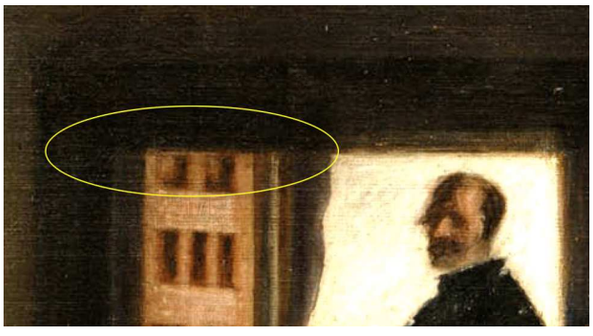

Figure 16: *Las Meninas, a perspective "licence" (source of image* [12]*, cropped and marked by author)*

integrated with a magisterial graphic feature. But there is more in this painting making it so unique: a mirror. Reflection is then included in this perspective, that is, another perspective into the perspective representation [7, 9]. As we said, King Felipe IV and Queen Mariana de Austria appear there, smaller than Nieto despite mirror hangs on the wall at same distance from our point of sight, which is a proof that they show in a mirror. What we see on the mirror, indeed, is the projection of the virtual image of the Royal Couple, geometrically formed beyond the surface of the mirror, at the same distance of that from the mirror King and Queen were into the real room in that moment. That is supposed to be, in front of the painter who was depicting them, while he and the other bystanders were attentively looking at them. As well as they seem looking at us. Based on this hypothesis, the sight point of *Las Meninas* should be the same viewpoint of the King. Of course, many authoritative hypotheses have been proposed, since we can not see what Velazquez is actually painting on his big canvas. Our goal will be about proving the projective consistency of what we see depicted on the canvas. Or, the consistency of Geometry, as the "bones of truth".

7 Projective proof

Projective analysis and graphic reconstruction have been carried on a digital copy of the painting imported in a CAD system. Some tolerances have been considered, due to the incomparable major resolution of CAD visualization in relation to the real painting. We sometimes thought that pencil and strokes, ruler and compasses, might have been better tools to use. On the other hand, CAD system would have allowed us to carry on 1:1 perspective investigations, and to store all the constructions in one file, reason why we decided to stay on it, working in the consciousness of the mentioned technical gap. The perspective reconstruction is made of two parts, one of them related to the reconstruction of the *Galería de Mediodía*, the other one focusing on mirror and its reflected image.

Compared with the richness of the composition, the painting offers a limited set of perspective elements. Apart from the clear front view of the rear wall with the mirror, whose dimensions were known, together with those of the two big canvas hung on it, the only usable foreshortened geometrical element are balconies and the paintings hung on the wall on the right. The first check has been about extending the depth lines in search for the main vanishing point of the structure. Initially, we tried to assume that this point was on the finger of the left hand of Nieto, consequently implying a horizon line passing through the baseline of the mirror reflecting the royal busts as well as through Velázquez's brush. This looked very convincing at the beginning, especially from a metaphoric point of view, as if also Nieto, the second *aposentador*, was involved, together with the *aposentador major*, in the perspective construction, by indicating that crucial vanishing point. Nevertheless, at the end of more accurate investigations, the choice of a little higher vanishing point appeared more correct (Figure 17), either because of its better connection with the whole perspective pattern, or, and most of all, because the projection of the right half of the baseline of the rear wall on the baseline of the canvas, nearly shows the corresponding real length, according to the historical map of the room (Figure 18). This means that Velázquez could use the baseline of the canvas as a perspective ground line. As we can see, the right endpoint of this segment actually lays outside

the boundary of the canvas. However, we decided to trust on this point, reasonably supposed to be part of the canvas before it was cut on the two sides after the fire, as we mentioned before. It was pivotal in this decision the recognition of a quite invisible point in the foreground, visible between Nicolastico's legs, which is the intersection point between the floor and the left jamb of the first balcony, only partially included in the image. This point, connected with the graphically reconstructed lower right corner of the rear wall, generates a line extensible to the vanishing point in question. The last issue, definitely convincing us, was the importance that the ground line would have at that time to carry on perspective constructions.

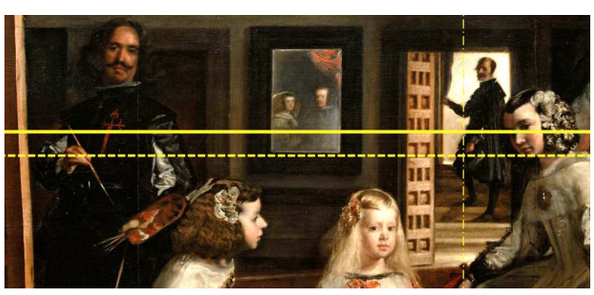

Figure 17: *Horizon line, first hypothesis (below), final hypothesis (above) (source of image* [12]*, cuts and diagram by author)*

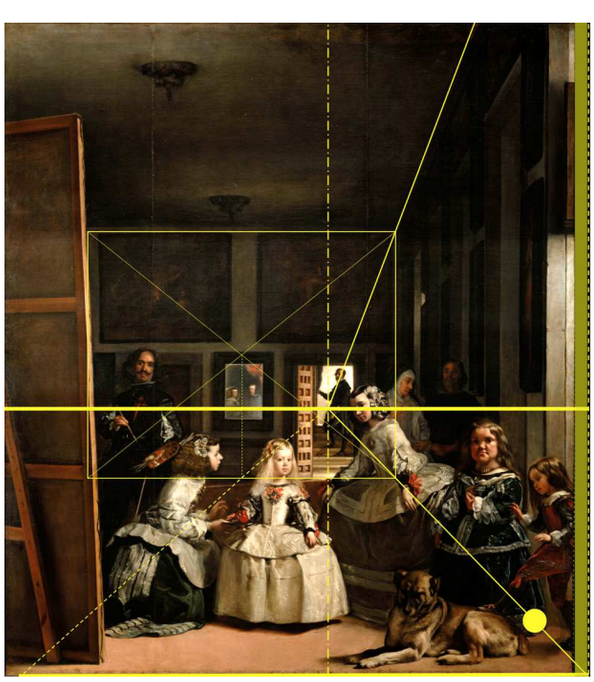

Figure 18: *The assumed basic perspective pattern (source of image* [12]*, diagram by author)*

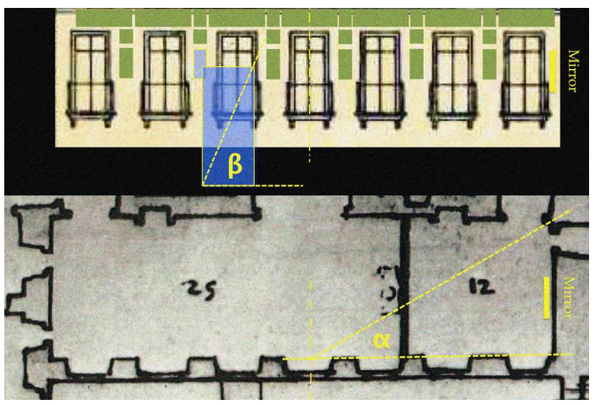

Figure 19: *Basic angles for the perspective reconstruction (source of images* [1]*,* [3]*, cuts and diagrams by author)*

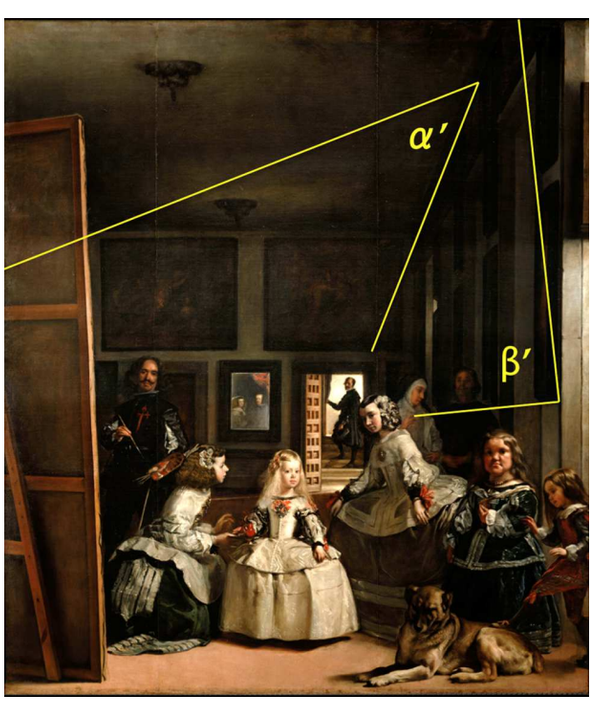

Figure 20: *Basic angles, transcription on the painting (source of images* [12] *diagrams by author)*

Once set the main bundle of lines, we had to work now on the foreshortenings in order to find the main distance and locate the viewpoint for the perspective reconstruction. To do this two angular data, that is, two directions were required. Since we already had the main vanishing point, related to the direction of the visual axis and orthogonal to the picture plane, we only needed another known direction recognizable in the painting. Given the absence of any geometrical reference on the floor, it was necessary to go back again to the information available from the 1626

plan by Juan Gomez de Mora [1, 3]. Whereas not the entire room is represented in the painting, whereas it was not possible to trust on the width of the windows drawn in the map because of the graphic imprecision, whereas it was not possible to estimate the width of balconies because of the unknown dimension of the chamfers in the painting, it was decided to consider an auxiliary diagonal running on an area having half the length of the room, extended from the midpoint of the medial balcony to the rear wall. Once drawn on the map, we could measure the true angle that this line formed with the southern wall (Figure 19). The same diagonal has been traced in perspective on the ceiling in the painting (Figure 20), and extended to the horizon line to find its vanishing point, which finally allowed us to draw a circle whose chord on the vertical visual axis was as long as the required main distance of the perspective construction. As a further proof, we repeated the procedure on the vertical plane of the wall, considering as a perspective reference for the metric data one of the paintings hung on between the balconies. At the end only a slight difference arose between the little shorter distance obtained with this additional construction, and the previous one, which we actually adopted (Figure 21). Now the main distance and the related distance circle allowed us to apply homological procedures for a true-to-size graphic reconstruction of the depicted elements (Figure 22). In addition, we also wanted to reconstruct the part of the room outside the pictorial space, that is, the part invading now our own space, corresponding to the area where King and Queen were during the painting session (Figure 23). Concerning metrics, we used to convert *pies* in *centimetres*, while the scale of graphic reconstruction, was 1:1, as we already said. The reconstruction confirmed the projective correspondence between the real room as it is drawn in the map and the depicted room, as well as the reliability of people, dog and furniture (Figure 24). Based on these parameters, the picture plane would be located at two thirds of the width of the first gate partially visible in the painting, measured from the painter's position, while the Royal Couple would be seated just behind the door located in front of the painter. Width and position of this door has been of course deduced only from the map that, as we saw, can be a little inaccurate in this kind of details. On our opinion, this door would be specular to the opposite one where we see Nieto, what should make the visual field more corresponding to what the painting suggests.

The pictorial set was in this way completely reconstructed (Figure 25). The last proof concerned the credibility of the reflected image of King Felipe and Queen Mariana. To make the proof it was first of all necessary to find the oblique plane to which the canvas belongs, and to determine its virtual specular outline beyond the mirror. This latter outline was determined by imposing symmetric vanishing elements, corresponding to those of the plane of the canvas represented in the painting, according to the distance circle. To complete the test, point of the reflected image of the King, namely a point between the eyes, was

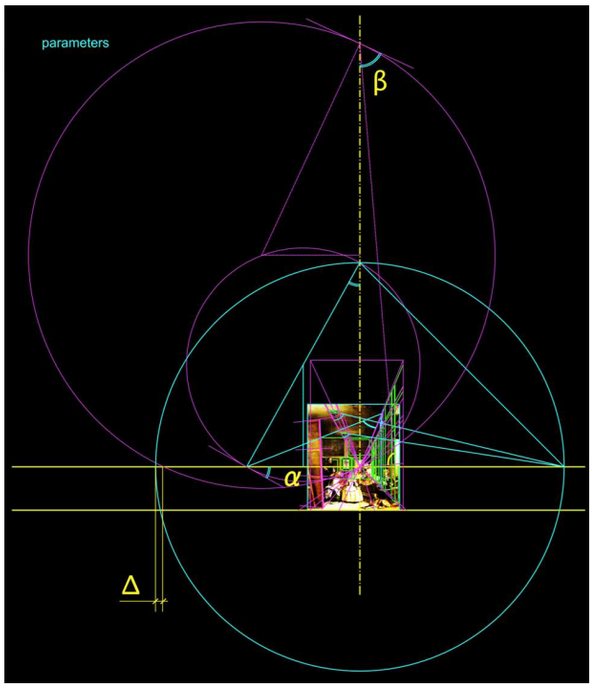

Figure 21: *In search for the perspective set: auxiliary circles and distance circle (dawn by author)*

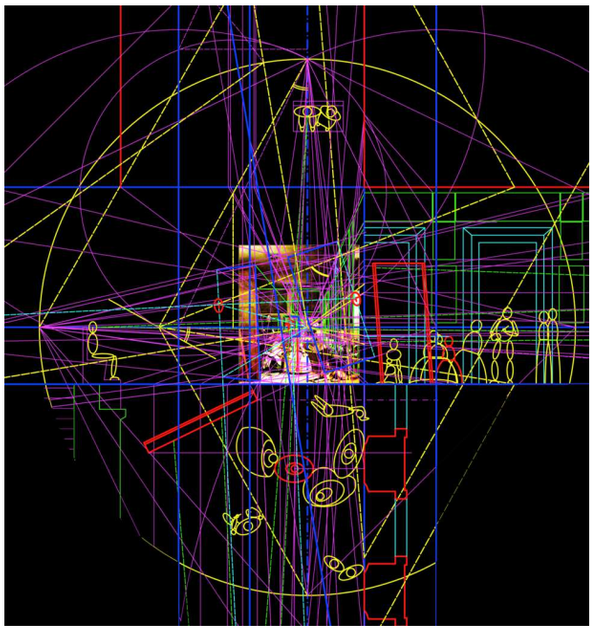

Figure 22: *Homology at work. Space and sight point: detail of the true-to-size reconstructions (drawn by author)*

translated from the virtual image of the mirrored oblique plane of the canvas, to the oblique plane of the canvas in front of Velázquez. The translation run on a depth line, belonging to a vertical plane perpendicular to the mirror in the real wall. As a final result, the point matches the canvas, meaning that the image of King and Queen we see in the mirror can really be the reflex of their portrait painted on the canvas, so that the sovereigns could see and follow the pictorial work going on in real time (Figure 26). By the way, since the portrait in the mirror seems complete, *Las Meninas* might represent the end of the pictorial session, then justifying the arrival of Nieto from the opposite side of the room. Taking advantage of homology, the graphically deduced true-to-size of the canvas shows that the hypothesized real position of the face of the King painted on the canvas, would be about one meter far from the oblique edge and about one and half meter high from the ground, which seems perfectly at hand for a painter about one meter and seventy centimetres tall portraying a man sitting at the mentioned distance from him. The perspective analysis of the painting has been also proposed to the students of my elective course *Geometrical Complements of Graphic Representation* at the School of Architettura e Societá of Politecnico di Milano in the academic year 2014-2015. During the course, as double check, physical models (Figure 27) and digital animations (Figure 28), where for the sake of "projective philology" gaps in the 3D models correspond to hidden areas in the painting, have confirmed this hypothesis. On the other hand, it would have been easy for Velázquez to set the elements and the chair for the royal husband and wife in the correct position in the real space beforehand as a proof, since this room was his *atelier*.
Concerning the adopted methodology, it has to be said that for the graphic reconstruction we used the modern homological method of Projective and Descriptive Geometry, which during the XVII Century was still under development. In addition, the use of *rabatment*, which we used to have the true profiles available on the same plane, requires and enormous graphic space, especially for the auxiliary constructions. For sure the method adopted by Velázquez was one allowing him to have all the basic auxiliary constructions on the canvas, maybe also together with the help of optical instruments, a matter that could be explored in new researches. Anyway, his strong background in perspective, optics and catoptrics is clear from his paintings. Moreover, it has been highlighted that he took care of his own education in these fields. At his death, indeed, 154 books were found in his library, mostly about math, geometry, optics, astronomy, including treatises and books by Luca Pacioli, Aguilonius, Dürer, Witelo, Guidobaldo Del Monte, Serlio, Benedetti, Zuccaro, Cousin, Barbaro, Tartaglia, Euclid, Alberti, Egnatio Danti, Vignola, Leonardo da Vinci, Cespedes, together with graphic instruments and a series of mirrors [7].

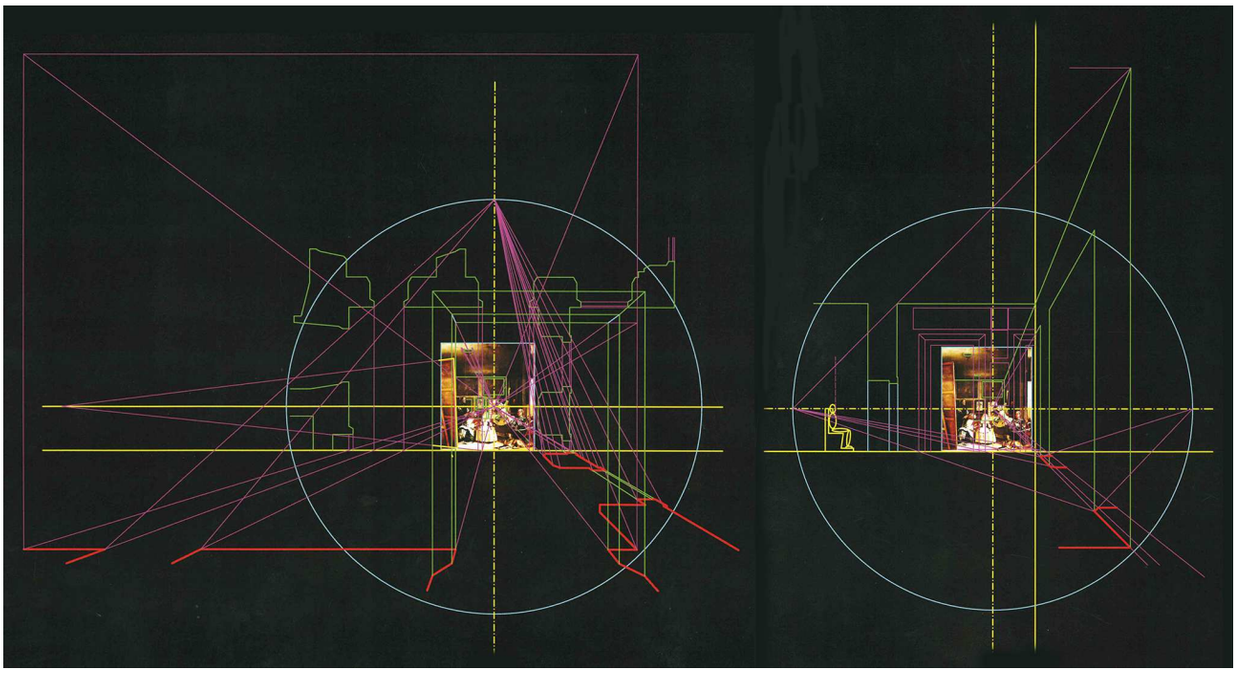

Figure 23: *Behind the canvas, inside our own space: perspective reconstructions (drawn by author)*

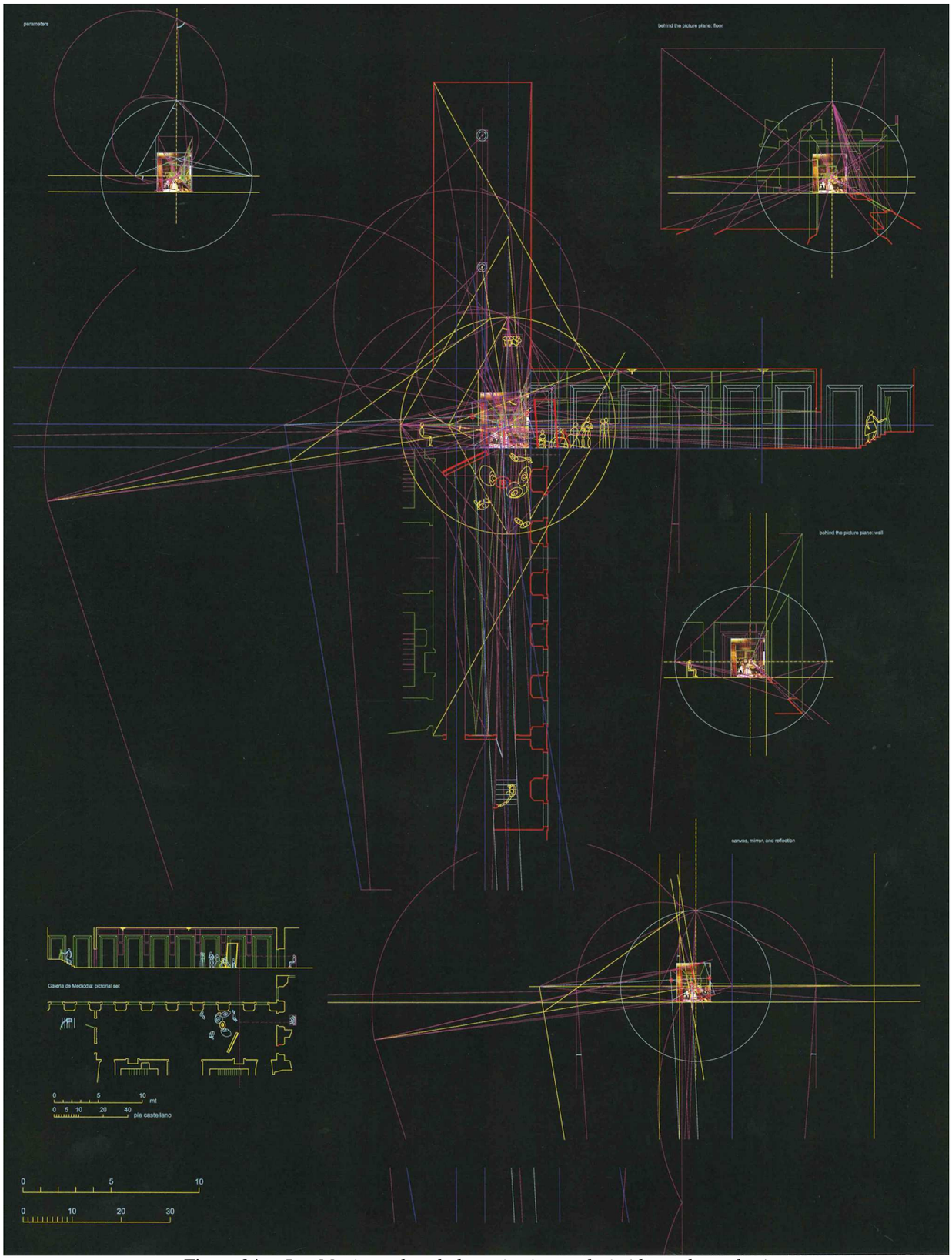

Figure 24: *Las Meninas, the whole projective analysis (drawn by author)*

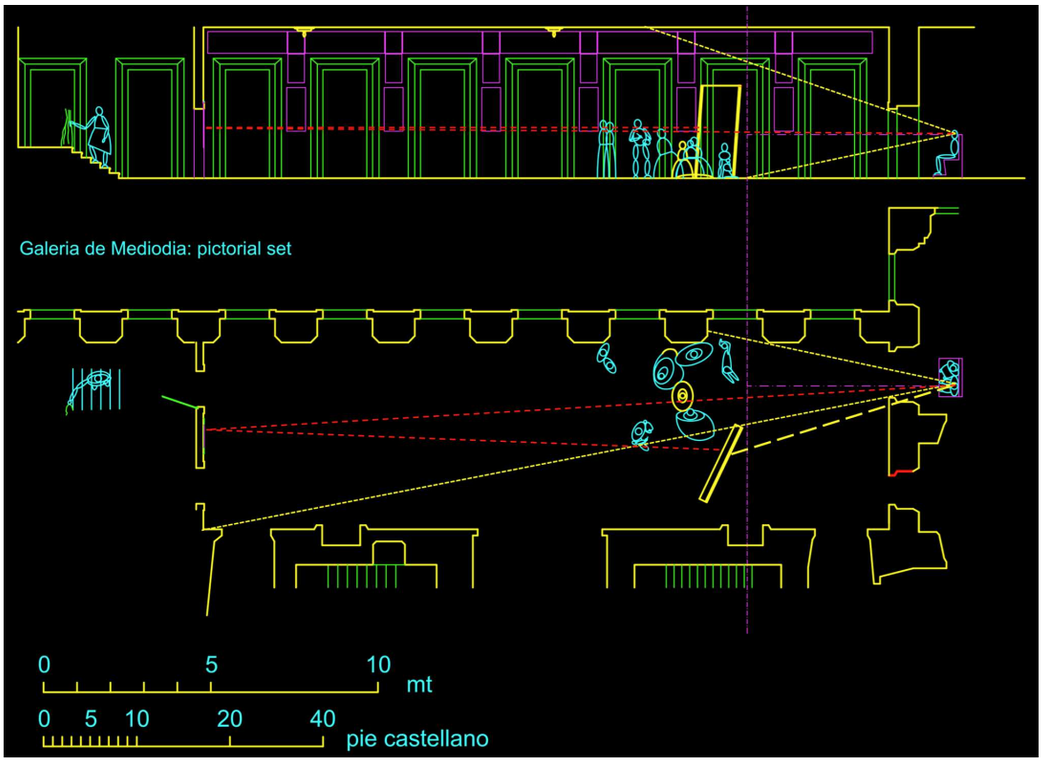

Figure 25: *Las Meninas, reconstruction of pictorial set and visual field: plan and section (drawn by author)*

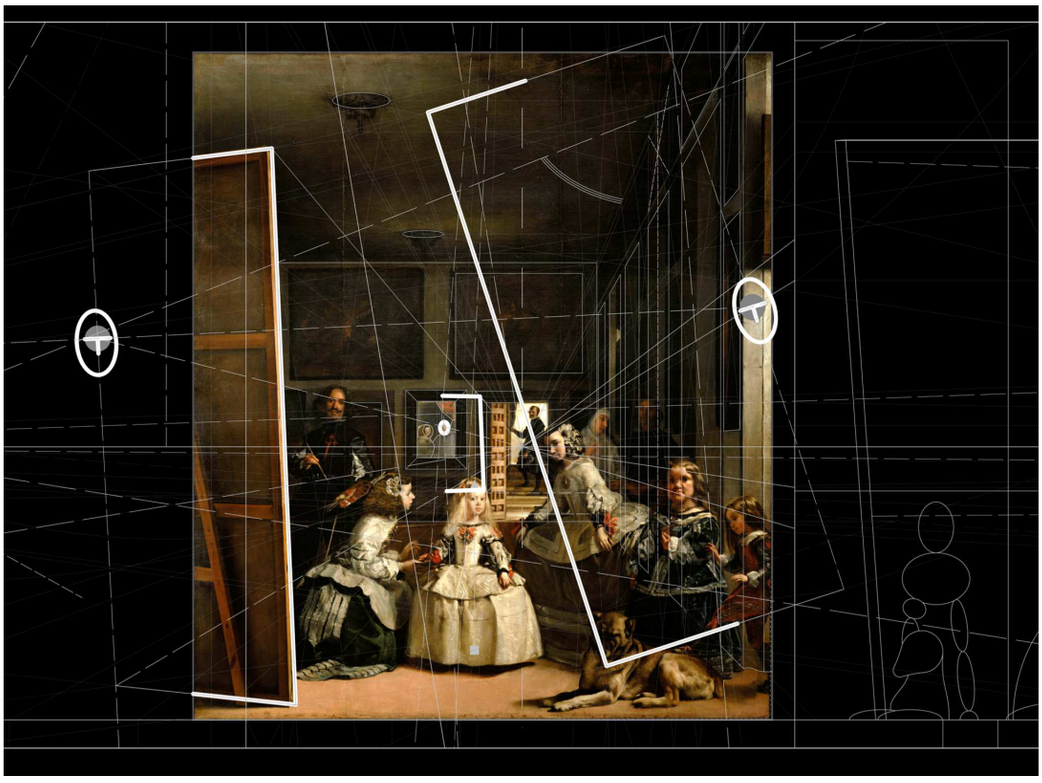

Figure 26: *Las Meninas, into the enigma of mirror via homological investigation (drawn by author)*

Figure 27: *Las Meninas, physical replica. Photographic view from the designated sight point (model and image by Aamir Ahmed Patel and Abhay Kaushik)*

Figure 28: *Las Meninas, "philological" digital replica: gaps in the 3D model correspond to hidden part in the painting (frames from an animation by Aamir Ahmed Patel and Abhay Kaushik)*

8 Conclusion

At this point, some comments about reason and meaning can be proposed. At a first glance the painting is shocking for the intriguing and flooring set as well as the pictorial virtuosity. But there is even more behind. Velázquez painted *Las Meninas* in his mature age, few years before he passed away, and thanks to his multiple offices across Art and Court he had a clear vision of the world around him [4]. He knew and showed the double side of reality, serious and mocking, light and dramatic, ironic and melancholy. *Las Meninas* is about all these. And its iconography is as precisely calibrated as a treatise, superbly integrating various aspects and levels. The representation of meaning follows a dynamic equilibrium, as well as we already saw in the pictorial composition, even more emphasized by the alternation of bright and dark areas in the pictorial space. All the basic hierarchical ranks of the Court and typologies of human beings appear on the canvas, in an interesting order, since backstage is of a dog, together with a midget and a dwarf, while King and Queen are the smallest figures, little dimed because of the reflection in the mirror. In opposite, the most shining figure is that of Infanta Margarita, at very barycentre of the scene, may be the real main subject of the painting, representing the future and the hope of the reign. This fact can not be clear without considering the heavy series of mourning afflicting the King, at his second wedding and having Margarita as his only son at that moment. On the other hand he was getting old, something consistent with his fading image in the mirror.

However, mirror is a pivotal enigmatic point in *Las Meninas*, and the duplication of the pictorial space a recurring obsession for the painting. We can mention *Christ at the house of Martha and Mary*, painted nearly four decades before, integrating two spaces in the same painting, or *Venus and Cupid*, better known as *Venus Rokeby*, painted seven years before, a nude where the face of the goddess is revealed into a small mirrored handed by Cupid. Some comparisons have been carried on with The *Arnolfini Portrait* by Jan van Eyck, realized more than two centuries before, in 1434. Anyway, considering the different typology of reflection, in van Eyck generated by a curved mirror, and apart from the superficial evidence of the presence of a mirror depicted in the scene, we do not see other significant similarities. Like in the *Venus Rokeby*, in fact, both subjects and their mirrored images appear on the canvas, while in *Las Meninas* we see only the mirrored image, but not the King and the Queen. To find the reason, it has been suggested to search into the literary genre of the *speculum principis*, or the mirror of prince, inspired by an ancient Roman tradition starting with Isocrate's *To Nicocles*, including booklets and manuals focusing on how to educate a Prince [10]. The basic idea was that mirror never fails, and that reality looked through a mirror can be dominated, like in the case of Perseus and Medusa Gorgon. At the time this literary genre was widely diffused in the European area. In Spain, it was known ad *espejo de principe*, where vices and virtues were compared and analysed by using various literary formulas and expedients. In the modern era some reference works were *Il Cortegiano* by Baldasar Castiglione in 1528, *Agudeza y arte de ingenio*, and *El criticon* by Balthasar Gracian, respectively in 1648 and 1651. About Italy we could remind *De Principatibus* by Nicolò Machiavelli, date back to 1513. But it seems that the main reference to Velázquez was the book *Idea de un principe politico Christiano*, that means the ideal Christian political prince, written in 1640 by Don Diego de Saavedra Fajardo, who was minister and ambassador, closely in touch with the King of Spain, and most of all, knight of the Order of Santiago, the Order that Velázquez was struggling to join at the time, as we saw before (Figure 29). Back to *Las Meninas*, mirror could allow king and queen to be there and not there at the same time, in the purity of a reflected image without contaminations with the real space. In other words, they could be there as a reflected image to represent the pure principle of being sovereigns, that is, as the mirror of their darling Princess (Figure 30).

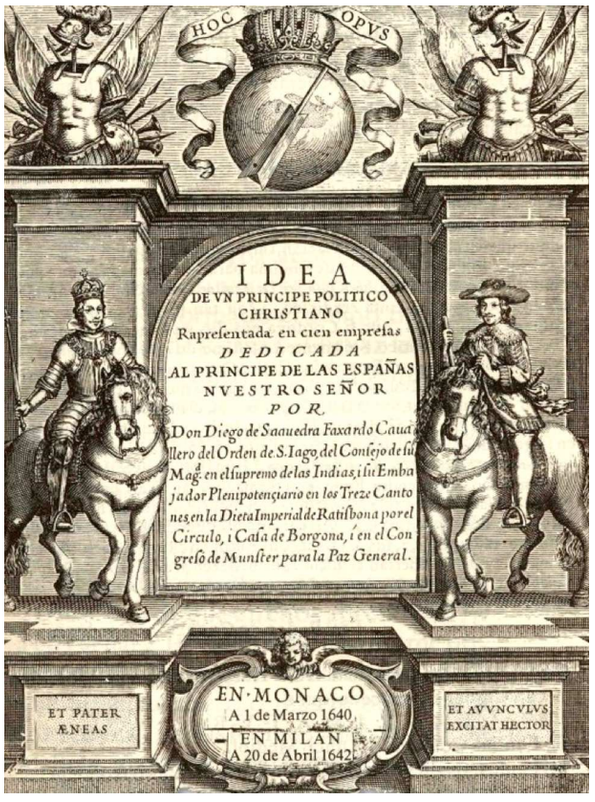

Figure 29: *Frontispiece of the book "Idea de un principe politico Christiano", written in 1640 by Don Diego de Saavedra Fajardo (source of image* [13]*)*

Figure 30: *The Infanta Margarita, darling daughter of Felipe IV and Mariana de Austria, seen through the pinhole of the model (picture by Georg Glaeser)*

The mirror is also connected with the two copies of Rubens hung above, namely *Minerva Punishing Arachne*, on the left, and *Apollo's Victory over Marsyas* on the right. They tell mythological stories of the dramatic consequences on humans who dared to challenge gods. As we know Arachne was turned in a spider and Marsyas ended up being flayed. What is also interesting to see is the correspondence in genders, since the feminine story is set above Queen and the masculine above King, to remind the limited power of human beings, no matter how much is their role in this world. But since Apollo is patron of Arts and Minerva's patron of Wisdom, their presence also symbolizes a wider admonishment, involving Velázquez himself, who is just at work on a painting. At the time, indeed, painters and were considered artisans working with hands, to whom the shift to high society was impeded. Proof is the hard work Velazquez was still doing, in spite of his multiple prestigious offices at Court, to be accepted as a member by the Order of Santiago. The two mythological stories seem then to have, first of all, a double meaning, as auspices for a divine protection as well as defences from the ire of deities due to the arrogance and haughtiness of the painter. He knew there might have been reasons for that. Why?

At the end, Royal Family, officers and servants show in his *atelier*. There are similar cases of pictorial scenes located in painters' ateliers, among the most well known we could remind *The Arkidukes Albert and Isabella Visiting a Collector's Cabinet* in 1623 by Jan Brueghel the Elder and Hieronymus Francken, and *The Gallery of Cornelis van der Geest Visited by the Regents* in 1628 by William van Haecht [8]. Nevertheless, the mood in *Las Meninas* is quite different, and definitely stronger. We see the painter himself looking into our space and our eyes, together with several other people in the painted space, in a way that his figure can not be removed without trivializing the scene. His silhouette stands out over the other characters, imperious and concentrated, despite the light *penumbra* around him. Considering the size on the canvas, it is large and detailed enough to be cut out as a self-portrait apart. Anyway, the additional and maybe most significant meaning comes from the fact that the painter in person is acting in the community of sovereigns, dignitaries, and deities. Moreover, he also involved goddes in his work, in a way that they could see the work in progress on the canvas, as if it was something worthy of their consideration and worries. This point is related to Velázquez's main aim, that is, release and redemption of painting and painters. Challenging task, in *Las Meninas* it seems fully realized, at the point that painting itself brings together history and mythology, which is not possible to achieve outside the boundaries of Art, in this case, of Painting. Where perspectival and optical interplays are of crucial importance to achieve the goal [7-10]. In this sense, as proposed in the title of this paper, we see the alchemic contribution of perspective in making Image able to set a reality. In this case, as a kind of *augmented* reality, enriched by supernatural presences and new meanings. That is, more than what would be possible to realize in the tangible space of the every day life. From the Golden Age of the Spanish Painting, Velázquez carried on in this painting a revolutionary enhancement, for some extents comparable to the one carried on in Italy by Leon Battista Alberti during the XV Century. This makes this masterpiece relevant not only for Art, but also in a wider social, cultural, and historical sense.

Therefore, and not only for technical reasons, we believe that the scene depicted in *Las Meninas* has not been simply outlined from a whole image reflected in a big mirror put in front of the artist, which would have implied an *imitation*, given that painting would be explicitly shown here as a *creation*. An intellectual, besides manual, creation, or, re-creation. Secondarily, a specular image would have weakened that exclusive *mirror of prince* effect provided by the specular image of the royal couple. In a way, there should have not been room for mirrored image as model of virtues, apart from the sovereigns. Another point reinforcing this hypothesis comes from the observation of the canvas in front of Velázquez, whose content we can only suppose but not see directly. In our opinion, this is one of the strongest metaphors incorporated in this pictorial manifesto, telling us that art is not revealed, if not to the artist, goddess wishing. In which is also an eternal enigma of Art. One more reason to avoid mere imitations of images reflected by a mirror. Art is a fleeing construction of genius and intelligence. In conclusion we have no other chances

but agree with Jonathan Brown's opinion: "A painting as rich in ambiguity as it is in subtlety, *Las Meninas* has long been recognized as a masterpiece of Western art, a pictorial tour de force rarely equalled and never surpassed. But when we attempt to explain its greatness, we soon realize how it seems to evade the grasp both of intuitive and rational understanding". Nevertheless, the prospective meager expected results have been largely offset by the wealth of experience resulting in the geometric study and graphic analysis of this, which is not only a masterpiece of genius, but also a superb educational example of scientific and artistic dedication as well as professional ennobling. Would we be able to achieve comparable goals in our research, educational, and professional field nowadays?

Acknowledgments

I would like to express my thanks to Professor Maria Grazia Sandri for helping me with the historical sources and Professor Dario Angelo Maria Coronelli for reviewing the English text. Thanks to my former student Shuyang Li for reviewing the final draft.

References

[1] J. M. BARBEITO, *El Alcázar de Madrid*, Colegio Oficial de Arquitectos de Madrid, Madrid 1992.

[2] J. M. BARBEITO, Velázquez y la decoración escultórica del Alcázar, in L. Alba Carcelén (editor), *Velázquez: esculturas para el Alcázar*, Real Academia de Bellas Artes de San Fernando, Madrid, 2007, 113–131.

[3] J. BROWN, *Images and Ideas in seventeenth-century Spanish painting*, Princeton University Press, Princeton, N.J., 1978.

[4] J. BROWN, *Velázquez, Painter and Courtier*, Yale University Press, London, 1986.

[5] K. CLARK, *Looking at pictures*, Holt Rinehart and Winston, New York, 1960.

[6] L. COCCHIARELLA (editor), *The Visual Language of Technique Between Science and Art*, Volumes 1-3, Springer International Publishing Switzerland, Cham, Heidelberg, New York, Dordrecht, London, 2015.

[7] M. KEMP, *The Science of Art. Optical themes in western art from Brunelleschi to Seurat*, Yale University Press, New Haven and London, 1990.

[8] M. MILLER KAHR, Velázquez and Las Meninas, *The Art Bulletin* **57(2)** (1975), College Art Association, 225–246.

[9] J. R. SAERLE, "Las Meninas" and the Paradoxes of Pictorial Representation, *Critical Inquiry* **6(3)** (1980), The University of Chicago Press, 477–488.

[10] J. SNYDER, "Las Meninas" and the Mirror of the Prince, *Critical Inquiry* **11(4)** (1985), The University of Chicago Press, 539–572.

[11] A. S. VELÁZQUEZ, Genius Loci. Anaparástasis del Alcázar vejo de Madrid a partir de la reconstrucción tridimensional de Las Meninas, *Cuadernos de los Amigos de los Museos de Osuna* **15** (2013), 138–147

[12] Source of the image of Velázquez's *Las Meninas*: `wikipedia.org`

[13] `en.m.wikipedia.org`

Luigi Cocchiarella
e-mail: luigi.cocchiarella@polimi.it
Politecnico di Milano, Department of Architecture and Urban Studies – School of Architettura e Societá
Milan, Italy

How to get KoG?

The easiest way to get your copy of KoG is by contacting the editor's office:

Marija Šimić Horvath
msimic@arhitekt.hr
Faculty of Architecture
Kačićeva 26, 10 000 Zagreb, Croatia
Tel: (+385 1) 4639 176
Fax: (+385 1) 4639 465

The price of the issue is €15 + mailing expenses €5 for European countries and €10 for other parts of the world.

The amount is payable to:

ACCOUNT NAME:	Hrvatsko društvo za geometriju i grafiku Kačićeva 26, 10000 Zagreb, Croatia
IBAN:	HR862360000-1101517436

Kako nabaviti KoG?

KoG je najbolje nabaviti u uredništvu časopisa:

Marija Šimić Horvath
msimic@arhitekt.hr
Arhitektonski fakultet
Kačićeva 26, 10 000 Zagreb
Tel: (01) 4639 176
Fax: (01) 4639 465

Za Hrvatsku je cijena primjerka 100 KN + 10 KN za poštarinu.

Nakon uplate za:

HDGG (za KoG), Kačićeva 26, 10000 Zagreb
žiro račun broj **2360000-1101517436**

poslat ćemo časopis na Vašu adresu.

Ako Vas zanima tematika časopisa i rad našeg društva, preporučamo Vam da postanete članom HDGG-a (godišnja članarina iznosi 150 KN). Za članove društva časopis je besplatan.

ISSN 1331-1611